

PAVEMENT SUBGRADE PERFORMANCE STUDY

National Pooled Fund Study SPR-208

Test Section 709

Subgrade AASHTO soil type A-6 at optimum moisture content

by

Edel R. Cortez⁽¹⁾
Troy W. Arnold⁽¹⁾
Christopher E. Williams⁽¹⁾

Subgrade Moisture Content	AASHTO Soil Type			
	A-2-4	A-4	A-6	A-7-5
M1	Optimum 10 % TS 701	Optimum 17 % TS 702	Optimum 16 % TS 709	Optimum 20.4 % TS 712
M2	12 % TS 707	19 % TS 704	19 % TS 708	21 % TS 710
M3	15 % TS 703	23 % TS 705	22% TS 706	25 % TS 711

¹ U.S. Army Corps of Engineers, Engineer Research and Development Center
Cold Regions Research and Engineering Laboratory
72 Lyme Road,
Hanover, New Hampshire 03755, United States

EXECUTIVE SUMMARY

This report is one of a series of reports included in the pooled-fund research project titled Subgrade Performance Study (SPR-208). Current mechanistic design procedures incorporate results from the AASHO Road Tests conducted in the late nineteen fifties. However, the AASHO Road Tests were all conducted on only one soil type (AASHTO type A-6). The tests results reflected the combined effect of traffic loads and seasonal variations. Applying failure criteria based on the AASHO Road Tests to other soil types, at different moisture contents and different climate introduces significant uncertainty.

Computer technology and new sensors present new opportunities to characterize the stress and strain response of pavement structures to traffic loads. More accurate measurements will constitute the basis for the development of mechanistic pavement models and failure criteria that consider soil type and moisture condition.

Transportations agencies of nineteen US states and the Federal Highway Administration (FHWA) are participating in this research initiative. The subgrade soil types included in this study are the four most commonly found soils in the United States. The test plan includes three full-scale road test sections for each soil type. These three test sections differ only on the subgrade moisture content. One represents the subgrade soil at optimum moisture content. Each of the other two test sections contains subgrade soil at a particular wet of optimum level. The test sections consisted of 76 mm (3 in.) of asphalt concrete, 229 mm (9 in.) of crushed base, and 3 m (10 ft) of subgrade soil over a Portland cement concrete floor that simulates bedrock. This report deals specifically with Test Section 709 corresponding to the case of a subgrade soil AASHTO type A-6 built at optimum moisture and maximum density. According to the Unified Soil Classification System, the subgrade soil was type CL (low liquid limit, clay). According to laboratory modified Proctor tests, for this soil, the optimum moisture content was 16 percent.

Accelerated traffic was applied by means of a Heavy Vehicle Simulator (HVS). Each test window was subjected to one of various load intensities ranging from 20 to 53.4 kN (4.5 to 12 kips). The load was applied through a dual truck tire assembly representing a half axle of a standard truck. Therefore, a 40-kN (9-kip) load is equivalent to an 80 kN (18-kip) load applied with a complete truck axle. The tire pressures were kept at 689 kPa (100 psi).

The test section was built inside the Frost Effects Research Facility (FERF) testing facility where subgrade soil moisture and temperature conditions were controlled. The test section contained six test windows. Each effective test window was approximately 6.08 m (20 ft.) long and 0.91 m (3 ft.) wide. Additional acceleration and deceleration zones were provided for each test window. Loading was applied unidirectionally at an average speed of 12 km/hr. The test windows were subjected to approximately 600 load repetitions per hour. The HVS applied traffic 23 hours per day. The remaining hour was used for maintenance.

Stress and strain sensors were located at various depths in the base course and the subgrade. Stress, strain, and surface rut measurements were taken at various stages throughout the traffic testing. Permanent deformation (while no traffic was occurring) and dynamic deformation (during the passing of the tire assembly) were measured layer by layer from the asphalt surface down to a depth of 1.52 m. With this configuration, profiles of deformations with depth were constructed, and strain profiles were deducted from them.

The subsurface deformation measurements were calibrated in situ by equating the sum of layer deformations to the measured surface rut depth. Surface rutting was measured with a laser profilometer and verified by wedge thickness measurements.

This report contains a description of the test section, material properties, construction, instrumentation, traffic loading, and pavement response in terms of stress and strain. A forensic evaluation was conducted after the traffic tests.

CONTENTS

EXECUTIVE SUMMARY	i
CONTENTS	1
DESCRIPTION OF THE TEST SECTION.....	3
MATERIAL PROPERTIES.....	5
CONSTRUCTION OF THE TEST SECTION.....	8
ACCELERATED TRAFFIC	13
TRAFFIC LOADS.....	16
TEMPERATURE AND MOISTURE DURING TRAFFIC	16
DEFORMATION AND STRAIN.....	32
<i>a) Permanent Deformations and Strains.....</i>	32
<i>b) Dynamic Deformations and Strains.....</i>	39
STRESS	40
FORENSIC EVALUATION.....	43
SUMMARY AND CONCLUSIONS	54
APPENDIX A.....	59
SURFACE PROFILE TEST RESULTS	59
APPENDIX B.....	66
PERMANENT DEFORMATION MEASUREMENTS.....	66
APPENDIX C.....	71
PERMANENT STRAIN MEASUREMENTS	71
APPENDIX D.....	75
DYNAMIC STRAIN MEASUREMENTS	75
APPENDIX E.....	79
STRESS MEASUREMENTS	79
APPENDIX F	82
FALLING WEIGHT DEFLECTOMETER MEASUREMENTS.....	82

INTRODUCTION

A national pooled fund study number SPR-208 titled Pavement Subgrade Performance Study was conducted with participation of nineteen U.S. states and the Federal Highway Administration (FHWA).

The study includes twelve full-scale test sections. The test sections were built indoors in the Frost Effects Research Facility (FERF) at the Cold Regions Research and Engineering Laboratory (CRREL) in Hanover, New Hampshire. CRREL is a component of the Engineers Research and Development Center (ERDC) which is the research and development division of the US Army Corps of Engineers. The tests were conducted indoors at approximately 20°C (68°F). They were instrumented with stress cells, strain gages, moisture gages, and temperature sensors. The test sections were subjected to accelerated loading using CRREL’s Heavy Vehicle Simulator (HVS). Pavement failure was defined at 12.5 mm (0.5 in.) surface rut depth, or the development of asphalt cracks 9.5 mm (3/8 in.) wide. Surface rut depth measurements were taken periodically during the accelerated load tests. At the same time, subsurface stress and strain measurements were also taken. A detailed overview of the test plan can be found in Janoo, et al. (2002). The test sections consisted of a 76-mm (3 in.) asphalt concrete (AC) layer, a 229-mm (9 in.) crushed gravel base and 3 m (10 ft) of subgrade soil over a 305-mm (12-in.) portland cement concrete floor. All the test sections in this research project were alike in geometry, instrumentation, and materials, except for the subgrade soil type and moisture content. The test sections were constructed using one of four subgrade soil types. For each soil type, one test section included subgrade soil at optimum moisture content and two test sections at each of two levels of wet of optimum. For each test section, provisions were made to maintain the temperature and moisture content as constant as possible. The test matrix for this study is shown in the table below.

Table 1. Experimental test matrix.

Subgrade Moisture Content	AASHTO Soil Type			
	A-2-4	A-4	A-6	A-7-5
M1	Optimum 10 % TS 701	Optimum 17 % TS 702	Optimum 16 % TS 709	Optimum 20.4% TS 712
M2	12 % TS 707	19 % TS 704	19 % TS 708	21% TS 710 Borderline soil A-6 and A-7-6
M3	15 % TS 703	23 % TS 705	22% TS 706	25% TS 711

This reports deals with the construction, accelerated traffic testing, and pavement response of Test Section 709. As shown in Table 1, the subgrade soil in this test section

was classified as AASHTO soil type A-6 conditioned at 16 percent gravimetric moisture content.

DESCRIPTION OF THE TEST SECTION

The test section consists of a 76-mm (3-in) hot mixed asphalt (HMA) layer, a 229-mm (9-in) crushed gravel base course, and 3 m (10 ft) of subgrade soil over a concrete floor that simulated bedrock. The subgrade soil was classified as AASHTO soil type A-6. This soil was conditioned to 16 percent gravimetric moisture content. This is the optimum moisture content for this soil according to modified Proctor test results. The laboratory CBR test results indicate that, at this moisture content, the subgrade soil had a CBR of 15 percent.

The test section was divided into six test windows. A test window is the area where traffic is applied. An effective test window was 0.91 m (3 ft) wide by 6.08 m (20 ft.) long, excluding acceleration and deceleration areas. The thickness and material properties for all test windows were intended to be constant, but the traffic load was set to one of several values for each of the test windows.

Each test window was instrumented with embedded sensors to measure in-situ stress, strain, moisture and temperature at various locations within the pavement structure. Dynatest® and Geokon® stress cells were used to measure stress in the unbound base course and the subgrade. ϵ mu coils were installed in stacks to measure deformation between coil pairs in vertical, longitudinal and transverse directions. Vertical deformations were measured in ten layers to a depth of approximately 1.52 m (5 feet). Strains were deducted from the layer deformation measurements. Campbell Scientific® CS615 sensors were used to record volumetric soil moisture content in the base course and subgrade during the accelerated traffic period. Additionally, strings of thermocouples were used to record subgrade, base course, asphalt, and air temperatures.

The test section was built indoors where the temperature and soil moisture were controlled. The test basin where the test section was built consisted of 3 concrete walls, a concrete floor and an access ramp also made of concrete.

Ordinary construction equipment was used to build the test sections, but the quality control testing was more rigorous than that of typical construction.

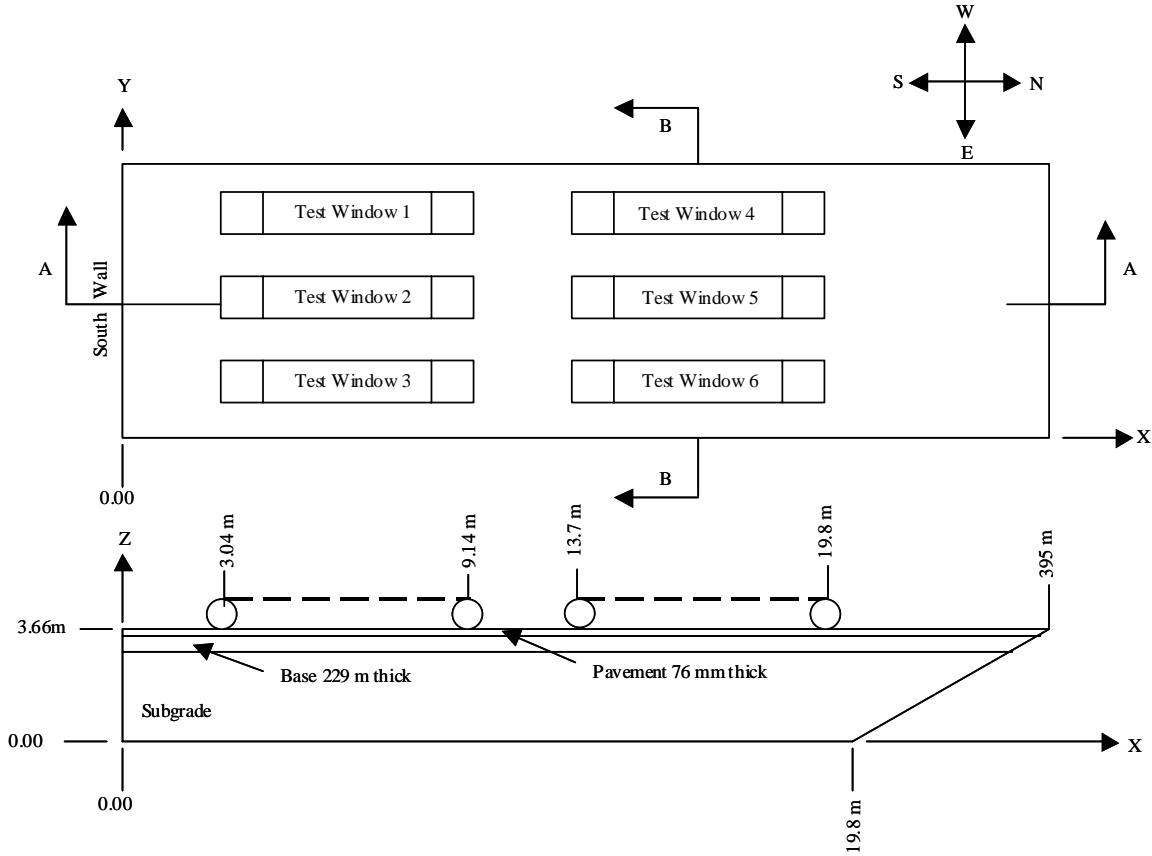


Figure 1a. Plan view and longitudinal cross section of test section.

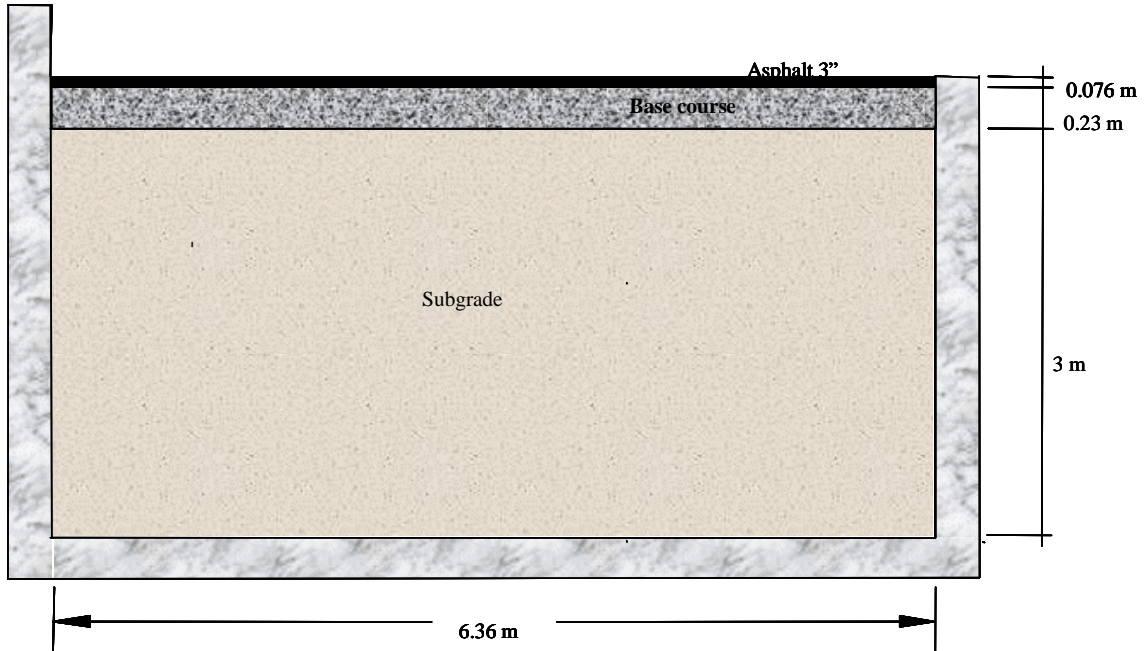


Figure 1b. Transversal cross section.

MATERIAL PROPERTIES

Laboratory tests were conducted on representative samples of the subgrade soil and the base course soil. The battery of tests included modified Proctor, laboratory CBR, grain size distribution, specific gravity, liquid and plastic limits, and hydrometer tests.

Figure 1 shows grain size distributions for the subgrade soil and for the base course soil. The subgrade soil has approximately 92 % passing the 0.074-mm (#200) sieve. The average liquid limit (LL) and plasticity index (PI) of the soil were 29 % and 13 % respectively. The average specific gravity of the subgrade soil was 2.70. According to the American Association of Highway & Transportation Officials (AASHTO) soil classification system, the subgrade soil was type A-6. According to the Unified Soil Classification System (USCS), the subgrade soil was type CL (low liquid limit clay).

The base course material was made of unbound crushed stone. It was classified as an AASHTO type A-1 soil. According to the Unified Soil Classification System, the base course soil was type GP-GM (mix of poorly graded gravel and silty gravel). About 11 percent by weight of the base course soil particles passed through the 0.074-mm (#200) sieve. The fines were classified as non-plastic. The base course soil met the New Hampshire specification 301.4 for base course materials. This was a crushed stone obtained from a quarry in Lebanon, NH. The source rock is classified as amphibolite which is a metamorphic rock.

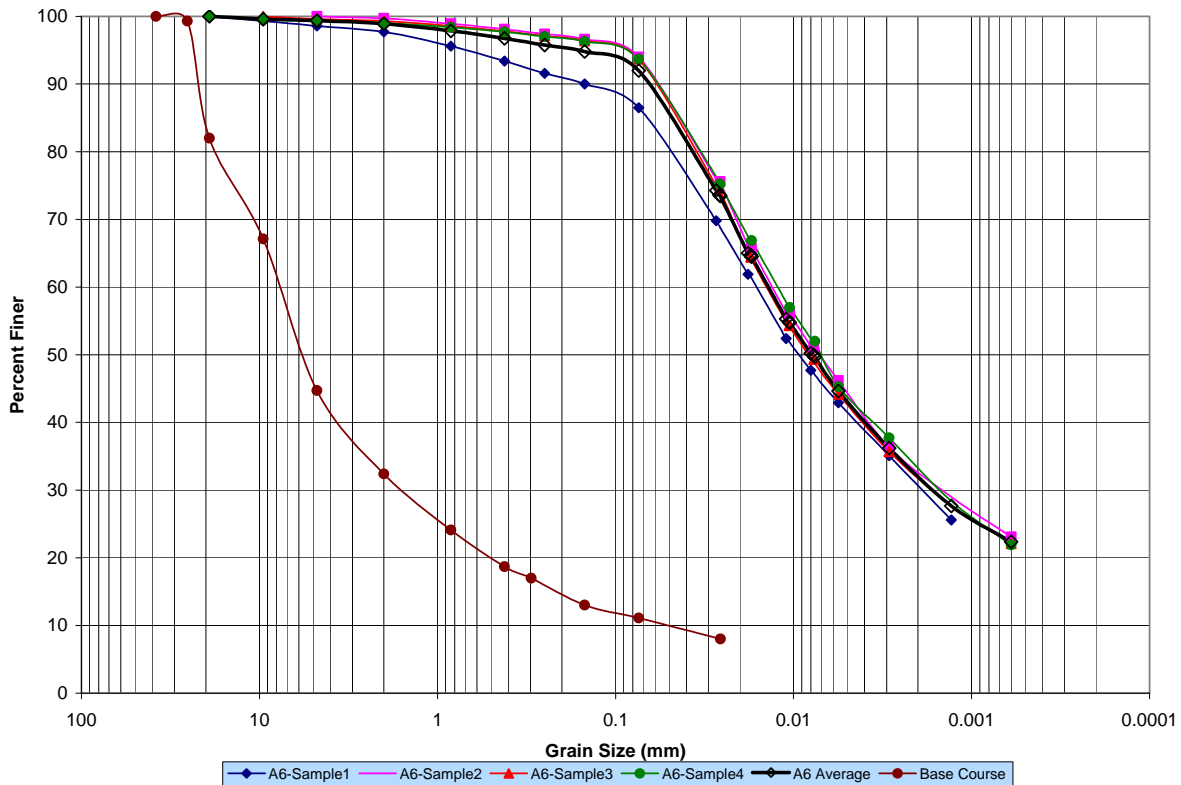


Figure 1a. Plan view and longitudinal cross section of test section.

Modified Proctor tests results show in Figure 3 indicated that the maximum density and optimum gravimetric moisture content for the subgrade soil were 1800 kg/m³ (112.5 pcf) and 16 % respectively. The design moisture content for this test section was the optimum moisture content, but the average as-built subgrade moisture content was 16.6 %. The laboratory CBR for this moisture content was approximately 13 percent.

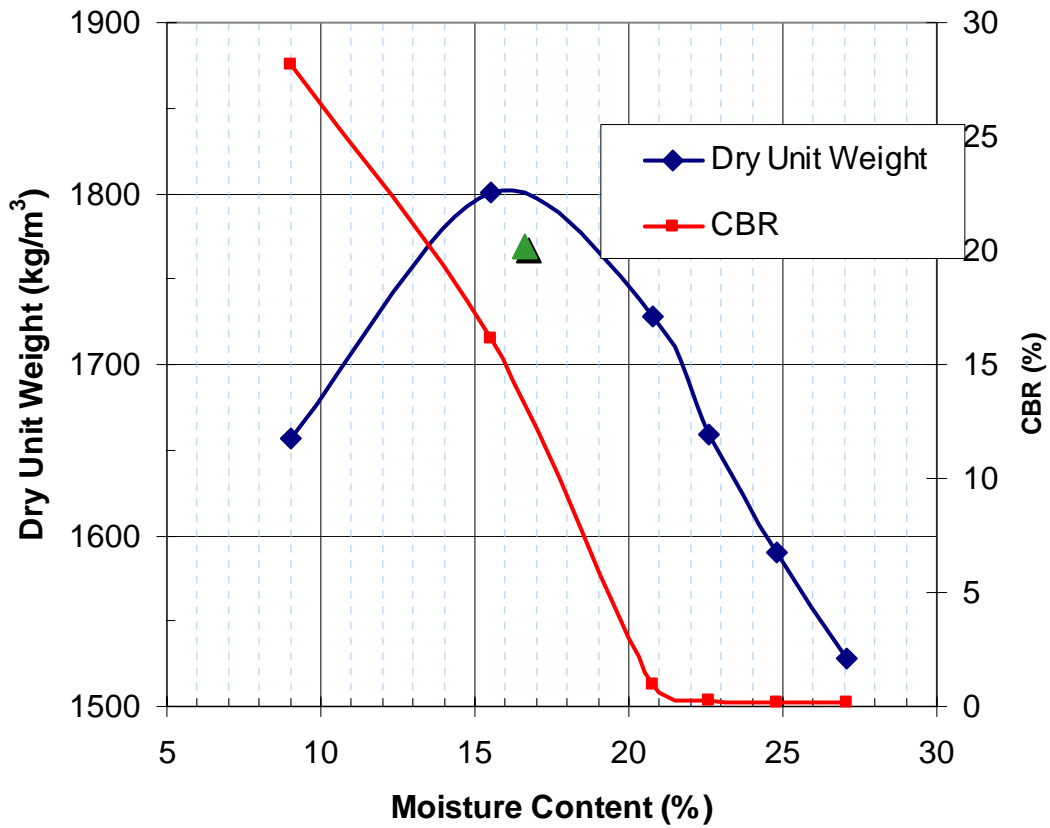


Figure 2. Modified Proctor and laboratory CBR test results for the subgrade soil.

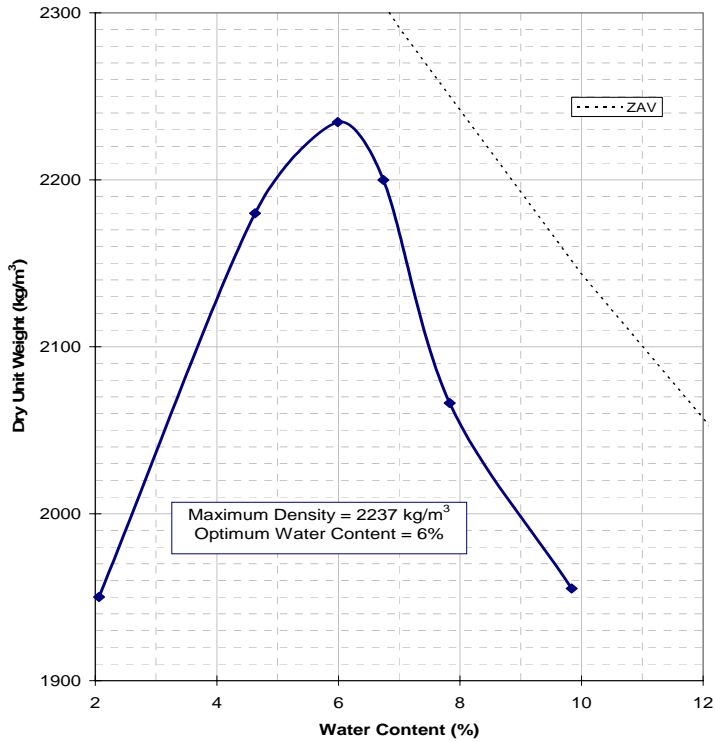


Figure 4. Base course modified Proctor test results.

The modified Proctor test results shown in Figure 4 indicate that the optimum gravimetric moisture content of the base course material was 6 percent and the maximum density was 2237 kg/m³ (139.5 pcf). Obtaining this moisture content with high hydraulic conductivity materials is difficult in practice. The average moisture content of the base course material during construction was 4.9 percent. The average moisture content of the base course material during the forensic evaluation was 3.2 percent. Apparently, the moisture content in the base course diminished gradually during the period of traffic testing. It appears that most of the moisture lost from the base course migrated down into the subgrade soil.

Table 2. Summary of properties of the subgrade soil used in Test Section 709.

AASHTO	A-6
USCS	CL
Spec. Gravity	2.70
LL (%)	29
PI	13
Optimum moisture content (%)	16
Maximum Density (kg/m ³)	1800
% passing #10	99
% passing #200	92

The asphalt concrete material of the binder course conformed to the Vermont Type II standard, with 19-mm maximum aggregate particle size and 4.5% of asphalt binder PG-58-34. The asphalt concrete material of the wearing course conformed to the Vermont Type III standard, with 13-mm maximum aggregate particle size and 5.3% of asphalt binder PG-58-34. The nominal thickness of the binder course was 51 mm. The nominal thickness of the wearing course was 25 mm.

CONSTRUCTION OF THE TEST SECTION

The subgrade was built in layers 150-mm (6-in.) thick. The soil was first placed at a moisture condition dryer than the target moisture content. The soil was rototilled, and moisture was gradually added until reaching the target. Then, the soil was compacted with eight passes of a 10-Ton (9,072-kg) steel roller in static mode. Moisture and density quality control measurements were conducted using a nuclear gauge. Additional roller compacting was applied as needed to obtain at least 95 percent of the modified proctor density for the given moisture content.

The base course was placed in 2 layers 114.3-mm (4.5-in.) thick for a total of 228.6 mm (9 inches). Finally, the AC layer was placed in two lifts for a total of 76 mm (3 inches).

CONSTRUCTION QUALITY CONTROL

During the construction of the subgrade, a series of tests were conducted on each of the compacted layers. Measurements included layer thickness taken with a survey level, and moisture-density measurements taken with a nuclear gauge. Falling weight deflectometer (FWD) tests were conducted on top of the asphalt concrete prior to traffic testing.

The mean moisture content of the test subgrade was 16.6 percent. The average moisture content of the base was 4.9 percent. The mean dry density of the subgrade was 1769 kg/m^3 (109.9 pcf). The mean dry density of the base course was 2356 kg/m^3 (147.1 pcf). The mean density of the AC was 2304 kg/m^3 (143.8 pcf).

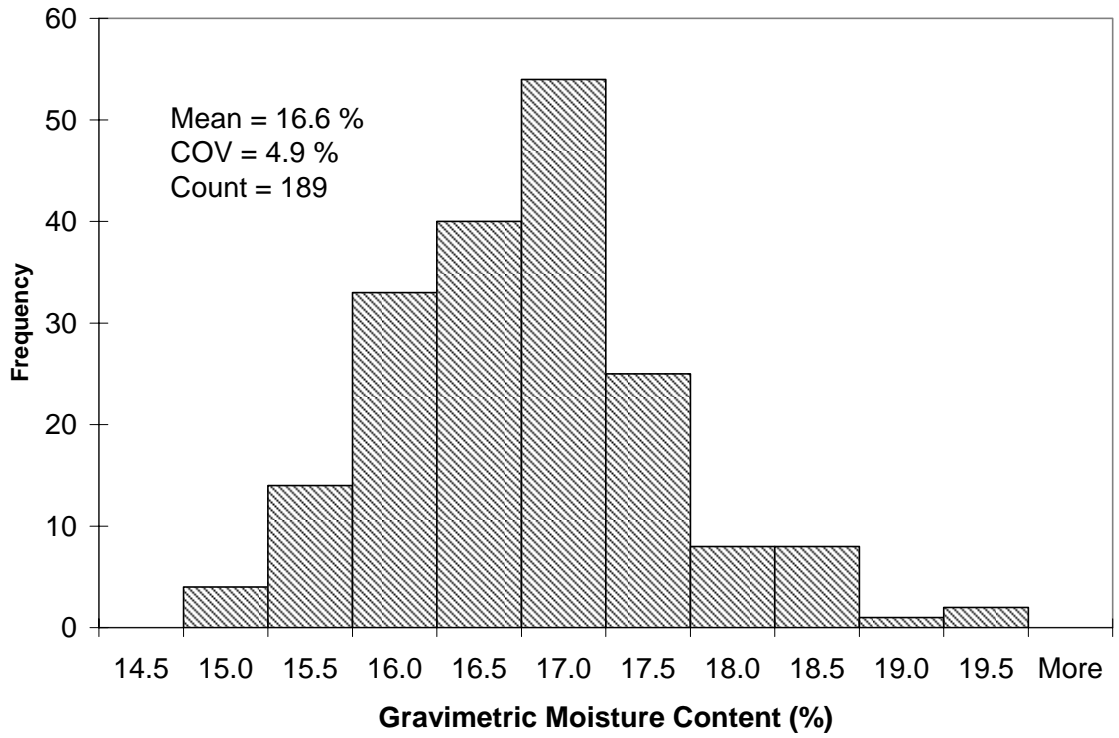


Figure 5. Subgrade moisture content.

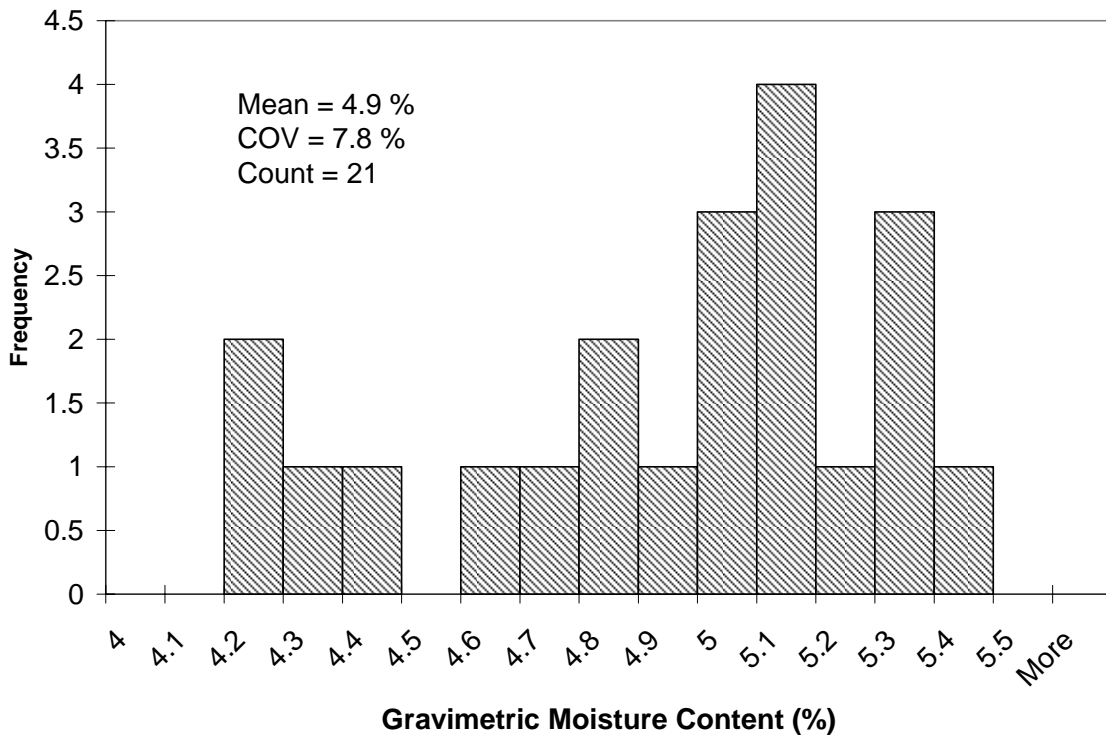


Figure 6. Base course moisture content.

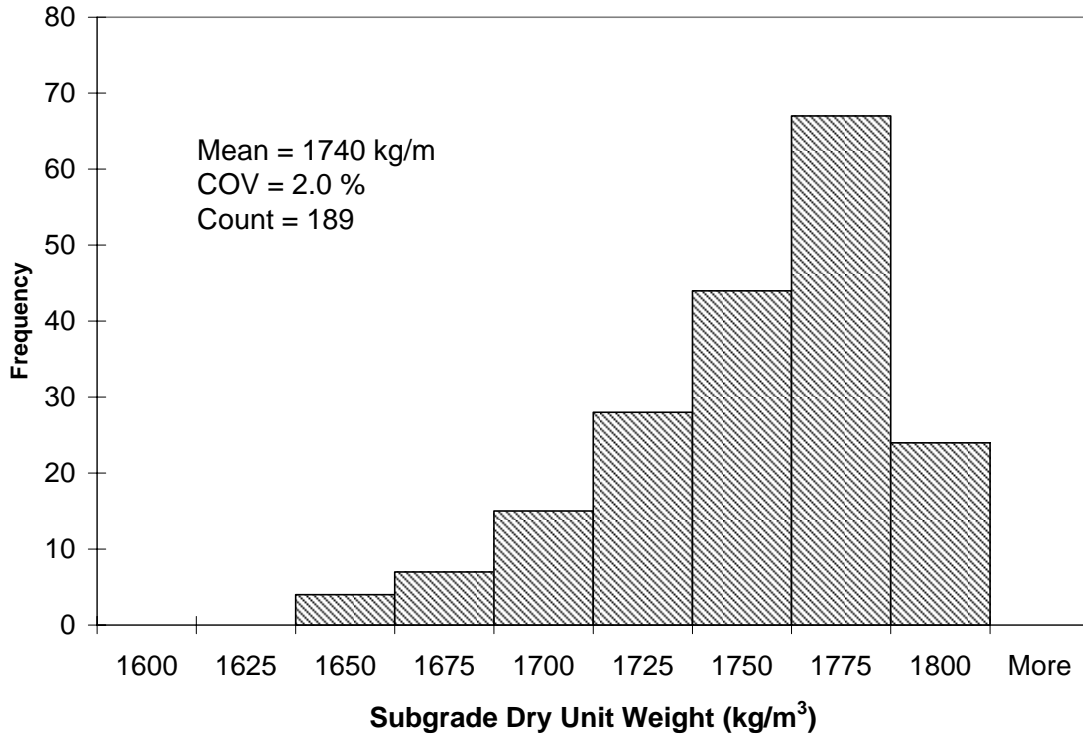


Figure 7. Subgrade dry unit weight.

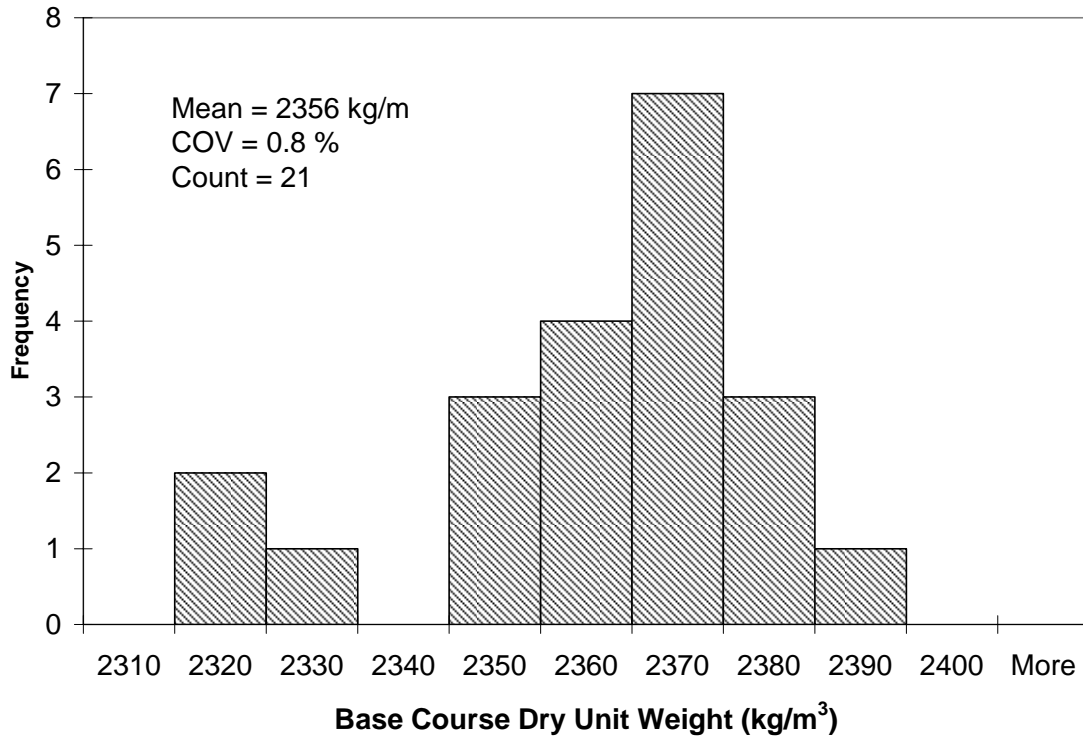


Figure 8. Base course dry unit weight.

INSTRUMENTATION

Instrumentation for measuring stress, strain, temperature, and moisture content were installed in the pavement structure during construction of the test section. More details about the instrumentation can be found in Janoo et al., 2002. The locations of the gages in the test section were similar to those in previous test sections.

Layer deformation measurements were made in the base and subgrade by means of ϵ mu coils. Strain can be deduced from deformation measurements between coil pairs in either coaxial or co-planar arrangements. The sensors were placed 150 mm center to center. Deformations were measured in the longitudinal (x), transverse (y), and vertical (z) direction of loading. Deformations in the vertical direction were measured to a depth of 1.52 m.



Figure 9. Emu coils in a co-planar arrangement to measure longitudinal and transverse deformations. A US 25-cent coin is included for scale reference.

A triaxial Dynatest® stress cell set was installed at a depth of 76 mm (3 in.) below the top of the subgrade in all test windows. In Test Window 2 an additional triaxial stress cell set was installed at a depth of 381 mm (15 in.) below the top of the subgrade. The diameter of the Dynatest® stress cells was 76 mm (3 in.).

Geokon® stress cells were installed in the middle thickness of the base course in each of Test Windows 2 and 5 in triaxial sets. In Test Window 6, Geokon stress cells were installed to measure only vertical stress at depths 51 mm (2 in.) below the bottom of the asphalt, at 25.4 mm (1 in.) above the base course-subgrade interface, and 127 mm (5 in.) below the top of the subgrade.



Figure 10. Dynatest® stress cell used in the subgrade.

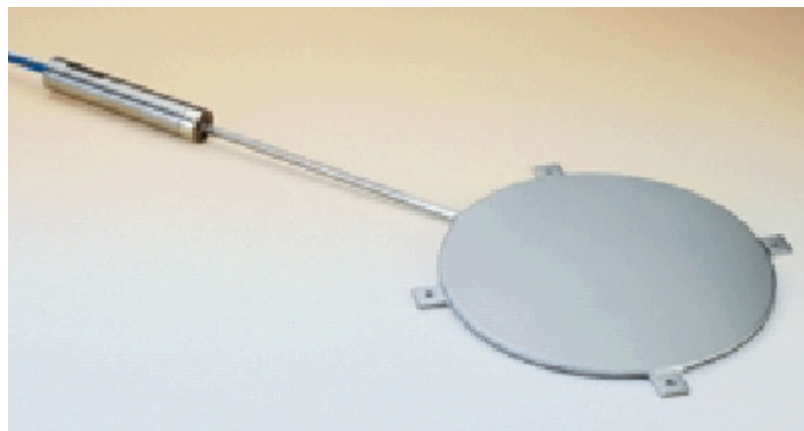


Figure 11. Geokon® stress cell used in the base course and subgrade.

Campbell Scientific® reflectometer soil moisture probes model CS615 were used to measure the moisture content in the base and subgrade during the traffic tests. These sensors measure the oscillation frequency between two rods embedded in the moist soil. The oscillation frequency is related to the dielectric constant that changes with moisture content, and to a lesser degree with temperature. The sensor readings are also affected by salinity, mineralogy and presence of organic materials. Volumetric moisture content is converted to gravimetric moisture content through weight-volume relationships and soil specific gravity. These sensors alone are not accurate enough for the purpose of this study, but this deficiency was corrected by oven dry measurements during construction and during the forensic evaluation.

Moisture sensors were located at three depths at each of three horizontal locations. There were moisture sensors in the middle of the base course, and in the subgrade at 15 cm (6 in.) and 61 cm (2 ft.) below the top of the subgrade.

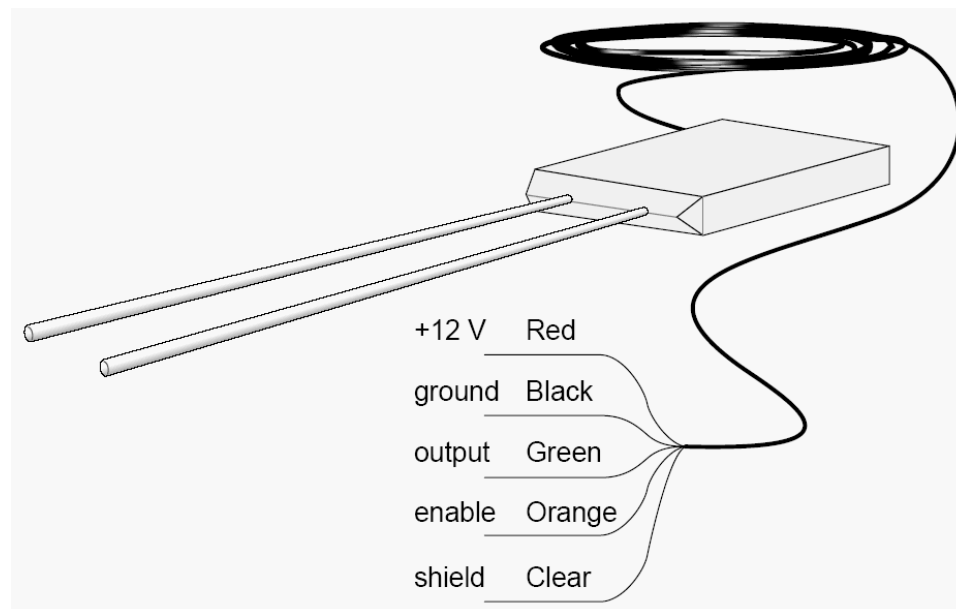


Figure 12. Campbell Scientific[®] reflectometer soil moisture probe model CS615.

Subsurface temperatures were taken using thermocouple sensors. The thermocouples have an accuracy of $\pm 0.5^{\circ}\text{C}$. The subsurface temperature sensors were installed at three horizontal locations within the test section in the asphalt concrete, base course and at two depths into the subgrade. Air temperatures were also measured.

ACCELERATED TRAFFIC

The test windows were subjected to accelerated traffic by means of CRREL's Heavy Vehicle Simulator (HVS).

The following tests were conducted:

1. Prior to the accelerated load tests, FWD measurements were conducted on the surface of the AC layer at locations in a predefined grid arrangement representative of the test section area.
2. Initial transverse profiles of each test window were measured using a laser profilometer. The laser source and sensor were located 45 cm (1.5 ft.) above the pavement surface. Each cross section was composed of 256 measurements spaced at 9-mm (3/8-in.) intervals. Twenty profilometer transverse cross section measurements at 0.3-m (1-ft.) intervals were taken at each window. Surface profile measurements were made at each traffic stop to define the progression of surface rutting throughout the traffic tests. Rut depth was defined as the difference between the surface depth at a given number of

passes and the corresponding depth measured at zero passes. A typical surface rut measurement and the definition of maximum rut depth are shown in Figure 15. Traffic testing was terminated when the average maximum surface rut depth of 12.5 mm was reached or exceeded.

3. In addition to the profilometer measurements, elevation measurements were conducted with a rod and level prior to the start and at the end of the traffic tests for each test window. Elevations were monitored at locations where the profilometer legs were placed during profilometer measurements to detect any potential change in elevation that would affect the profile measurements. In addition, the elevation of the projection of the vertical emu stack on the asphalt surface was also monitored with a rod and level system. The results from the level surveys indicated that the profilometer leg points were stationary throughout the test.



Figure 13. Laser profilometer.

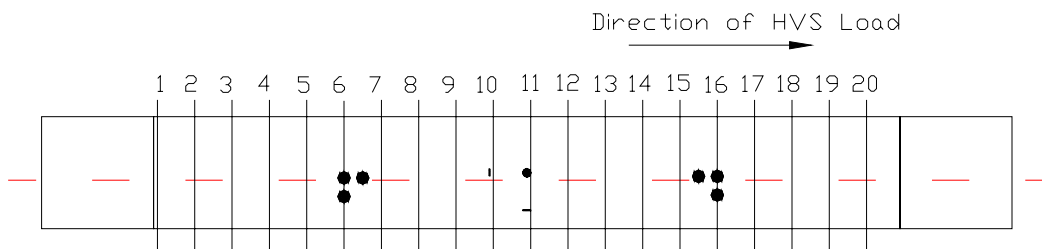


Figure 14. Locations for profile measurements in a test window.

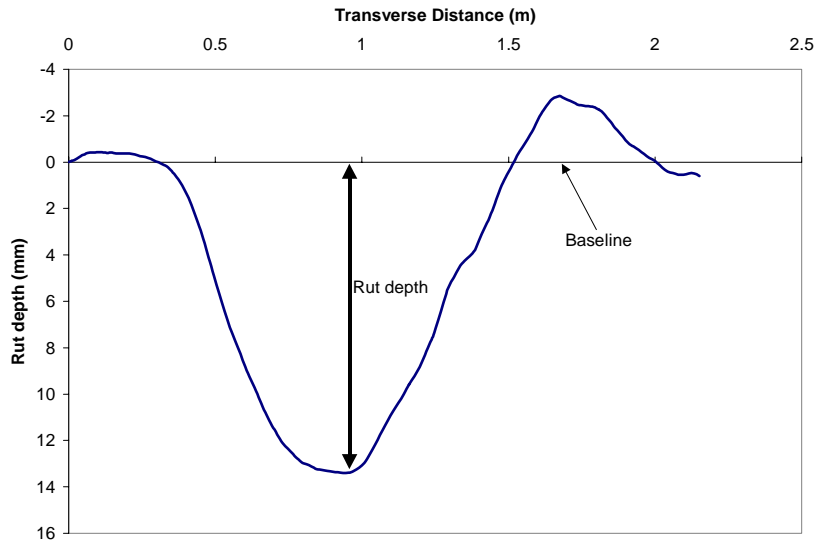


Figure 15. Definition of rut depth.

4. Subsurface stress and displacement measurements conducted in the vertical, longitudinal, and transverse directions relative to the direction of traffic. The measurements were conducted at various pass levels to define their progression throughout the traffic tests. The displacement measurements were conducted dynamically upon the passing of tire traffic, and also statically when no traffic was occurring. The dynamic deformations measured the resilient deformation during traffic load events. The static measurements were intended to measure permanent deformation.
5. In addition to the ϵ mu coils embedded in the pavement, a mobile coil was placed on top of the asphalt over the vertical stack of embedded ϵ mu coils as shown in Figure 16. This provided a means to measure the vertical permanent deformation in the asphalt layer.



Figure 16. Measuring vertical deformation between the AC surface and the top of the base course.

TRAFFIC LOADS

Traffic loading was applied by means of CRREL’s Heavy Vehicle Simulator (HVS). The tire assembly was a dual-tire standard truck half axle. The traffic speed was 12 km/hr. The traffic was allowed to wander across a width of 0.91 m (3 ft.). The mean applied loads are summarized in Table 3. The tire pressure was set to 690-kPa (100 psi).

Table 3. Mean semi-axial loads on test windows

Test Window	Applied Loads	
	kips	kN
709C1	6	26.7
709C2	9	40.0
709C3	12	53.4
709C4	7	31.1
709C5	9	40.0
709C6	4.5	20.0

Table 4. Sequence of HVS tests on test windows

Window	Start	End
709C1	04-May-2004	19-May-2004
709C2	30-Mar-2004	01-Apr-2004
709C3	19-Apr-2004	21-Apr-2004
709C4	22-Mar-2004	26-Mar-2004
709C5	22-Apr-2004	29-Apr-2004
709C6	05-Apr-2004	14-Apr-2004

TEMPERATURE AND MOISTURE DURING TRAFFIC

The test section was built inside the FERF building where temperature and moisture can be controlled. The mean air temperature during the traffic test period was 18.1 °C (65°F). Thermocouples embedded in the asphalt concrete, the base course and the top of the subgrade indicated that this was also the mean temperature in the pavement structure. Figure 17 shows the temperature measurements during the traffic test period. The air temperature shows three inverse spikes that corresponded to opening of the building gates that coincided with temperature scanning times. The building gates were

opened briefly very infrequently in order to move construction equipment in or out of the building. In each of these events, a gate was opened for less than five minutes. The heating equipment was able to counteract the effect of a short duration gate opening without measurable cooling of the asphalt concrete. Temperature and moisture measurements were taken at four hour intervals.

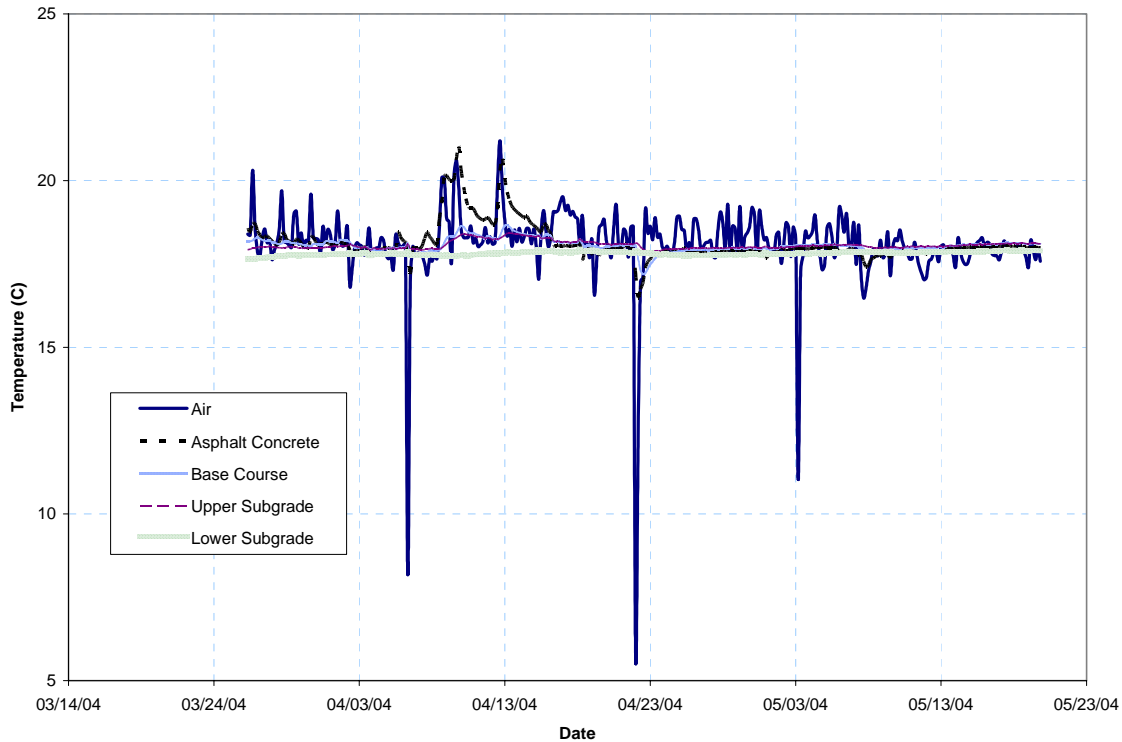


Figure 17. Air and pavement temperatures during the traffic test period.

The temperature oscillations in the asphalt concrete were not large enough to cause any significant stiffness variation. Thermocouples are accurate to ± 0.5 °C.

Moisture measurements were conducted by means of Campbell Scientific model CS615 sensors. These sensors measure the oscillation frequency between two rods embedded in the moist soil. The oscillation frequency is related to the dielectric constant that changes with moisture content, and to a lesser degree with temperature. The sensor readings are also affected by salinity, mineralogy and presence of organic materials. Volumetric moisture content is converted to gravimetric moisture content through weight-volume relationships and soil specific gravity. These sensors alone are not accurate enough for the purpose of this study, but this deficiency can be corrected by oven dry measurements during construction and during the forensic evaluation. Figure 18 shows the oven-dry corrected gravimetric moisture measurements in the base course, at 15 cm (6 in.) below the top of the subgrade and at 61 cm (2 ft.) below the top of the subgrade. The shape of the moisture curves suggests a small increase in moisture content in the upper subgrade during the traffic period. The test section is built above a portland cement concrete floor, it is surrounded by portland cement concrete walls and covered by

76 mm (3 in.) of asphalt concrete. Neglecting water vapor diffusion through these practically impermeable materials, one can consider the subgrade and base course system as a practically sealed system. Therefore, the increase in moisture content in the upper subgrade must come as a result of moisture migration within the test section. The moisture sensor data suggest that moisture near the top of the subgrade initially decreased slightly, and then increased as soon as traffic began. This suggests that traffic may contribute to moisture migration toward the top of the subgrade where the stresses are larger. The mechanisms of moisture migration within the subgrade are not sufficiently understood. Perkins and Cortez (Perkins and Cortez, 2004) suggested that pore water pressure may build at the top of the subgrade as a result of multiple traffic applications. Oven dry measurements taken during the forensic evaluation also indicated an increase of moisture in the upper subgrade.

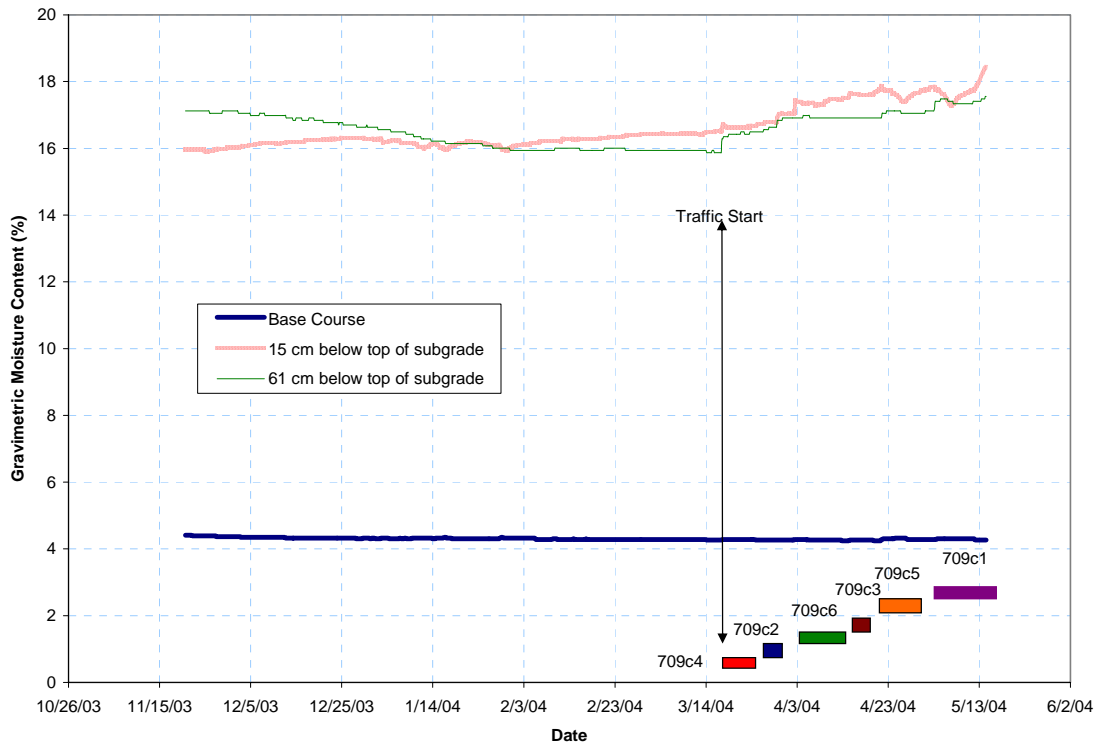


Figure 18. Moisture measurements in the base and subgrade in the period from construction to the forensic evaluation.

Figure 18 also indicates when traffic was applied for each test window. Figure 3 shows that for the AASHTO A-6 subgrade soil at optimum moisture content of 16 the laboratory CBR value is 15 percent. Figure 19 shows that this is equivalent to a resilient modulus of 97 MPa (14 ksi). If the moisture content increases to 17.5 percent, the laboratory CBR is reduced to 10 percent, or 76 MPa (11 ksi). The CBR and resilient modulus decreases rapidly with an increase of moisture content on this subgrade soil type. The effect of moisture increase on the visco-plastic behavior of fine grain soils such as this AASHTO A-6 soil may be more pronounced than the effect on its elastic behavior.

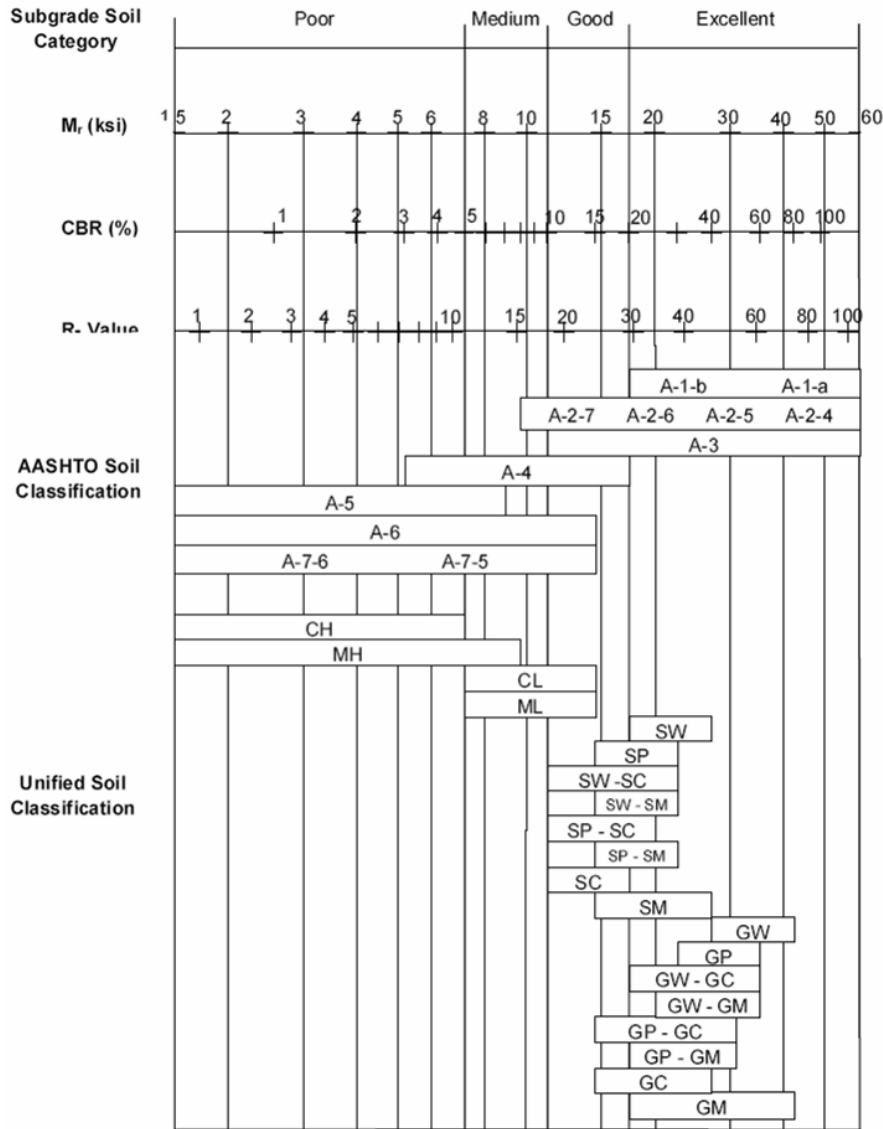


Figure 19. Relationships between CBR and resilient modulus for various soil types. (AASHTO M-E Guide, 2004).

SURFACE RUTTING AND OTHER DISTRESS

Transverse surface profile measurements were taken periodically during testing. Rut depth was calculated as the difference between the profile measurements taken at the given pass level and the profile measurements taken prior to testing (pass level zero). Cross sectional profile measurements were taken at 305-mm (1 ft.) intervals along the effective test window for a total of 20 locations.

The maximum rut depths from transverse profile measurements were used to develop the longitudinal profile. Longitudinal rut depths for each test window as a function of load repetitions are presented in Figures 27 to 32. The load applied to Test Window 709c2 corresponds to the equivalent of a 40 kN (18 kip) axle load. Figure 20

shows that this test window endured 5000 traffic repetitions to reach failure. The subgrade gravimetric moisture content was 16.6 percent. According to modified Proctor tests, the optimum moisture content for this AASHTO A-6 soil was 16 percent. Laboratory tests indicated that this soil's CBR value at 16.6 percent gravimetric moisture content was 13 percent.

The progressions of rut depths as a function of load repetitions in the various windows are presented in Figure 20. The average rut depth as a function of applied load was used to determine the number of load repetitions to reach the failure rut depth of 12.7 mm. In general, as the applied load increased so did the rate of rutting depth. However, the results from Test Windows 709c5 and 709c6 were anomalous because the asphalt concrete developed cracks and delamination prematurely. Test Window 709c4 was tested first. When the average rut depth was about the 12 mm, the asphalt surface course delaminated from the lower asphalt layer at a strip nearly including the northeastern portion of the test window. Cracking and shoving related to the asphalt delamination was observed as shown in Figure 23. The traffic was then stopped to avoid damage to the HVS, and the test was ended. The asphalt damage created cracks that later grew into Test Window 709c5. Test Windows 709c1 and 709c3 were then tested. The only distress observed in three test windows in the south region of the test section was surface rutting. No visible crack or other asphalt distress was observed in these test windows. Contrastingly, the three test windows in the north region of the test section had premature asphalt cracking, delamination, and shoving. Test Window 709c6 was tested next. The damage caused by traffic on Test Window 709c6 included cracks that grew quickly onto Test Window 709c5 when traffic was applied to this test window as shown in Figure 25. Therefore, the results from Test Windows 709c5 and 709c6 should be excluded from the analysis of Test Section 709. Notice the striations on the lower asphalt layer that are aligned with the direction of traffic. The exposed lower surface displayed a light colored, thin film of rock powder produced by grinding of aggregates during delamination and shoving. The premature asphalt failure was probably due to excessive cooling of the asphalt during placement and compaction. Paving occurred in a cold day at the end of the paving season. More detailed examination of the asphalt failure was conducted during the forensic evaluation, and the existence of delamination and poor bond between the upper and lower asphalt layers were confirmed. Interlayer bond in the south region of the test section that includes test windows 709c1, 709c2 and 709c3 was adequate.

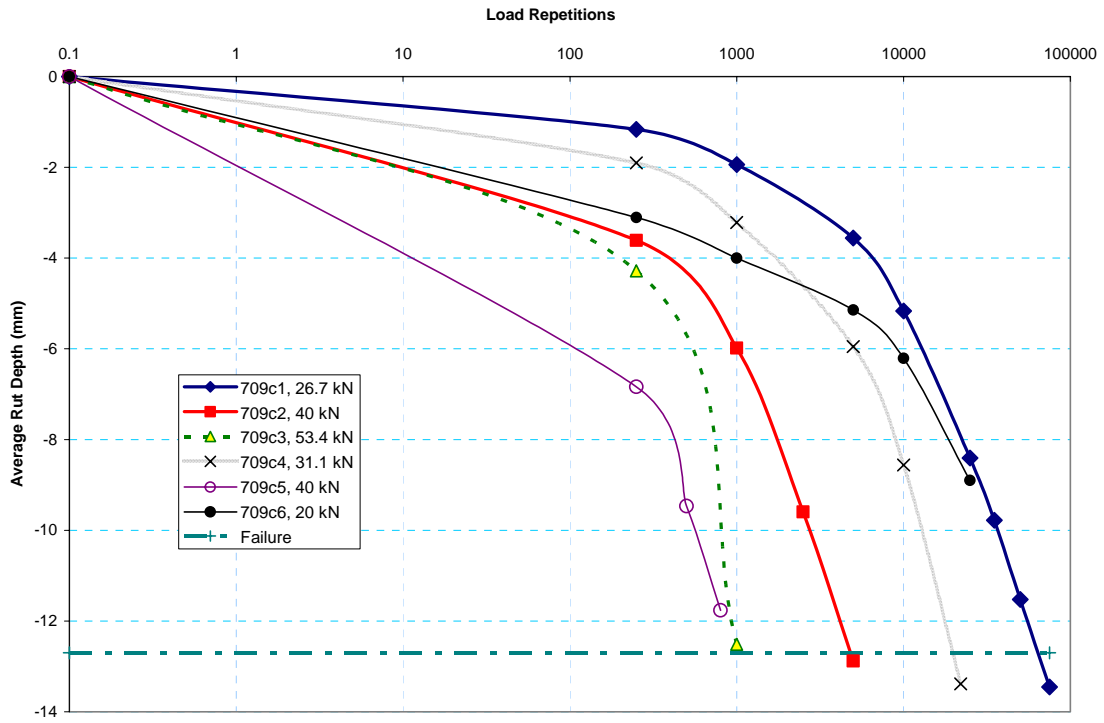


Figure 20. Average rut depth as function of semi-axial load intensity and repetitions.



Figure 21. Test Window 709c1 before HVS traffic.



Figure 22. Test Window 709c1 at the end of HVS traffic.



Figure 23. Test Window 709c4 at the end of HVS traffic.



Figure 24. Damage to Test Windows 709c5 caused by neighboring test windows.



Figure 25. Test Window 709c5 at the end of HVS traffic.



Figure 26. Close up of delaminated area showing striations on the lower asphalt layer.



Figure 27. Close up of asphalt cracking over the emu sensors.

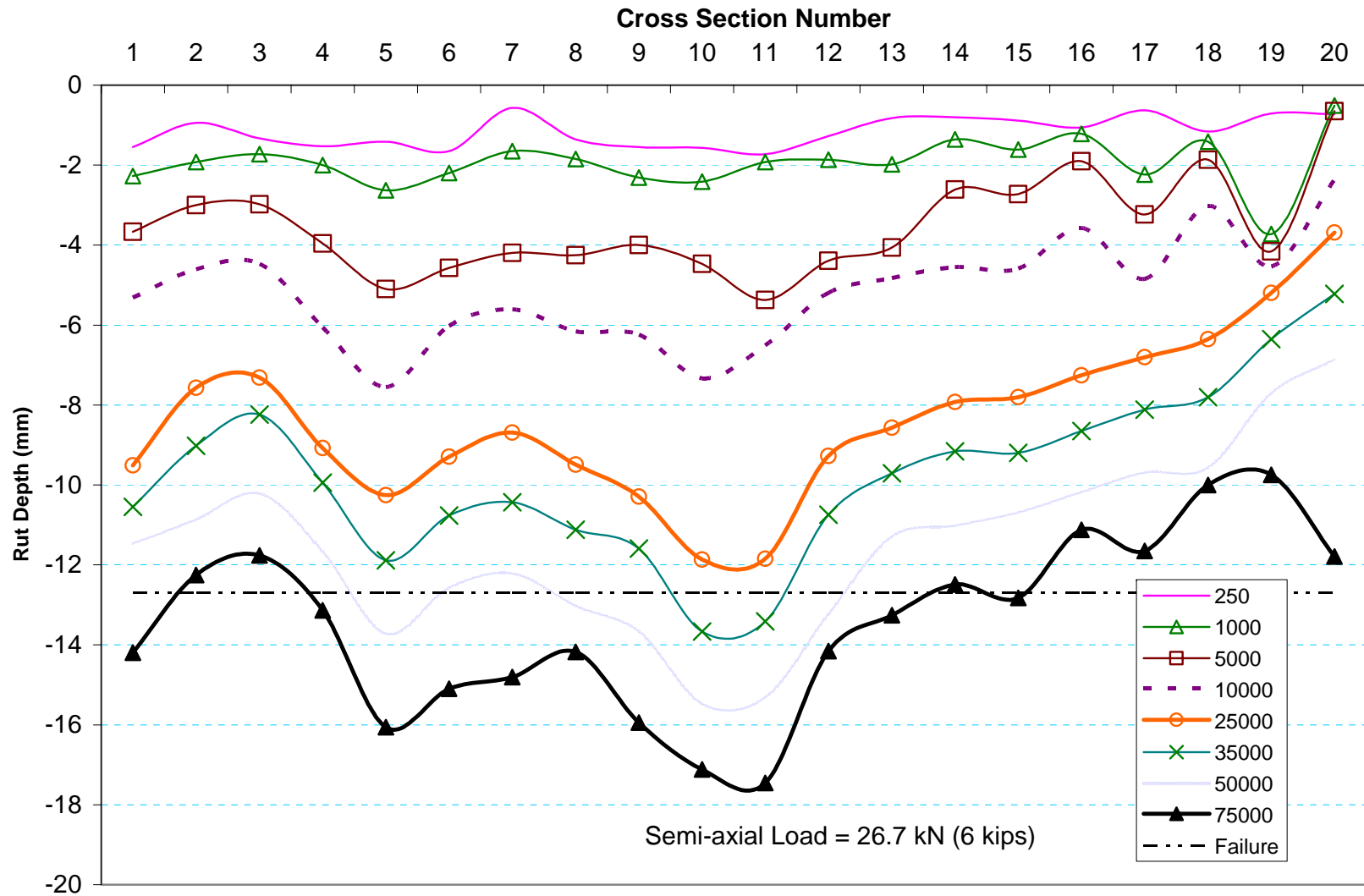


Figure 28. Progression of surface rutting along the center of the tire path in Test Window C1.

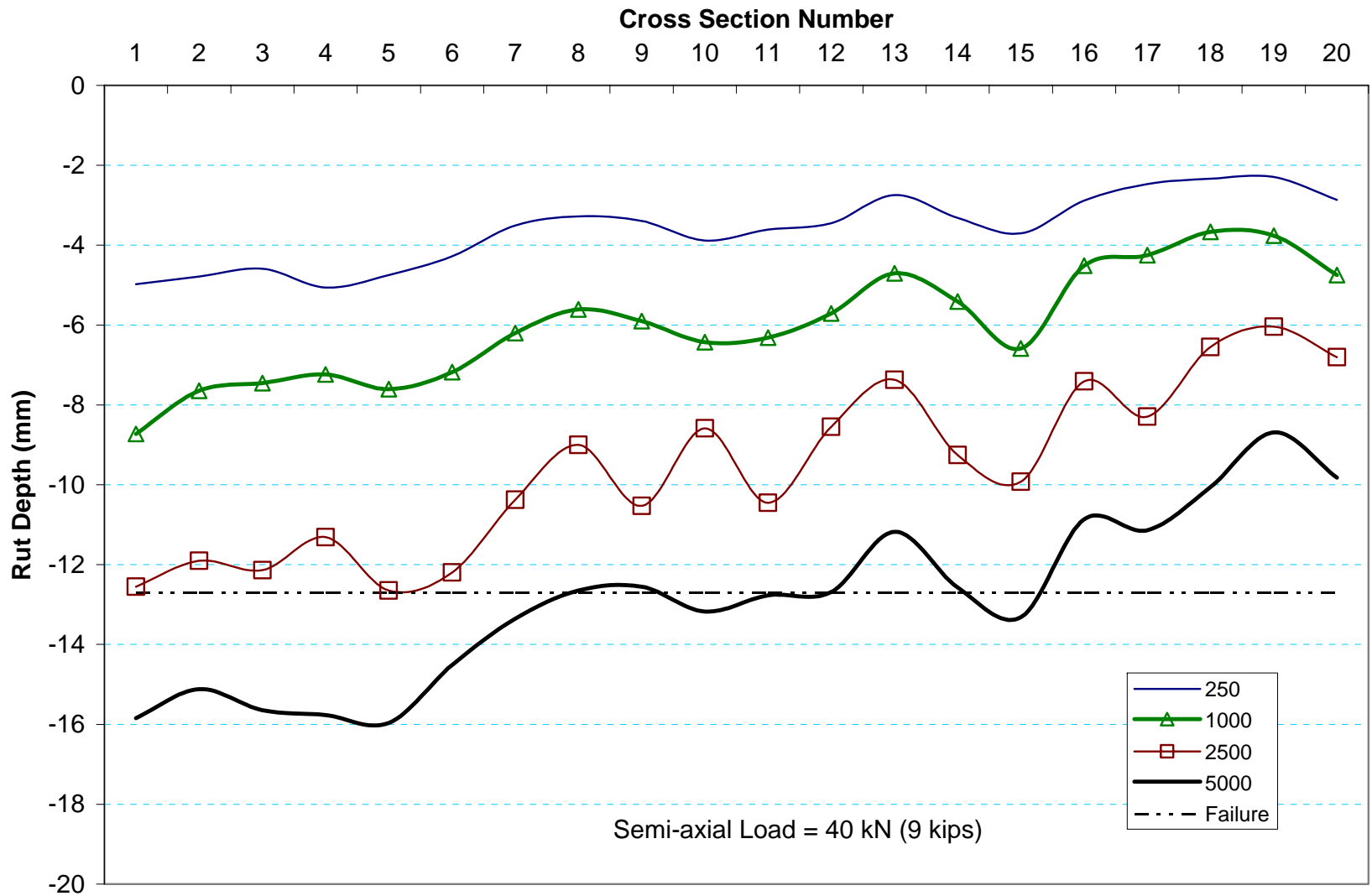


Figure 29. Progression of surface rutting along the center of the tire path in Test Window C2.

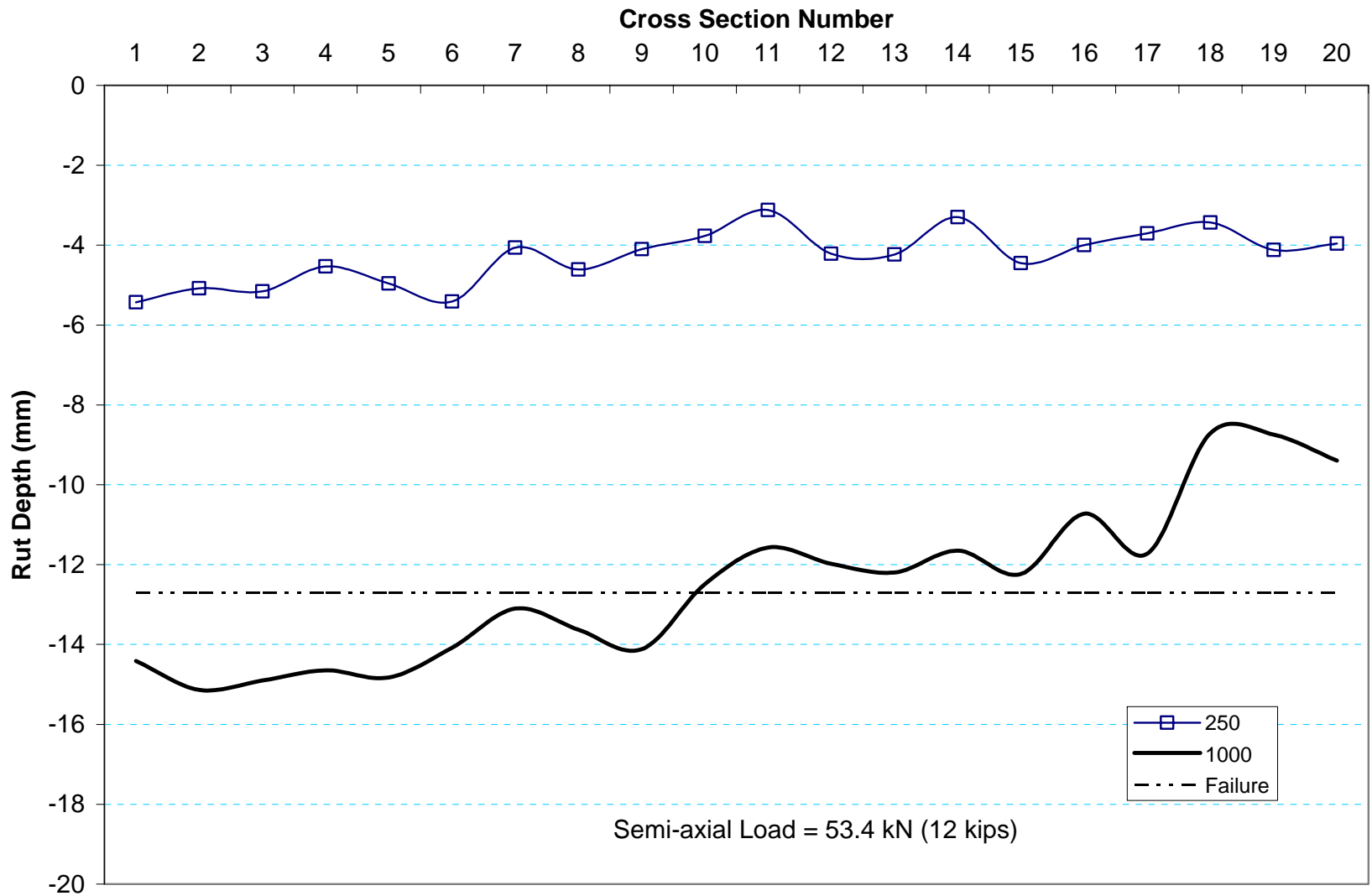


Figure 30. Progression of surface rutting along the center of the tire path in Test Window C3.

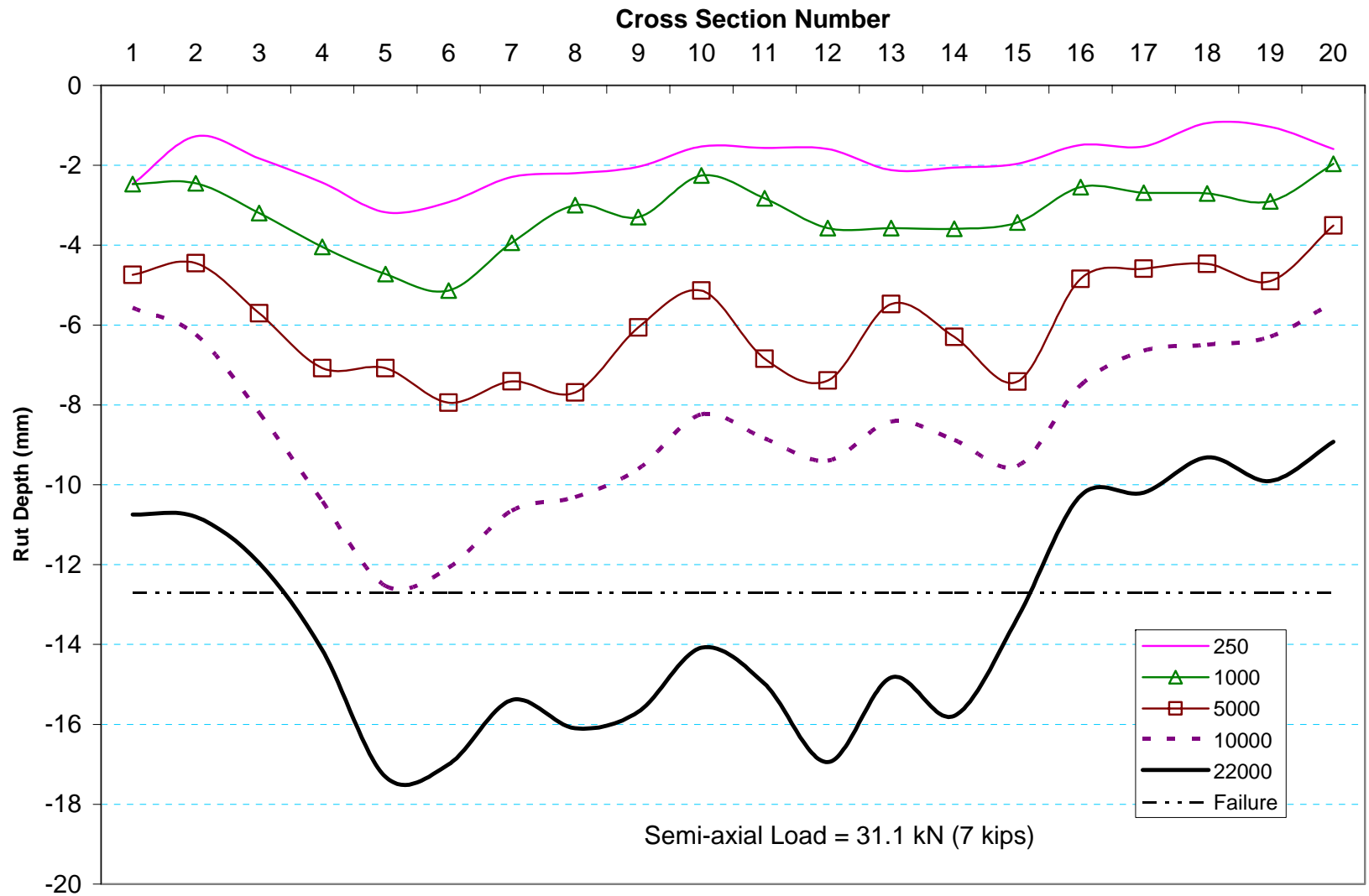


Figure 31. Progression of surface rutting along the center of the tire path in Test Window C4.

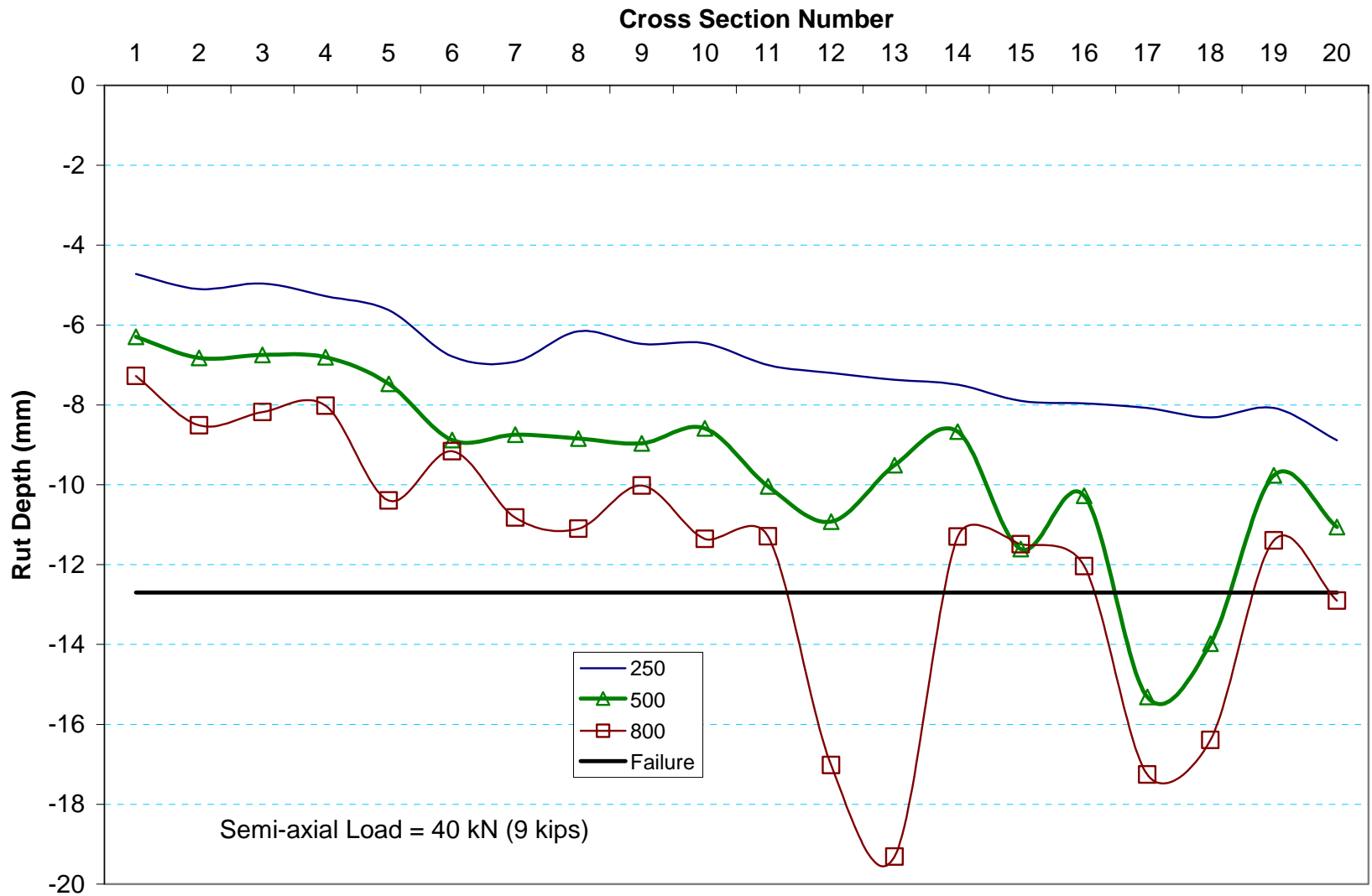


Figure 32. Progression of surface rutting along the center of the tire path in Test Window C5.

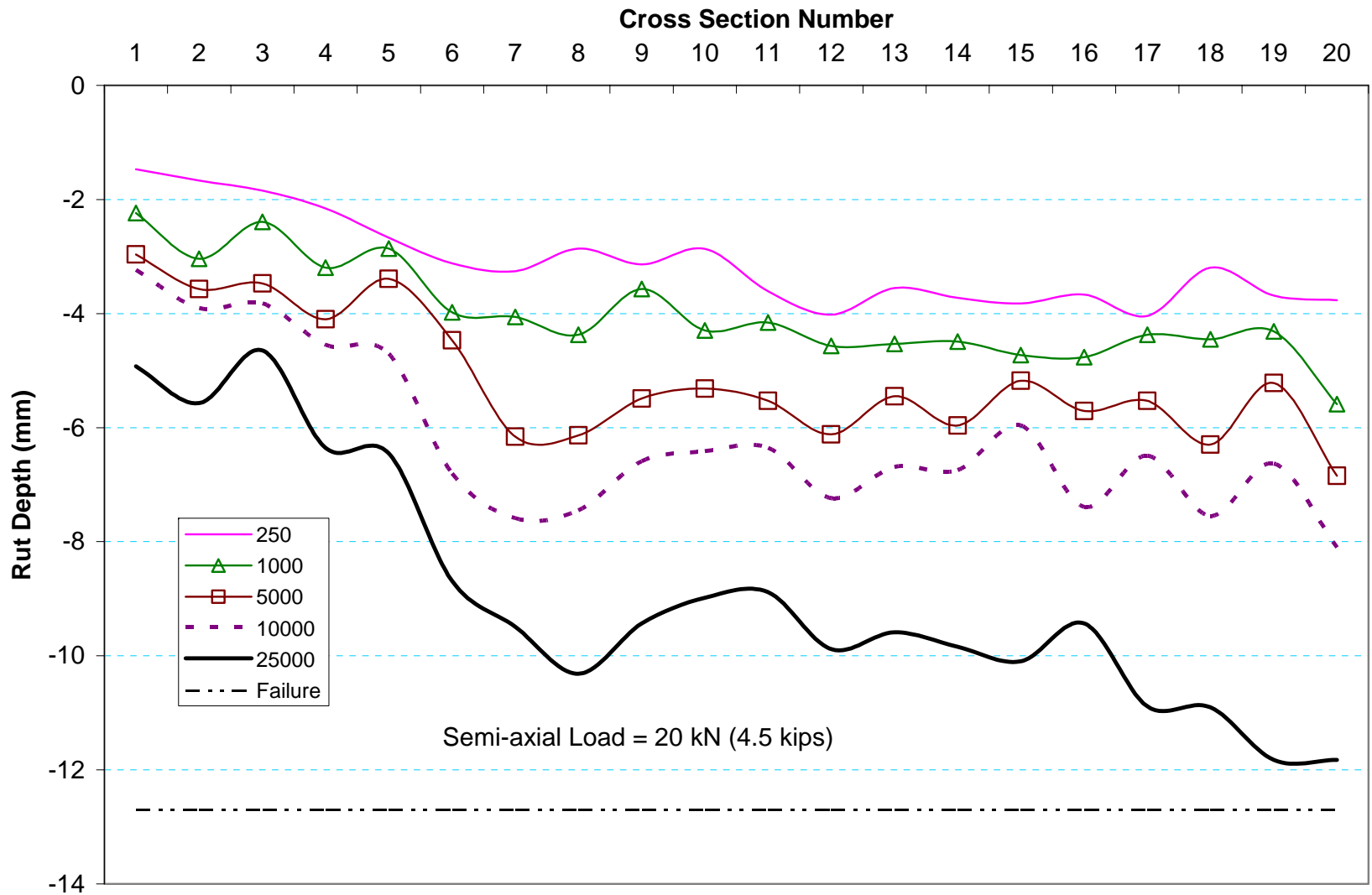


Figure 33. Progression of surface rutting along the center of the tire path in Test Window C6.

Table 8 shows the number of traffic passes that were required to cause a rut depth of 12.7 mm (0.5 in). The results from Test Windows 709c5 and 709c6 were excluded due to the premature asphalt concrete failures described above. Figure 34 graphically shows the relationship between load intensity and number of traffic passes to failure, and also a power function that fits the experimental data with an R^2 value of 0.996.

Table 8. Load Repetitions to reach failure of 12.7 mm

Test Window	Load (kN)	N_{failure}
c1	26.7	65000
c4	31.1	20200
c2	40.0	4800
c3	53.4	1000

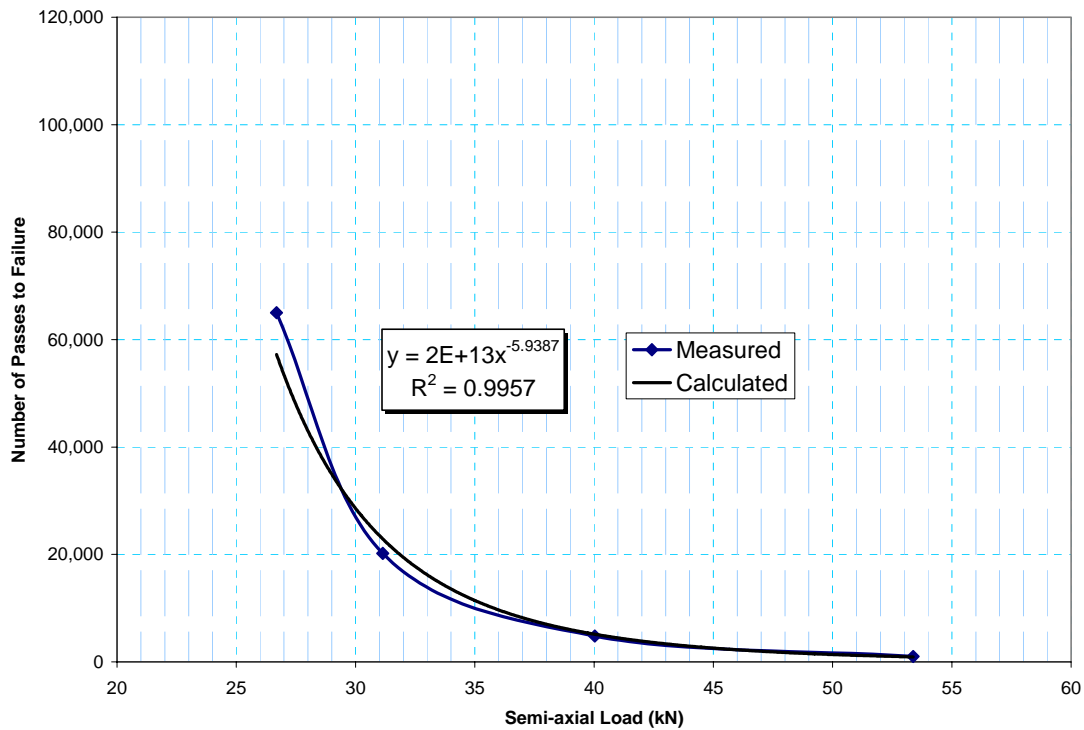


Figure 34 Load repetitions as a function of rut depth.

DEFORMATION AND STRAIN

εmu inductance coil sensors were used to measure the distance between pairs of coils at various stages throughout the traffic testing. Comparing the distance between a pair of coils to the initial distance, the deformation of the soil between the coils can be established. An average strain value can then be calculated by dividing this deformation by the initial coil distance. By convention, we assign this strain value to a point located in the middle between the coil pair. Coil distance measurements were conducted at stages with the HVS stopped to obtain permanent deformation, and also dynamically during traffic applications to obtain resilient deformations.

a) Permanent Deformations and Strains

Permanent deformation measurements were collected from εmu coils embedded in the base and the subgrade. Measurements were conducted before traffic began and at various stages throughout the traffic tests. An additional mobile εmu coil was placed at the asphalt surface and paired with a coil embedded just below the bottom of the asphalt concrete (AC) to measure the vertical deformation that occurred in the asphalt layer. Three stacks of εmu coils were embedded to form triaxial arrangements in the base and subgrade. Vertical pairs of εmu coils were embedded down to a depth of 1.52 m (5 ft) from the asphalt surface. Previous experiments have shown that, at this depth, the strains are normally small compared to electronic noise.

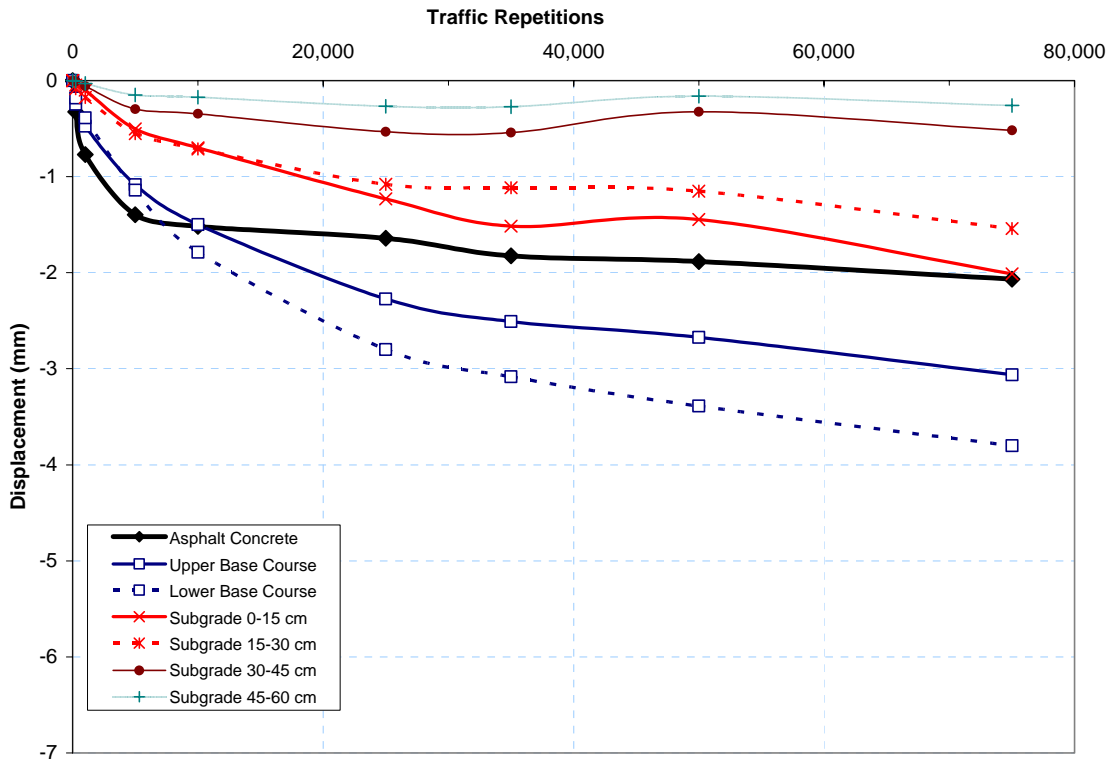


Figure 35a. Layer by layer vertical permanent deformation in Test Window 709c1 with 26.7 kN semi-axial load.

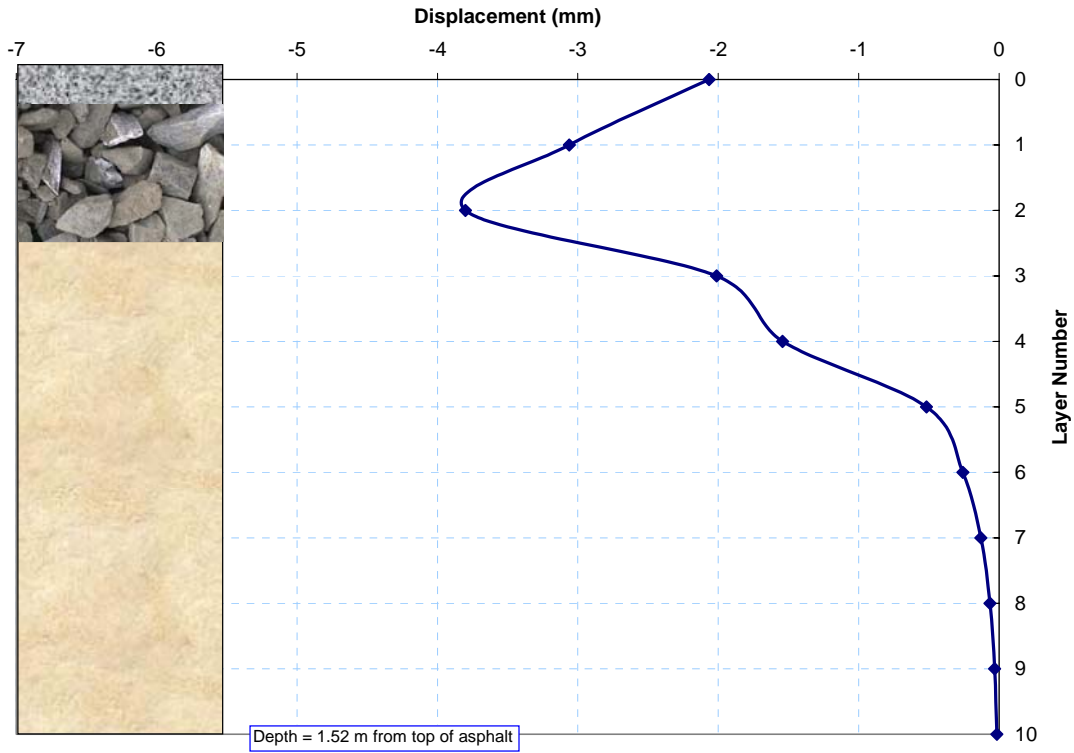


Figure 35b. Layer by layer vertical permanent deformation at failure in Test Window 709c1 with 26.7 kN semi-axial load.

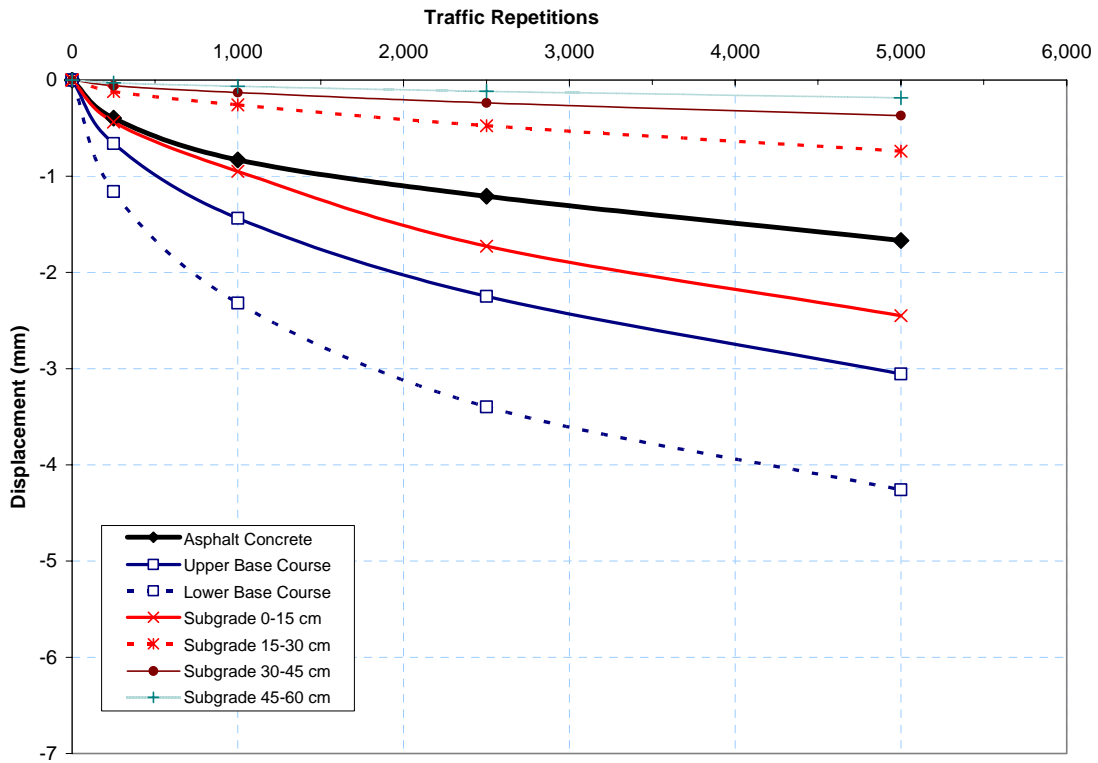


Figure 36a. Layer by layer vertical permanent deformation in Test Window 709c2 with 40 kN semi-axial load.

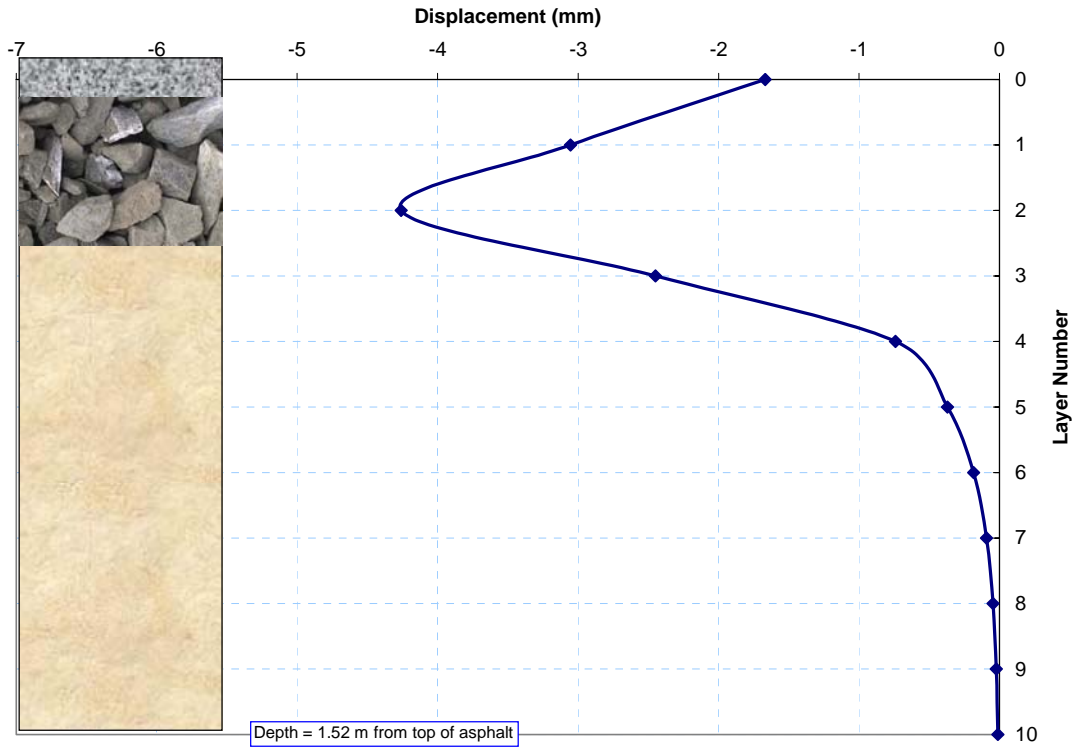


Figure 36b. Layer by layer vertical permanent deformation at failure in Test Window 709c2 with 40 kN semi-axial load.

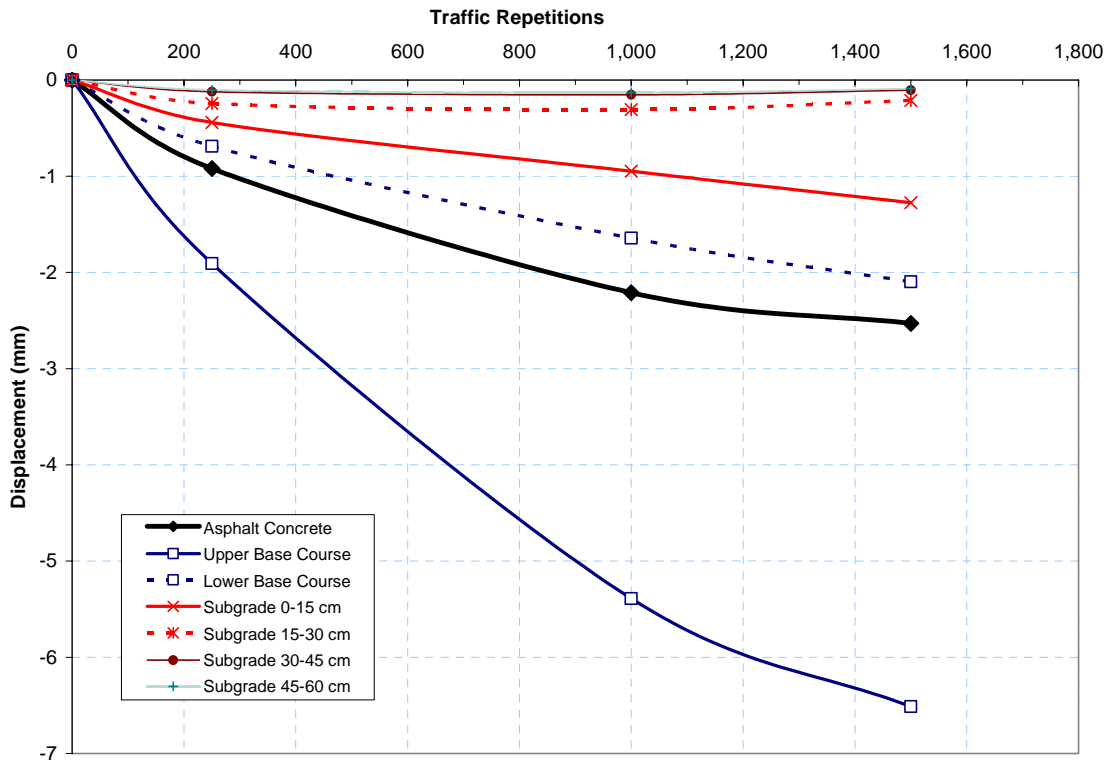


Figure 37a. Layer by layer vertical permanent deformation in Test Window 709c3 with 53.4 kN semi-axial load.

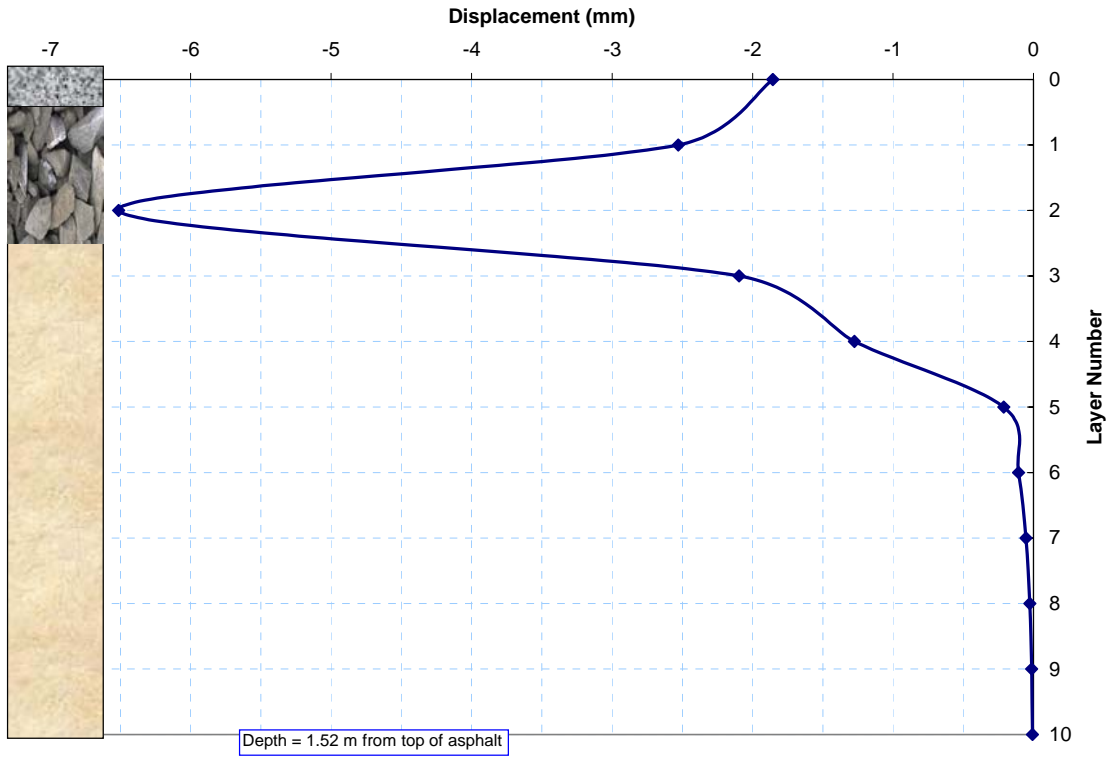


Figure 37b. Layer by layer vertical permanent deformation at failure in Test Window 709c3 with 53.4 kN semi-axial load.

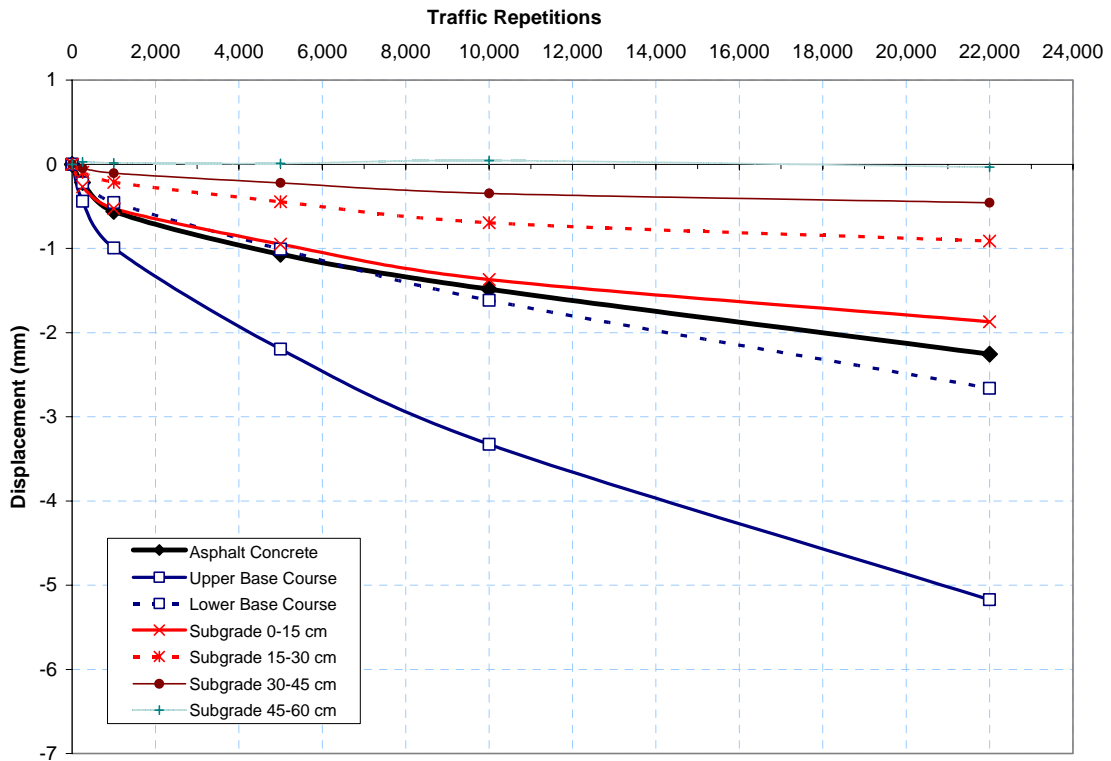


Figure 38a. Layer by layer vertical permanent deformation in Test Window 709c4 with 31.1 kN semi-axial load.

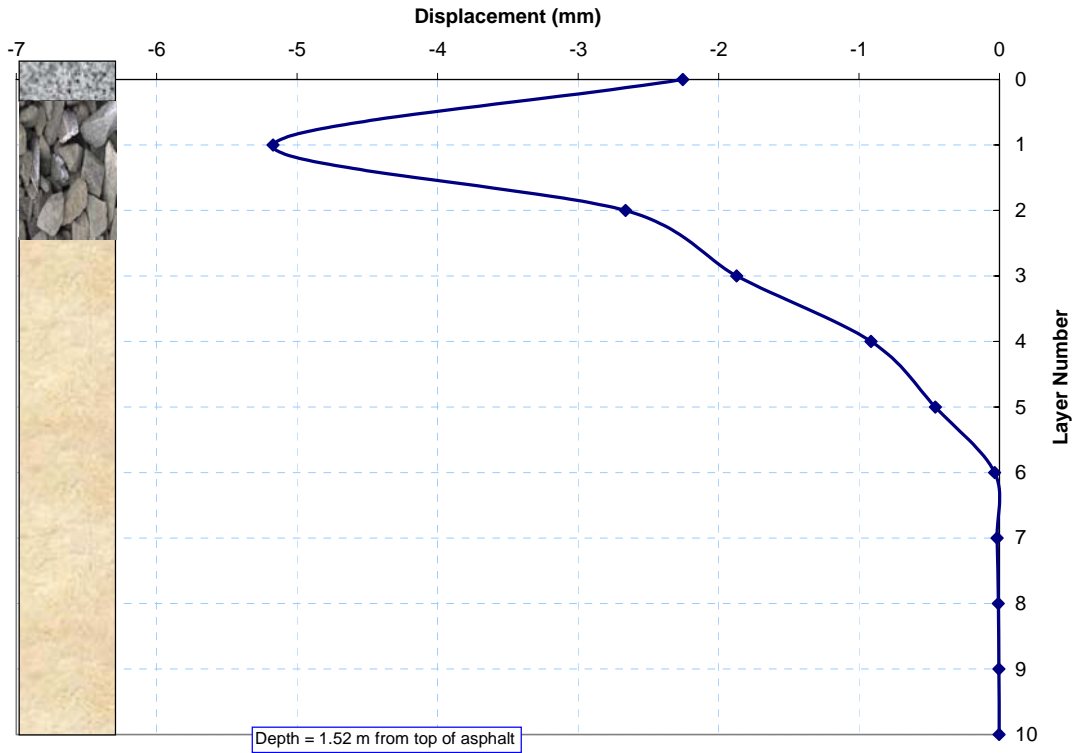


Figure 38b. Layer by layer vertical permanent deformation at failure in Test Window 709c4 with 31.1 kN semi-axial load.

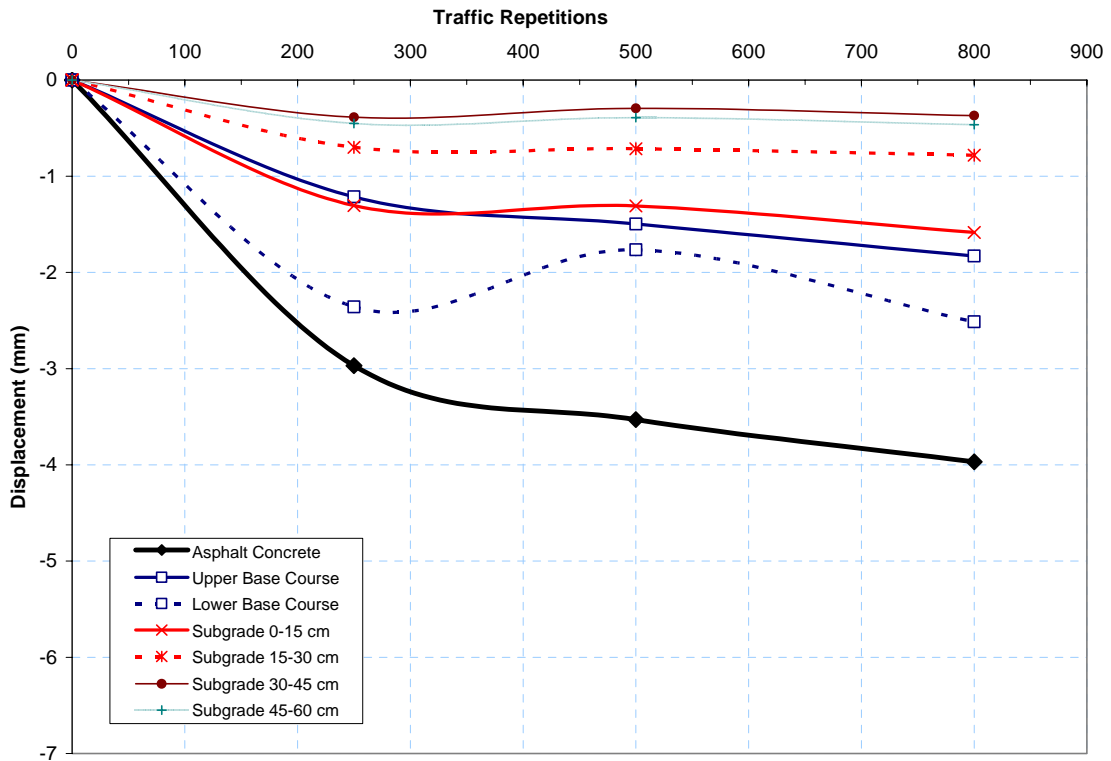


Figure 39a. Layer by layer vertical permanent deformation in Test Window 709c5 with 40 kN semi-axial load.

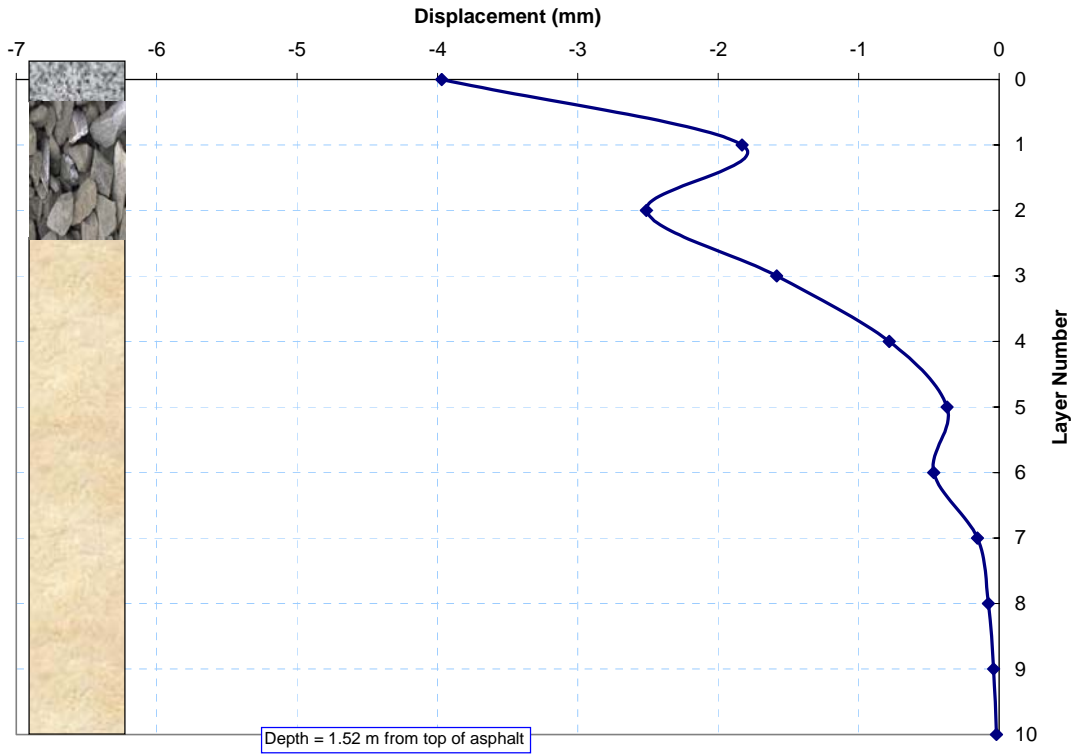


Figure 39b. Layer by layer vertical permanent deformation at failure in Test Window 709c5 with 40 kN semi-axial load.

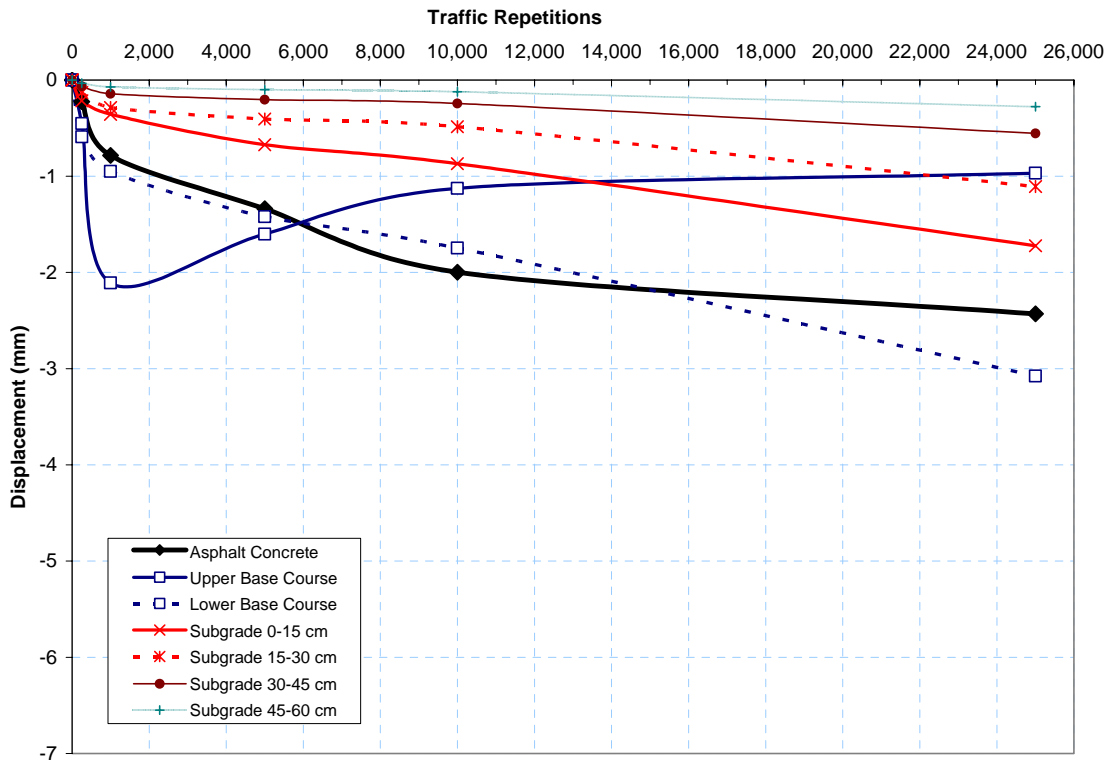


Figure 40a. Layer by layer vertical permanent deformation in Test Window 709c6 with 20 kN semi-axial load.

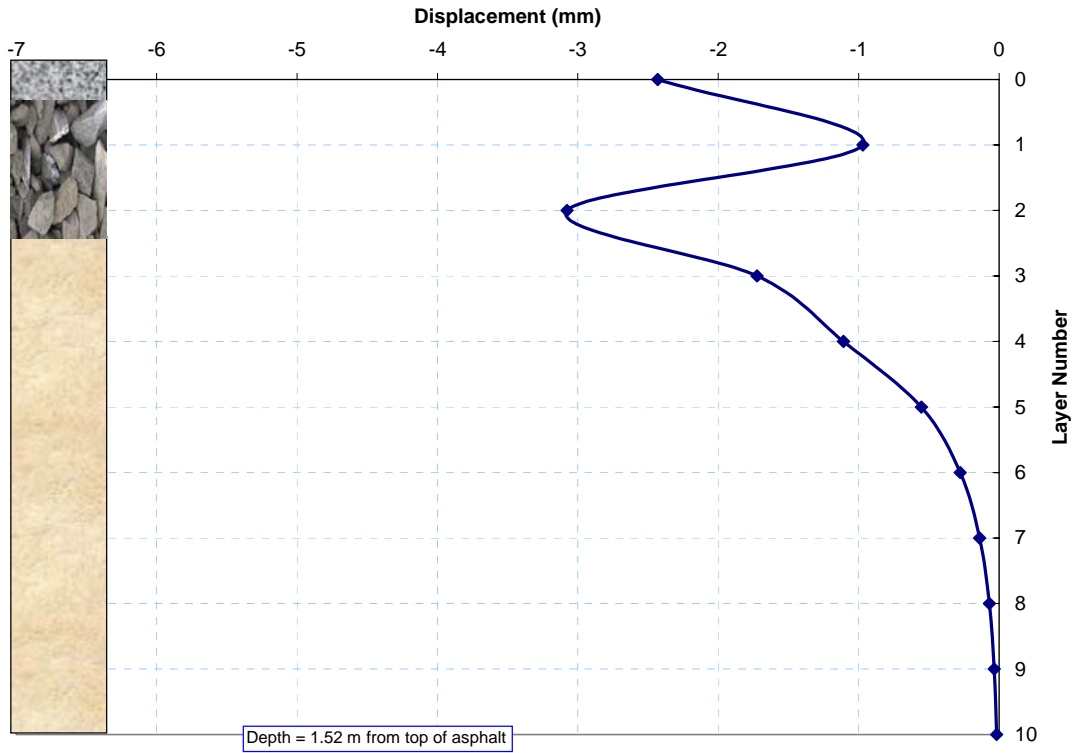


Figure 40b. Layer by layer vertical permanent deformation at failure in Test Window 709c6 with 20 kN semi-axial load.

The permanent deformations in Test Windows 709c5 and 709c6 were heavily influenced by premature asphalt failure in the form of delamination, cracking and shoving. These results should not be used in the general analysis of Test Window 709 because they could obscure valid trends observed in the remaining test windows.

The vertical permanent strains on the top of the subgrade as a function of load repetitions are shown in Figure 41. The strains were compressive. There appears to be good correlation between applied load and permanent deformation and strain.

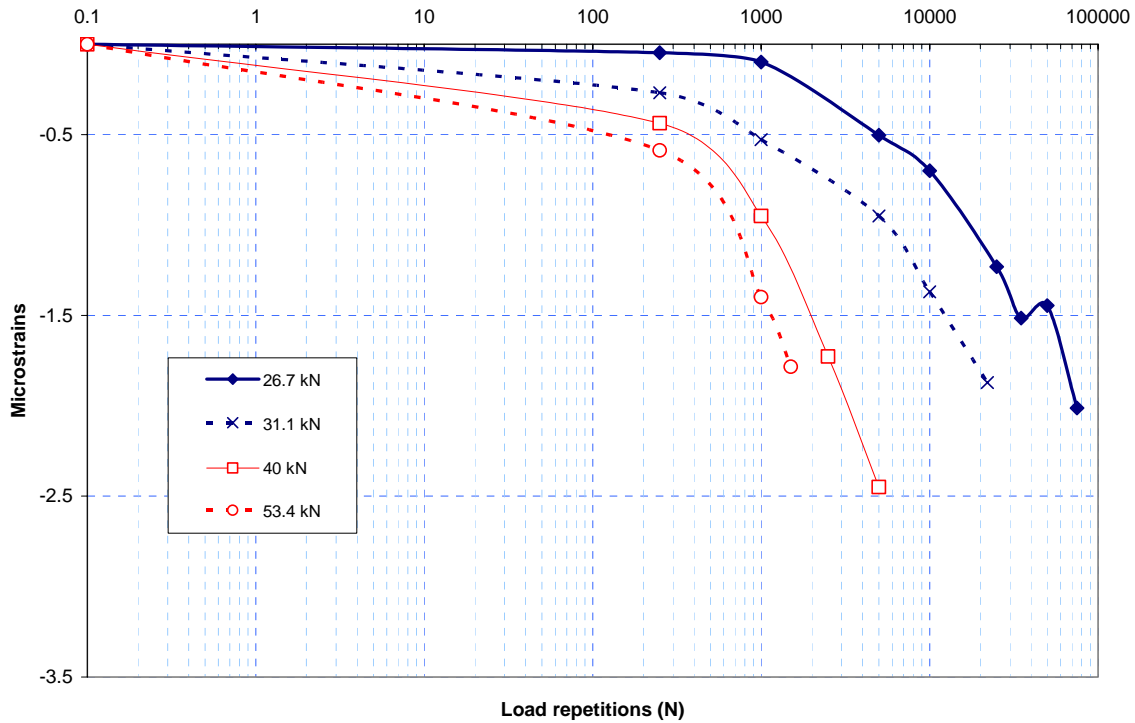


Figure 41. Permanent vertical deformation in the top 15 cm of the subgrade.

b) Dynamic Deformations and Strains

As with previous test sections, triaxial dynamic displacements were measured with the ϵ mu coil gages in the base and the subgrade. The vertical displacements and strains were compressive. The transverse displacements and strains were extensive. The longitudinal displacement and strains were initially compressive until the tire assembly was located directly above the sensors, and thereafter suddenly reversed into extensive displacement and strains. Dynamic displacements are primarily elastic. Observing the static permanent deformation and the dynamic measurements, one can conclude that for each traffic load event, most deformation is recoverable (resilient), but a small component of (permanent) deformation remains. However, the ratio of permanent to resilient deformations decreases when the number of traffic repetitions increases. This report we will focus on vertical stress and strains. A later report will examine relationships between vertical and horizontal components of stress and strain in order to model soil behavior, and define the mechanical behavior of the pavement structure as affected by multiple parameters.

In general, there was some correspondence between load intensity and resilient displacement and strain. Resilient strains as a function of load repetition at 76 mm (3 in.)

below the top of the subgrade are presented in Figure 42. It can be seen that, in this test section, the resilient strains remained nearly constant throughout the traffic tests.

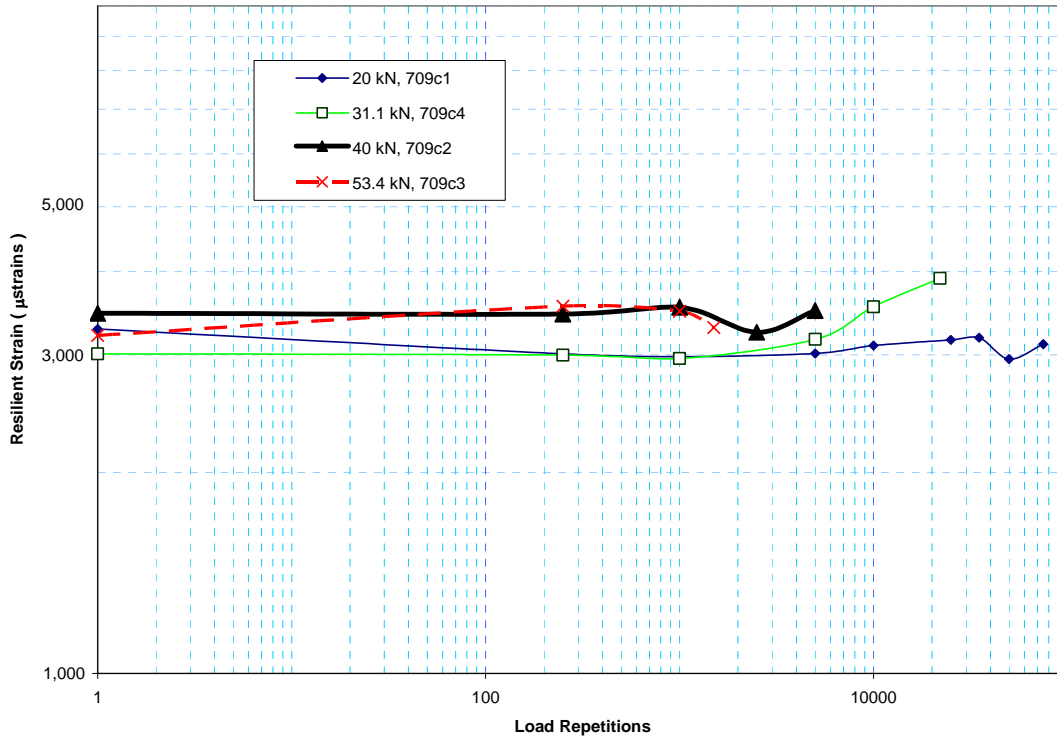


Figure 42. Resilient vertical strains 76 mm (3 in) below the top of subgrade as function of load repetitions

STRESS

Stress measurements were conducted by means of two types of gauges: Geokon and Dynatest. Figure 43 shows the stress measurements conducted in Test Windows 709c2 and 709c5, both loaded with 40 kN (9 kips) semiaxial load. The stress measurements in Test Window 709c5 was largely affected by a wide crack and delamination that occurred in the asphalt concrete. The stress measurements in Test Window 709c2 are good measurements of stress at points in the center of the thickness of the base course located directly under the tire path.

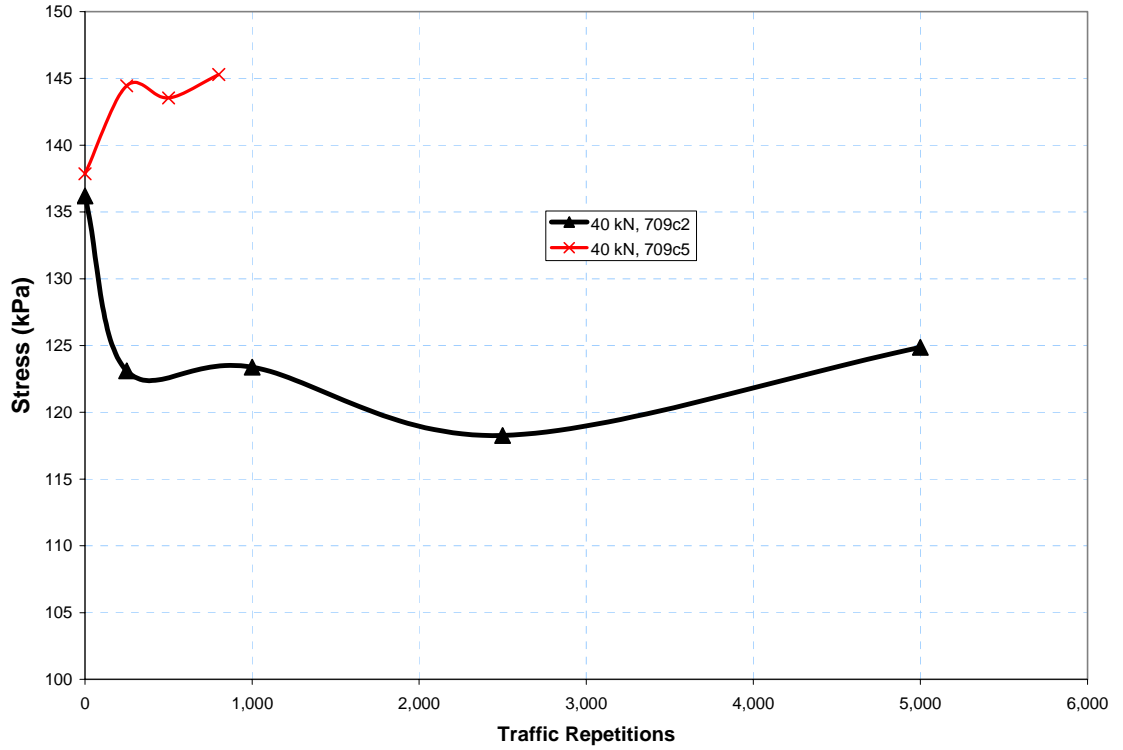


Figure 43. Stress measurements in the middle of the base course in Test Windows 709c2 and 709c5, both with 40 kN semi-axial load.

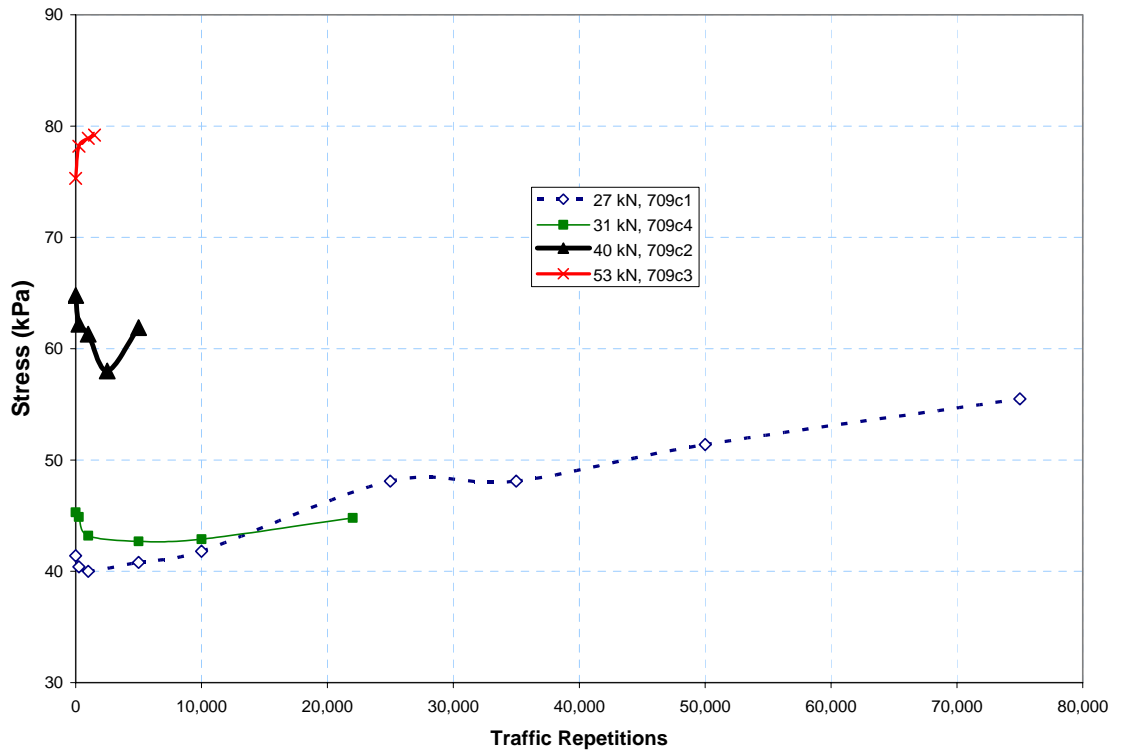


Figure 44. Stress measurements at a depth of 76 mm below the top of the subgrade for various semi-axial loads.

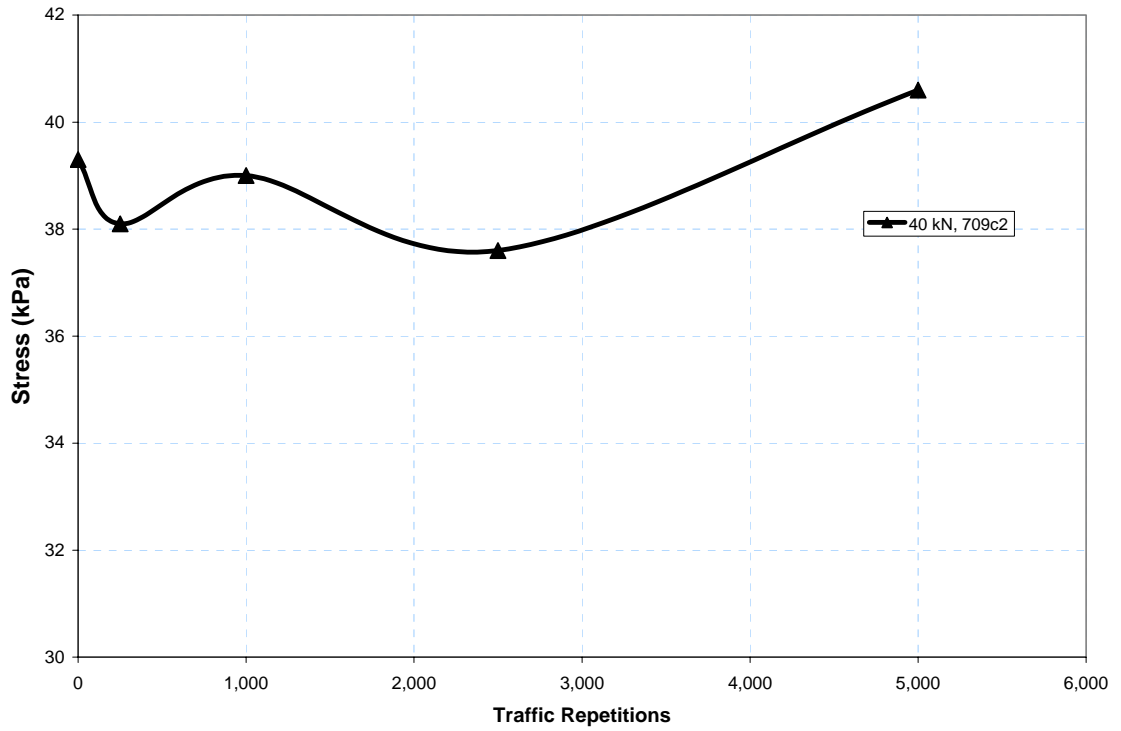


Figure 45. Stress measurements at a depth of 304 mm (1ft.) below the top of the subgrade for a semi-axial load of 40 kN (9kips).

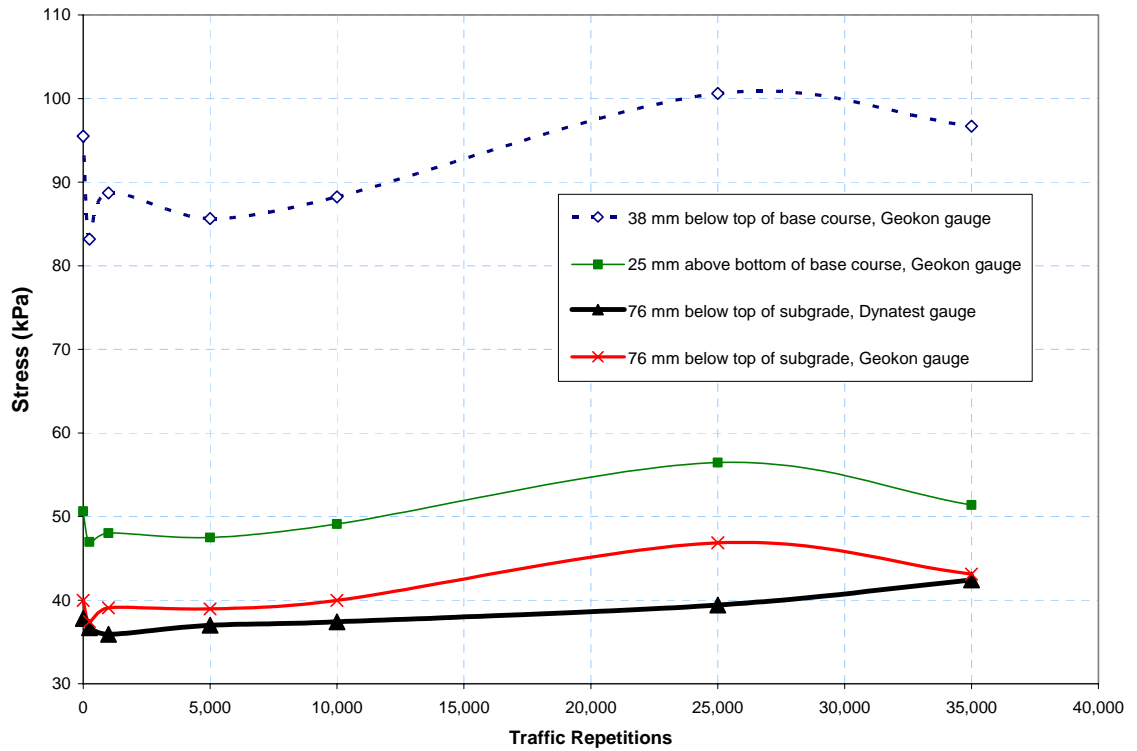


Figure 46. Stress measurements at various depths in Test Window 709c6 with a semi-axial load of 20 kN (4.5 kips).

In most cases, stress increased slightly with traffic repetitions. This is probably due to packing of soil particles under the action of traffic. Figure 46 apparently suggests that, under similar conditions, the Dynatest gauges registered only slightly lower stress than the Geokon sensors.

FORENSIC EVALUATION

A forensic evaluation was conducted to establish the condition of the pavement structure at the end of the traffic tests. Two trenches were cut across the test windows. One trench was excavated across test windows 1, 2, and 3 on the south region of the test section. This trench will be referred to as the “South Trench”. Another trench was excavated in the north region of the test section. This trench cut across test windows 4, 5, and 6. The boundaries of the trenches were carefully located and marked to avoid damaging the embedded sensors and wires. Dry saw cutting was used to avoid disturbing the base and subgrade moisture contents. Base course and subgrade soil samples were taken immediately after exposure to determine their moisture contents by the oven-dry method. The side surfaces were carefully scrapped and dusted off to be able to measure asphalt and base layer thickness.

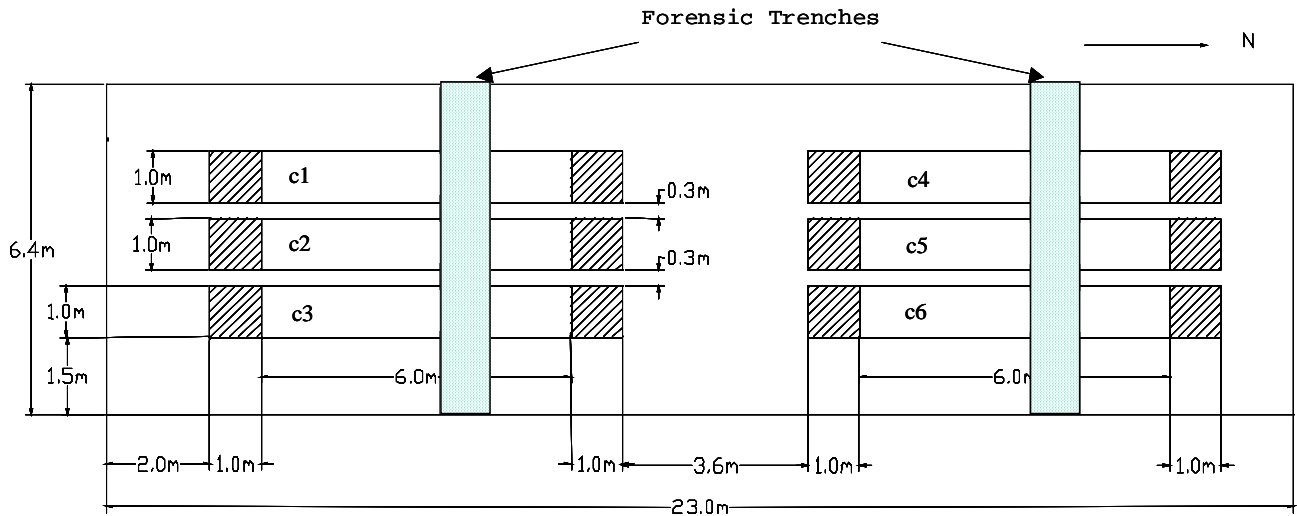


Figure 47. Location of the forensic trenches in Test Section 709

Figure 48 shows a view of the test section at the end of traffic. The distress mode in test windows 709c1, 709c2, and 709c3 were limited to smooth rutting. Contrastingly, the distress modes in test windows 709c4, 709c5, and 709c6 included delamination of the asphalt surface course, cracking and shoving. Test window 709c4 was traffic tested first. Only smooth rutting was observed throughout most the test. Delamination, cracking and shoving appeared suddenly near the end of the traffic tests. Therefore, the test results of Test Windows 709c4 should be valid. The test results obtained in test windows 709c5 and 709c6 should not be used to draw conclusions of general behavior because of their

premature asphalt failures and damage caused by traffic applied to neighboring test windows.

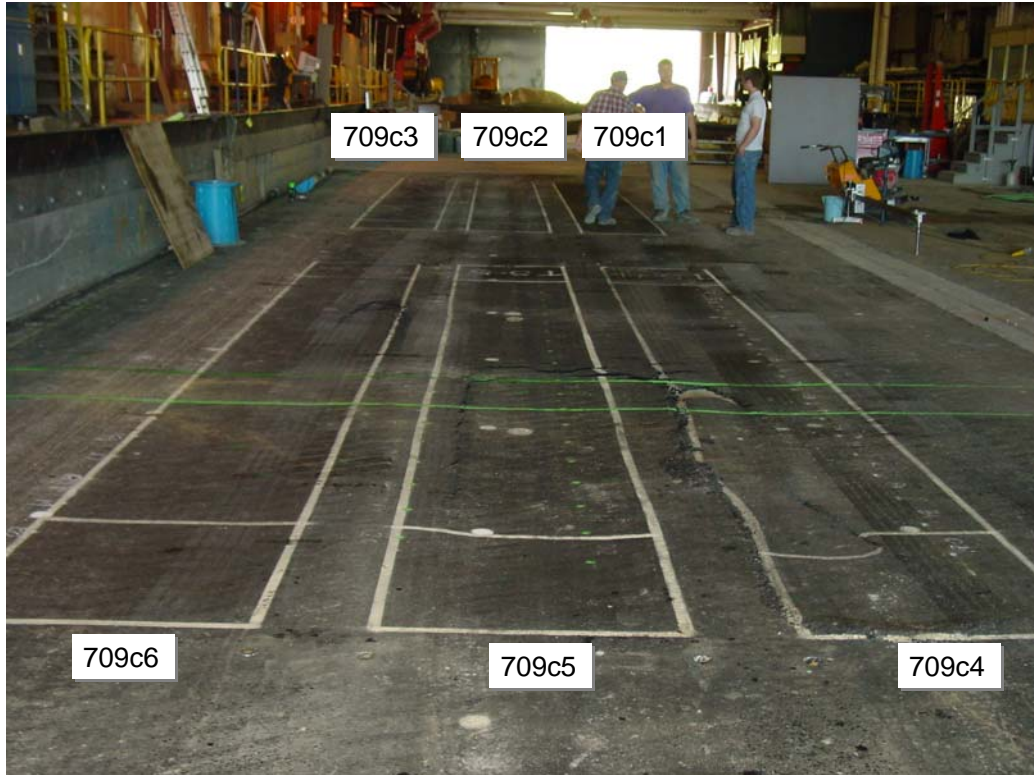


Figure 48. Forensic trenches.

Moisture and density measurements were conducted inside the trenches in the base course and in the upper subgrade down to a depth of 0.91 m (3 ft.) below the top of the asphalt concrete. Figure 49 and 50 show the gravimetric moisture contents in the south and north trenches respectively. The measured values are consistent with those obtained during the construction. Figures 51 and 52 show density measurements for the south and north trenches at each test window and also at locations outside the traffic areas at the east and west sides of the test windows. Most measured values are above 90 percent of modified Proctor density. Vane shear measurements were conducted at the top of the subgrade, at 0.30 m (1 ft.) and 0.61 m (2 ft) below the top of the subgrade. Figure 53 and Figure 54 show Vane shear measurements in the trenches at each test window and at side locations. Notice that the values for the top of the subgrade were omitted because the shear strengths exceeded the capacity of 140 kPa of the measuring device.

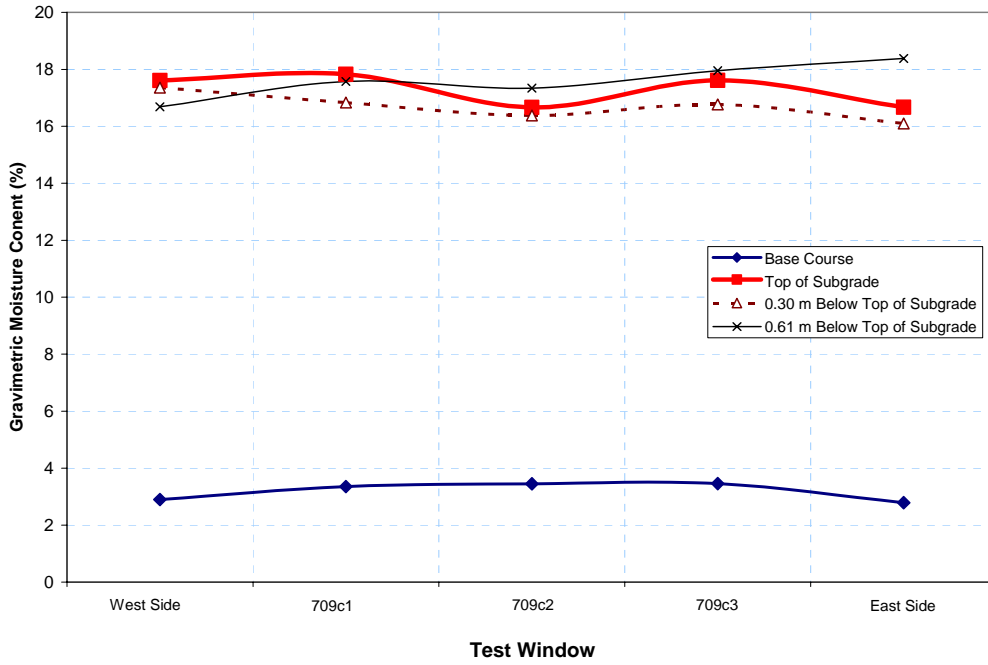


Figure 49. Moisture content in the base and upper subgrade in the south trench.

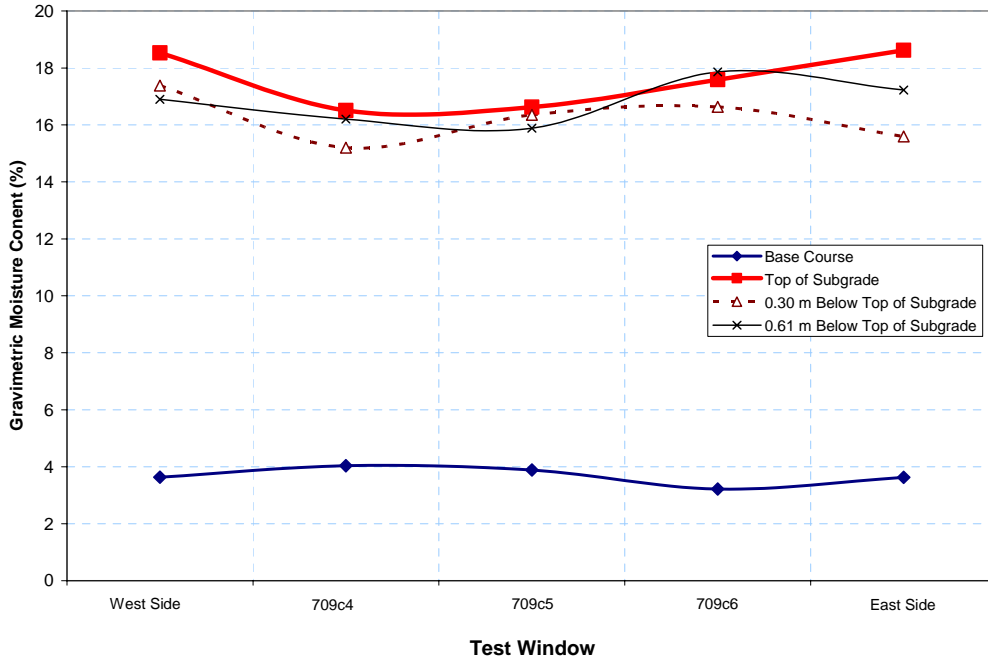


Figure 50. Moisture content in the base and upper subgrade in the north trench.

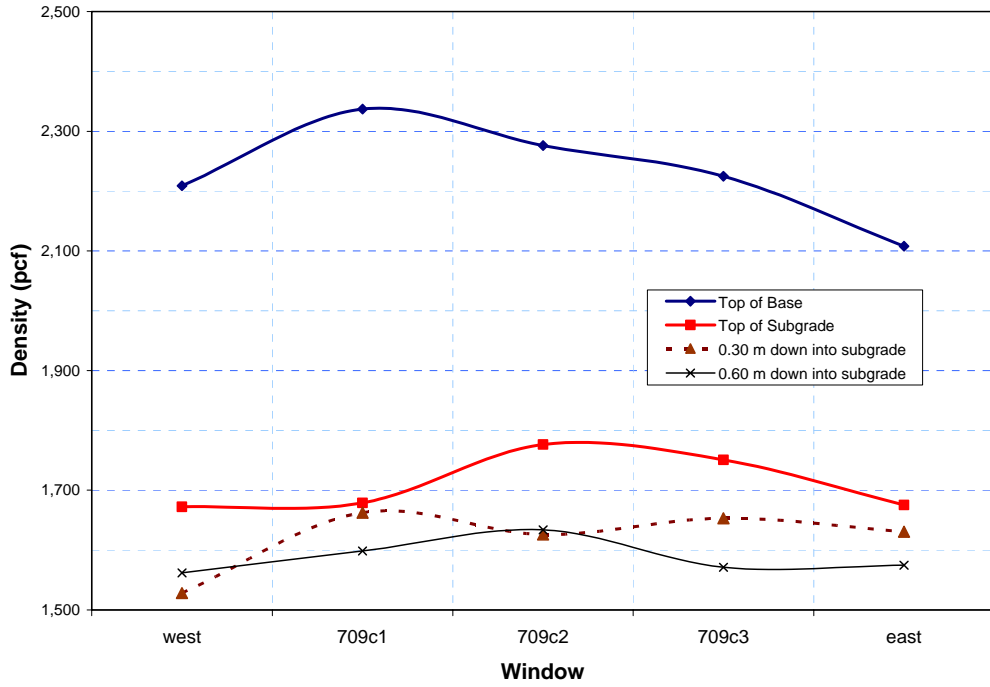


Figure 51. Density measurements in the base and upper subgrade in the south trench.

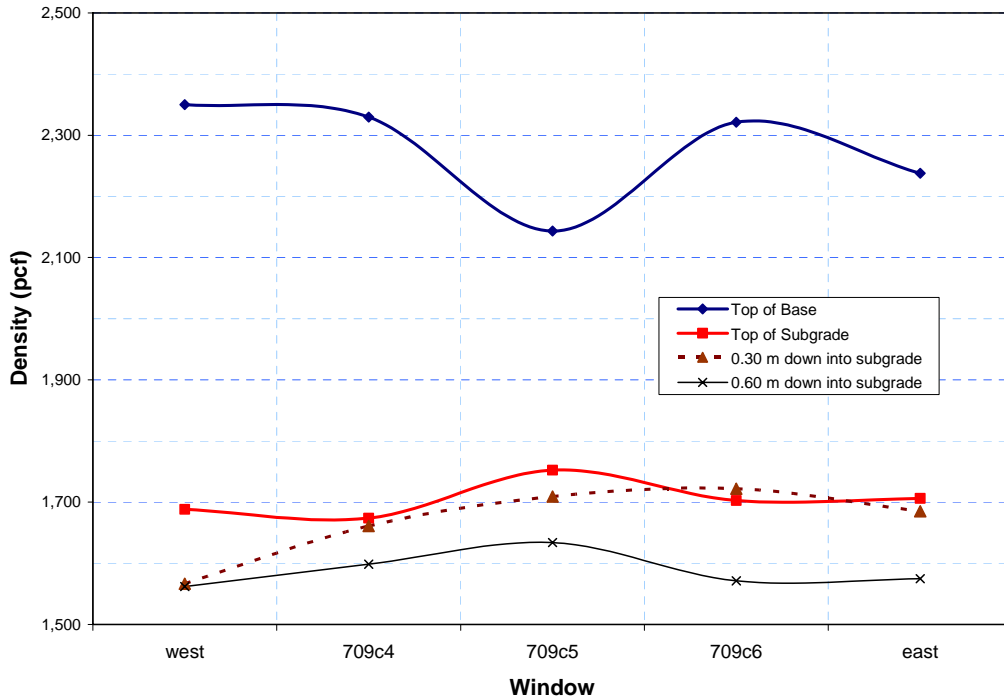


Figure 52. Density measurements in the base and upper subgrade in the north trench.

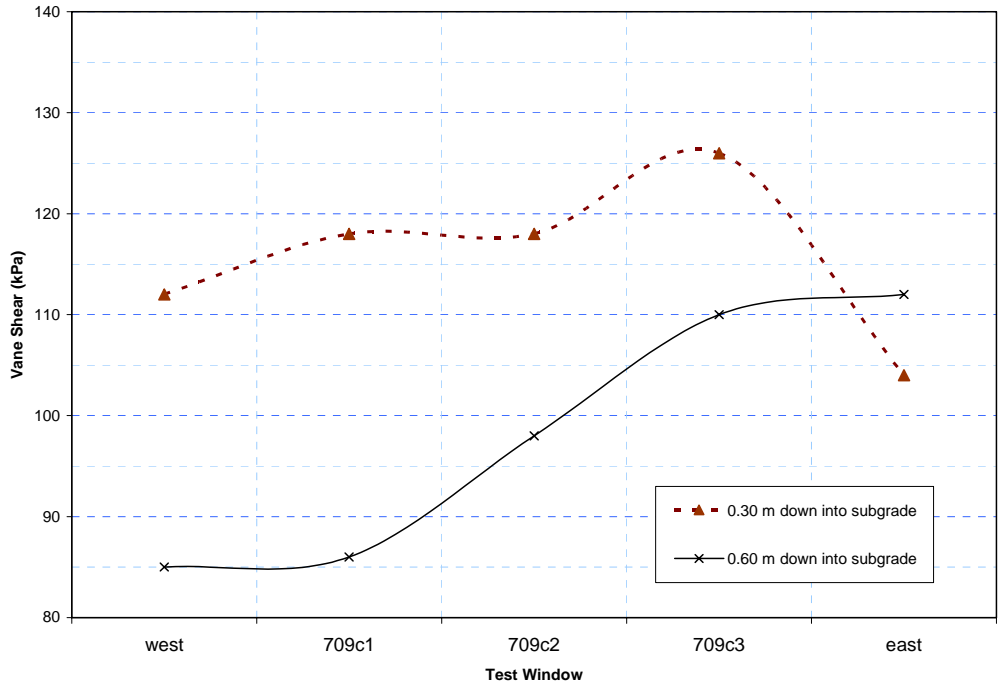


Figure 53. Vane shear measurements in the upper subgrade in the south trench.

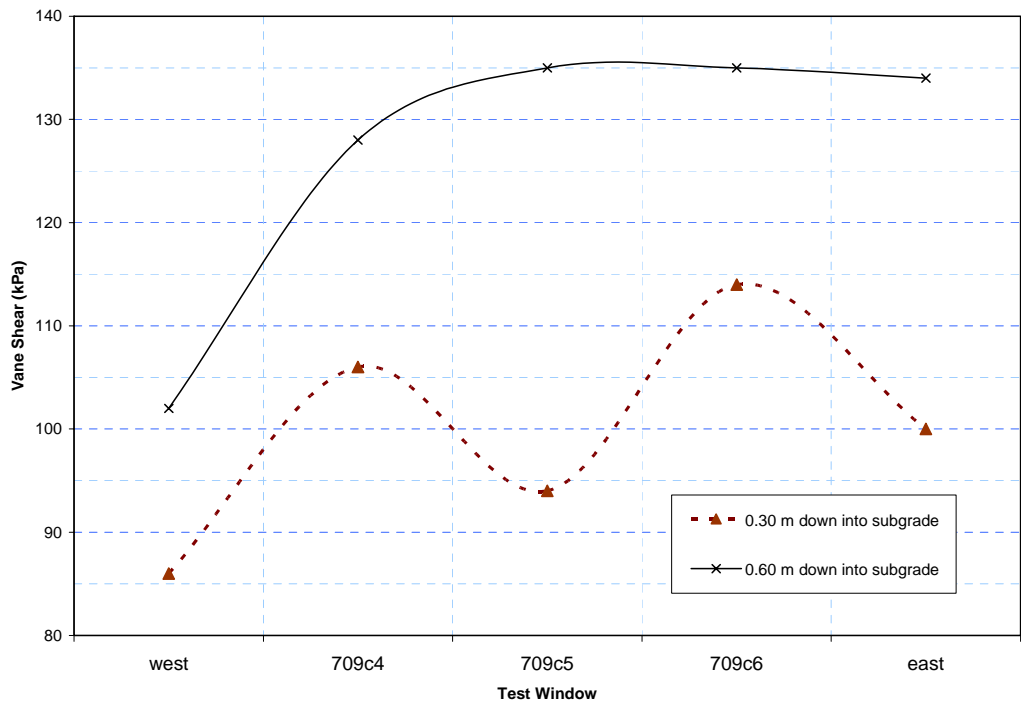


Figure 54. Vane shear measurements in the upper subgrade in the north trench.

Asphalt and base course layer thickness measurements for each test window are presented in Figures 55 through 60. In Test Window 709c1 the asphalt thickness was

slightly larger than intended. The average base course was near its design value of 229 mm (9 in.) but there were significant variations from side to side.

The average asphalt thickness in Test Window 709c2 was slightly larger than intended. The average base thickness was also near its intended value.

In Test Window 709c3, the average asphalt thickness was 10 mm (3/8 in.) larger than its design value of 76 mm (3 in.). The average base course thickness was as intended.

In Test Window 709c4 the average asphalt thickness was slightly less than intended, but its average base course thickness was 25 mm (1 in) less than its design value. This difference must be considered in the analysis.

In Test Window 709c5 the average asphalt thickness was 10 mm (3/8 in.) larger than its design value. The average base course thickness was 51 mm (2 in) less than its intended value. This is a very significant deviation that must be considered in the analysis. Undoubtedly this was an important contributing factor to the poor performance observed in this test window.

In Test Window 709c6 the average asphalt thickness was as intended, but the base course was 25 mm (1 in.) thinner than intended. This may have contributed to the poor performance of this test window.

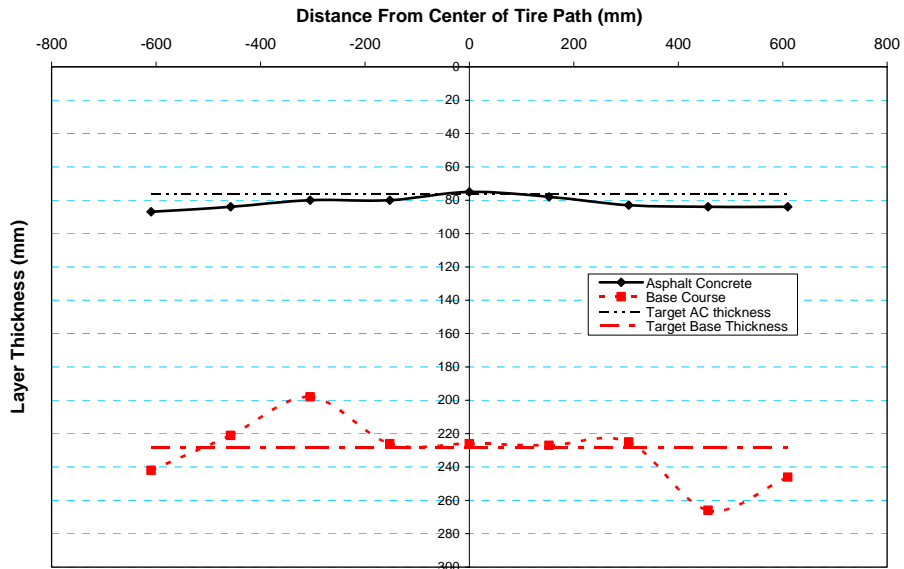


Figure 55. Layer thickness measurements across Test Window C1.

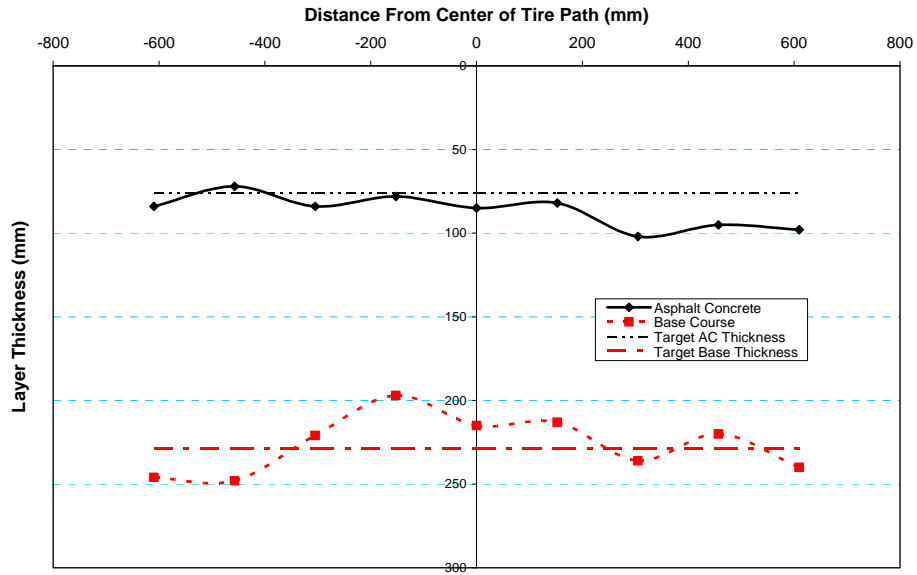


Figure 56. Layer thickness measurements across Test Window C2.

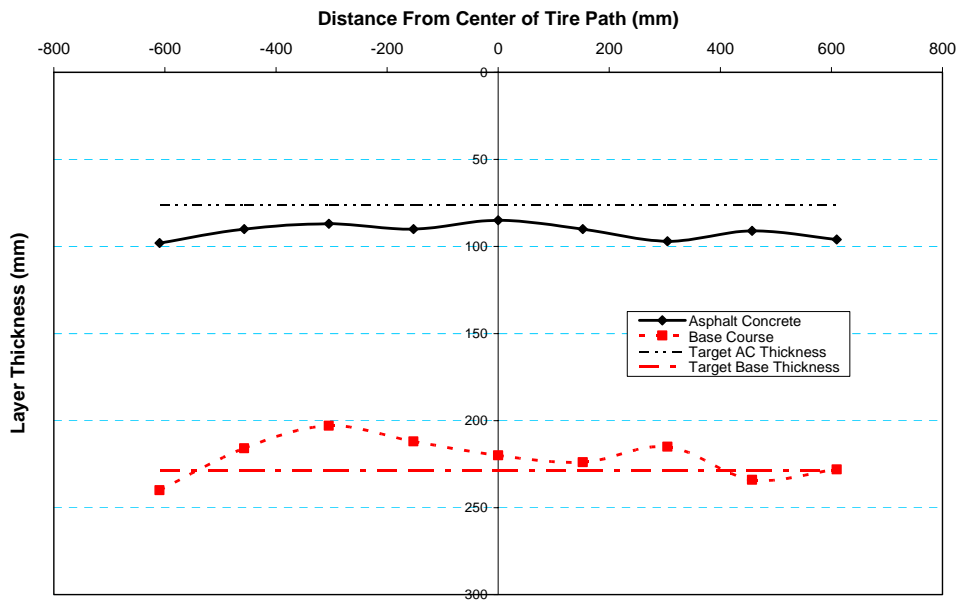


Figure 57. Layer thickness measurements across Test Window C3.

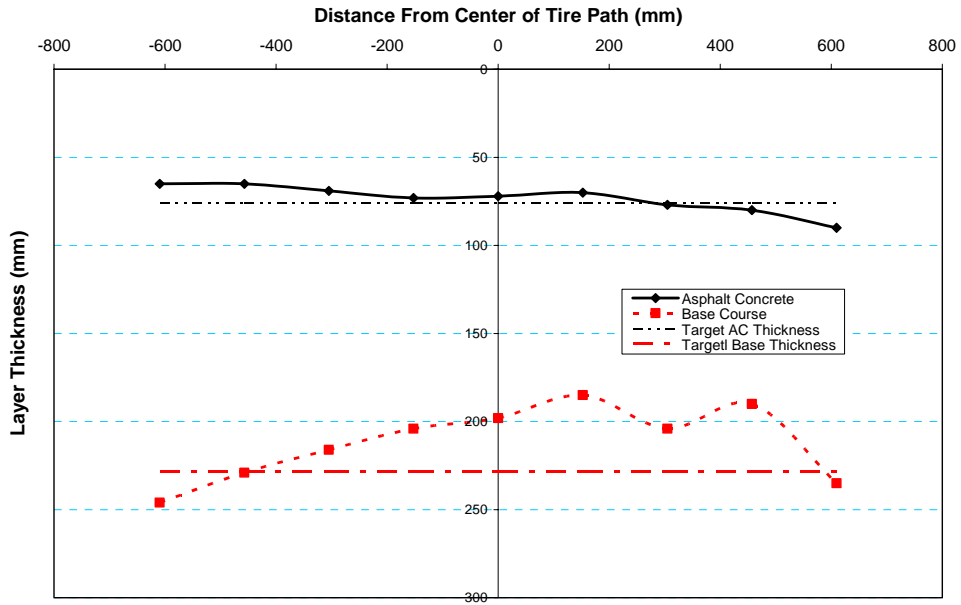


Figure 58. Layer thickness measurements across Test Window C4.

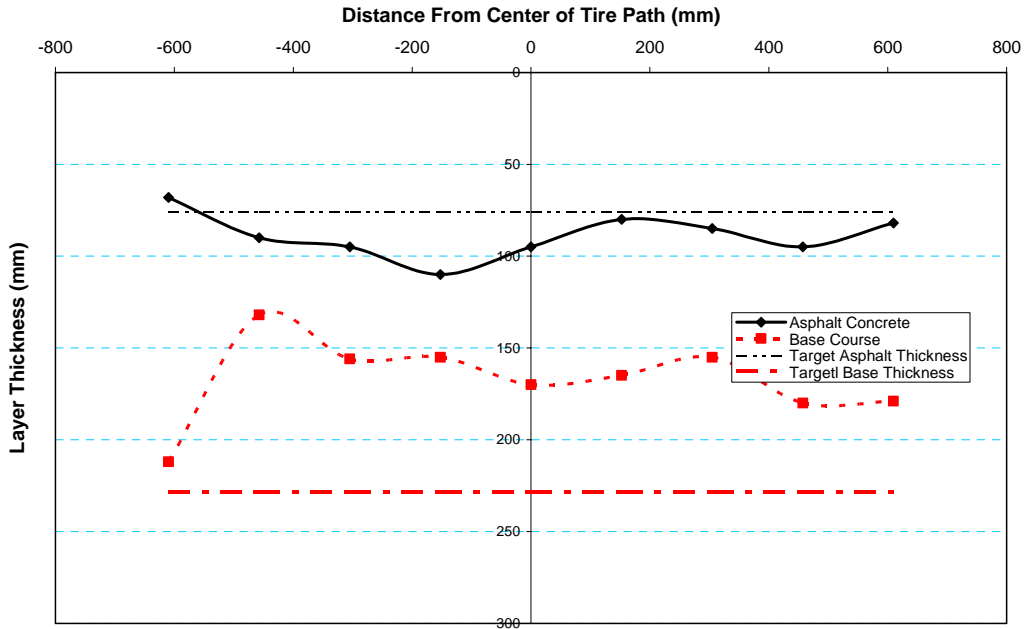


Figure 59. Layer thickness measurements across Test Window C5.

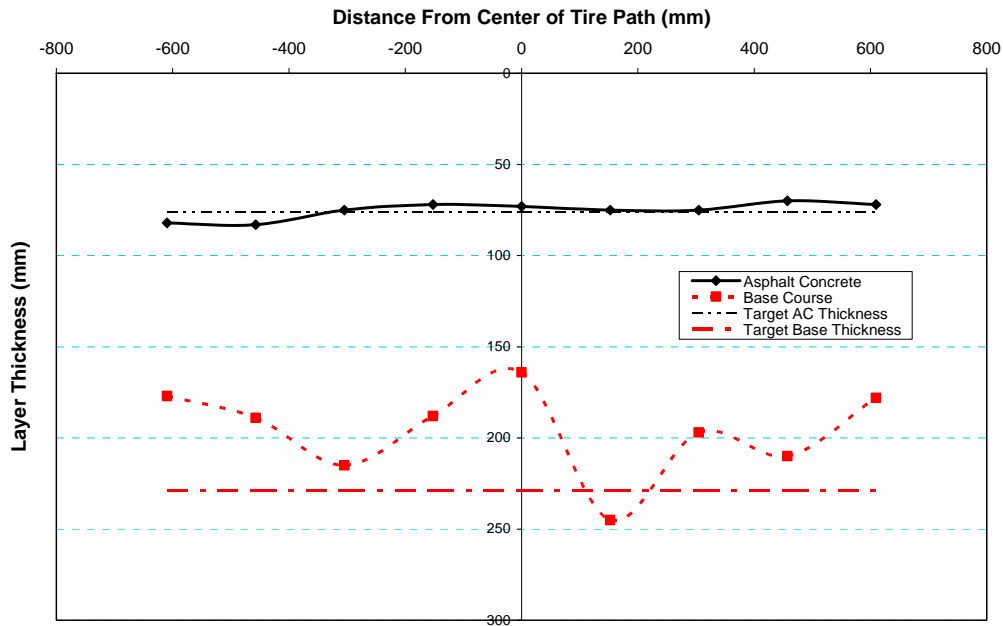


Figure 60. Layer thickness measurements across Test Window C6.

Dynamic cone penetrometer (DCP) measurements were conducted from the top of the subgrade down to a depth of at least 0.61 m (2 ft.). Figures 61 through 66 show profiles of CBR values obtained through DCP-CBR correlations. The average subgrade CBR value was 7 percent. According to Figure 19, this corresponds to a resilient modulus of 62 MPa (9,000 psi).

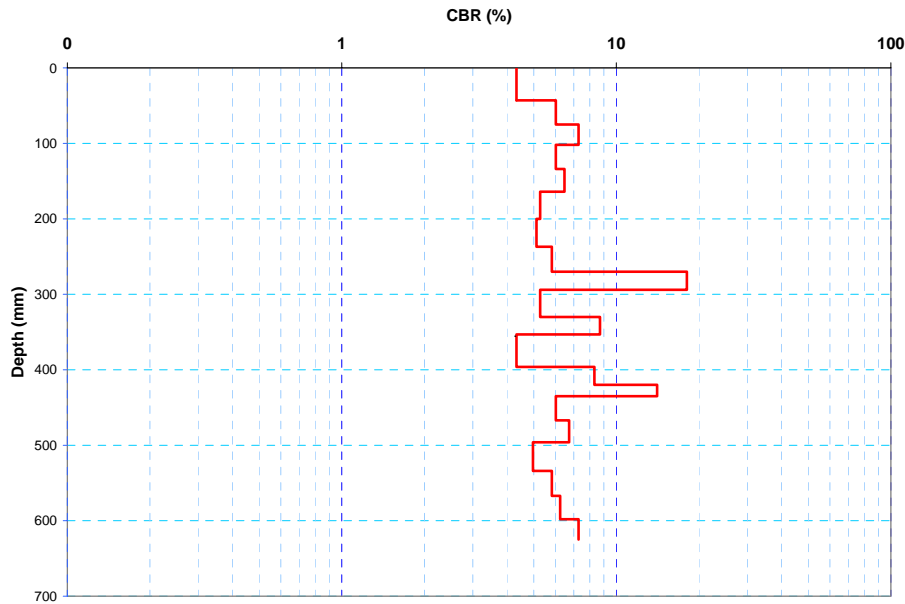


Figure 61. Subgrade CBR in Test Window C1.

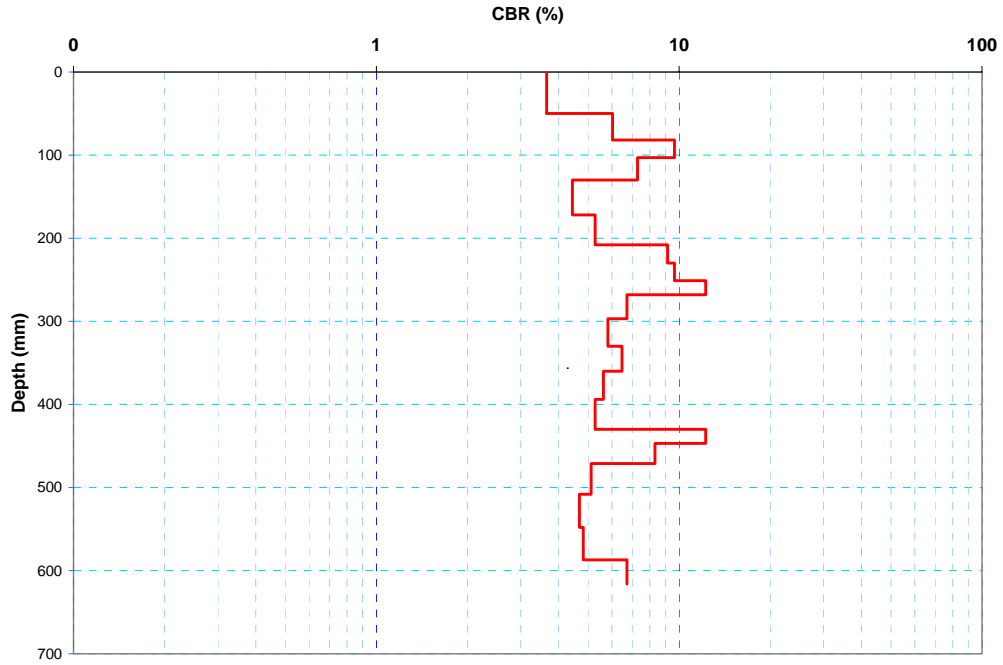


Figure 62. Subgrade CBR in Test Window C2.

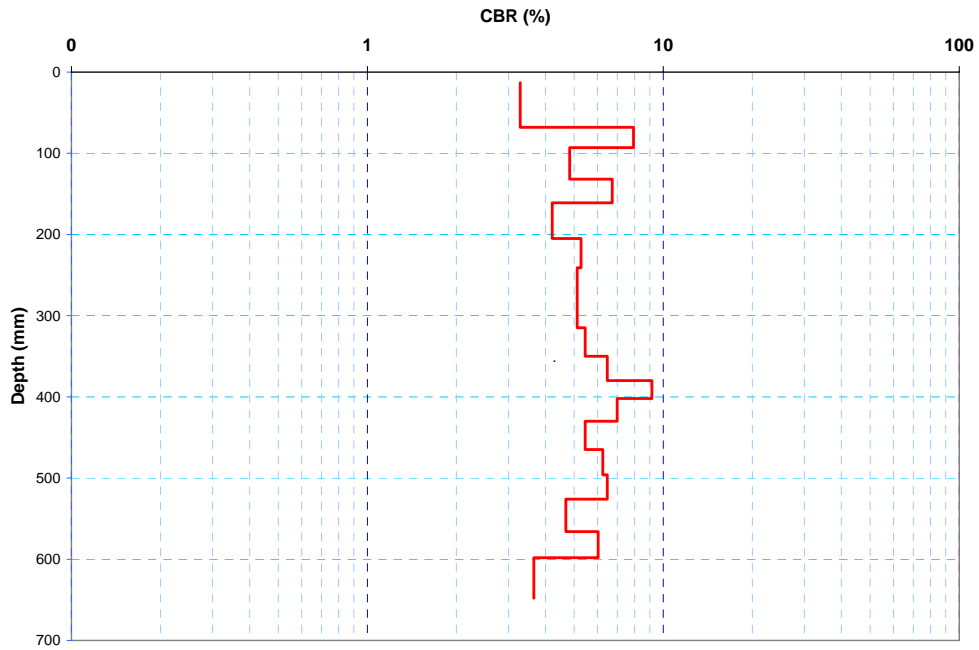


Figure 63. Subgrade CBR in Test Window C3.

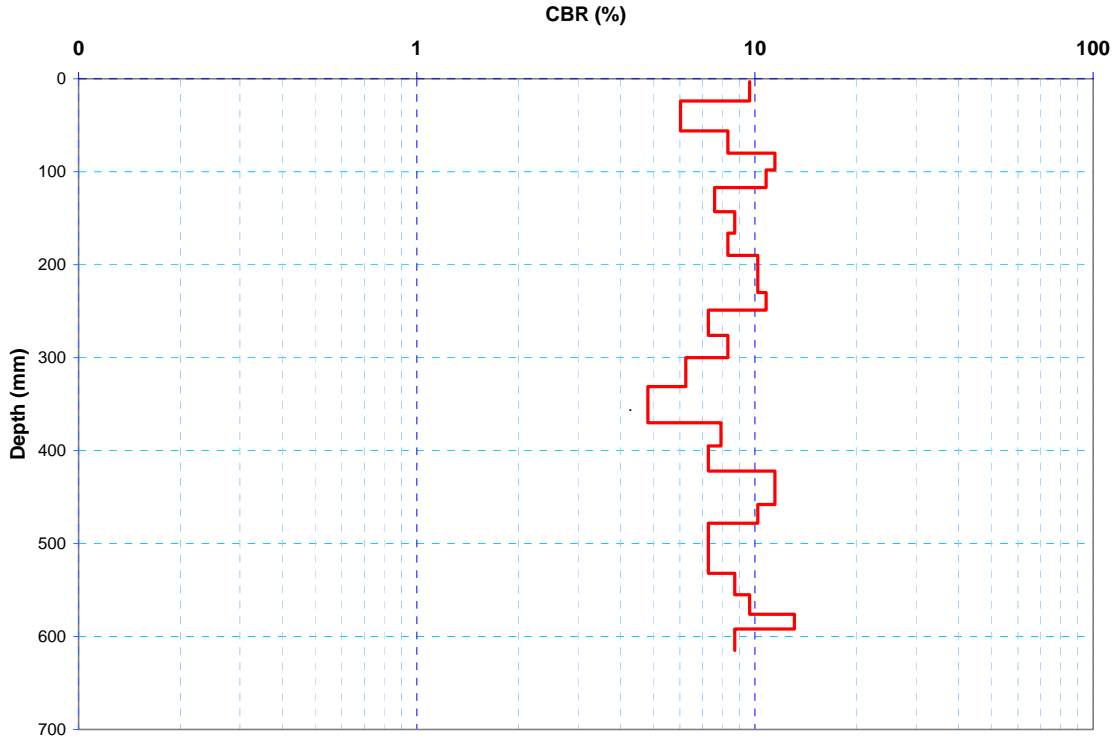


Figure 64. Subgrade CBR in Test Window C4.

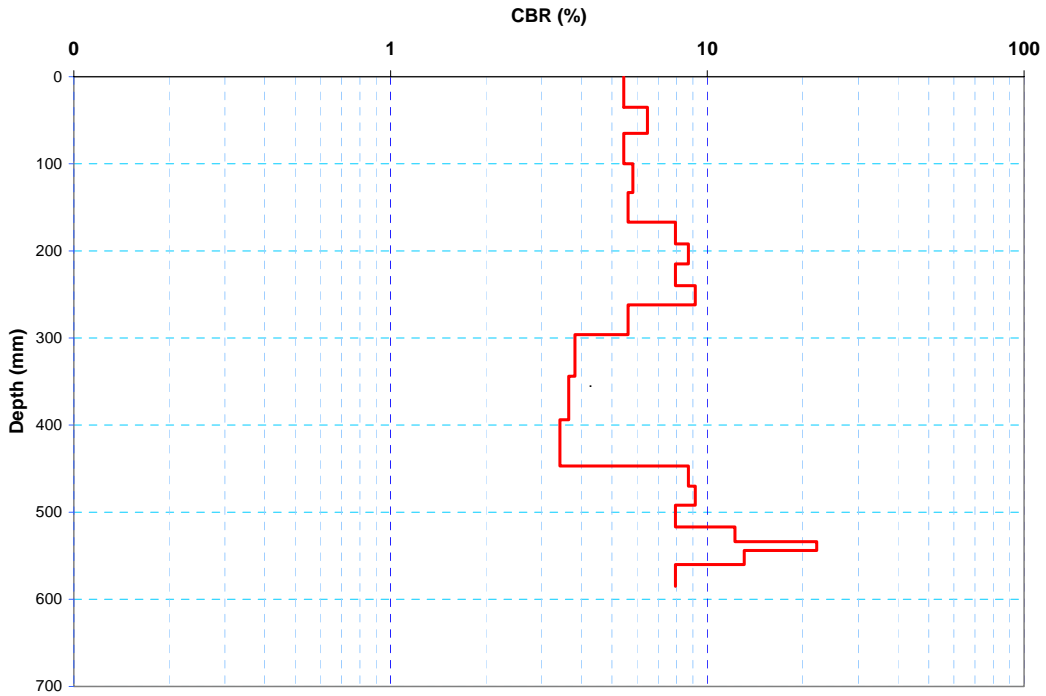


Figure 65. Subgrade CBR in Test Window C5.

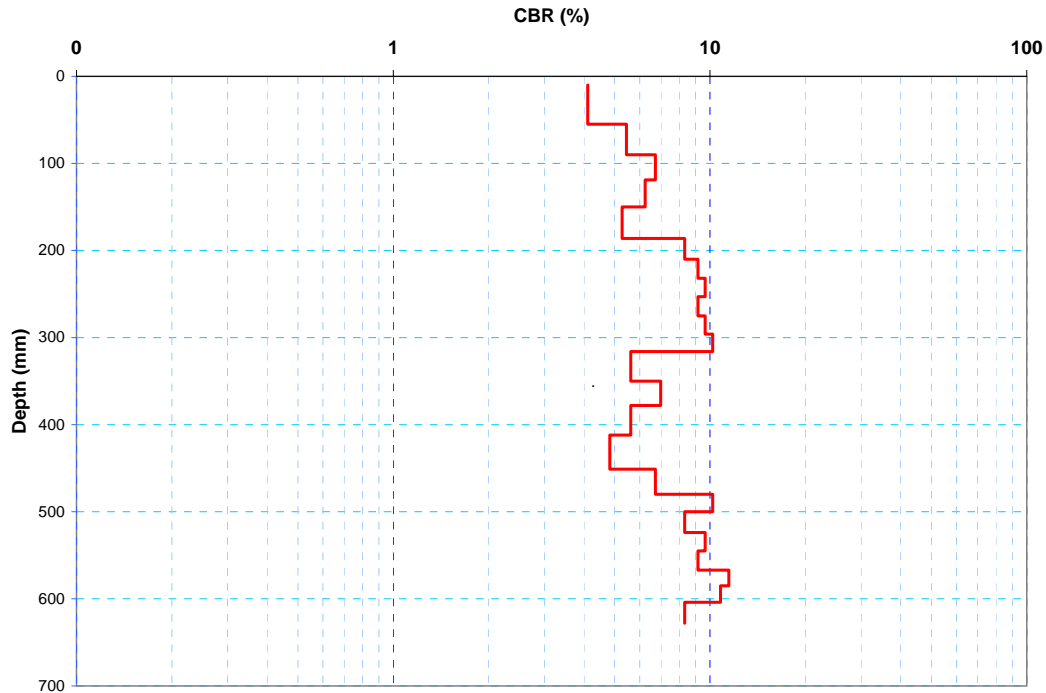


Figure 66. Subgrade CBR in Test Window C6.

SUMMARY AND CONCLUSIONS

Accelerated pavement testing (APT) was conducted on a test section with a subgrade soil that was classified as AASHTO type A-6 (USCS type CL). The subgrade was intended to be built at optimum moisture content that, for this soil is 16 percent. Laboratory modified Proctor and CBR tests conducted on this soil indicate that, at optimum moisture content, the laboratory CBR value is 15 percent (Figure 3). According to construction records, the actual average moisture content for the upper subgrade was 16.6. However, moisture sensors were located only at two depths in the subgrade. Oven dry measurements during the forensic evaluation indicated that the moisture content of the upper subgrade was 17.5 percent. The apparent moisture content increase in the upper subgrade may be due to vapor migration from the lower subgrade. This seemingly small moisture increase may have relatively large impacts on the mechanical behavior of the subgrade during traffic. Figure 3 shows that, at 17.5 % moisture content, the laboratory CBR of this soil is 10 percent compared to 15 percent at optimum moisture content. Dynamic cone penetrometer (DCP) measurements conducted during the forensic evaluation (Figures 61 through 66) indicate average CBR values of 7. Figure 19 shows that resilient modulus (M_r) for CBR of 15 percent is 97 MPa (14 ksi), whereas for a 10 CBR the M_r is 76 MPa (11 ksi). According to Figure 3, for this soil, the CBR and resilient modulus decreases rapidly with increase of moisture content. The moisture effects on the visco-plastic components of soil behavior may be more pronounced than the effect on M_r .

The test section was instrumented with stress, strain, temperature and moisture sensors. The test section was divided into 6 test windows. A test window is an area where traffic was applied by means of CRREL's Heavy Vehicle Simulator (HVS). All test windows are built equally in terms of materials and geometry, but the traffic load intensity is varied from test window to test window. However, the traffic load is kept constant throughout the traffic test for a particular test window. The test loads varied between 20 to 53.4-kN (4.5 to 12 kips). The load was applied by means of a standard dual truck tire assembly that constitutes half of a truck axle. Therefore, for example, 40 kN (9 kips) is equivalent to a full axial load of 80 kN (18 kips). The tire pressure was kept constant at 690-kPa (100 psi). Traffic speed was also kept constant at 12 km/hour (7.46 miles/hour) for all test windows. The effective test windows were 6.08 m (20 ft) long, excluding acceleration and deceleration zones. Traffic was evenly wandered within a strip 0.91 m (3 ft) wide. Traffic was unidirectional, i.e., the tire assembly applied load in one direction and returned to the initial point suspended in the air. Accelerated pavement testing was conducted over a period of 3 months. Because the experiments were conducted indoors, the ambient and pavement temperatures were practically constant throughout the test period. The average ambient temperature was 18.1 °C (65°F). Soil moisture was also kept as constant as possible. The bottom and sides of the test section were made of portland cement concrete, and the top surface was made of asphalt concrete. Aside for vapor diffusion, the pavement was practically a sealed system for soil moisture. However, some moisture migration from the lower subgrade to the upper subgrade may have occurred as explained above. At various stages during the accelerated pavement testing (APT), dynamic stresses, resilient strain, permanent strains, and surface rut depth measurements were collected for each test window. Arrays of sensors were embedded in each test window to measure vertical, longitudinal and transverse components of stress and strain at critical locations. Transverse profiles on top of the asphalt concrete were taken by means of a laser profilometer. Surface deformation profiles were produced by subtracting corresponding profiles at various pass levels to a baseline profile taken before traffic began. Surface rut progressions with traffic repetitions are presented in Figures 28 through 34. Subsurface deformation and stress data is presented in Figures 35 through 46.

Premature asphalt failures in the form of delamination between asphalt base and surface courses, cracking and shoving were observed in Test Windows 709c5 and 709c6. This resulted in abnormal rutting, stress and strain test results. The data from the anomalous test windows will be excluded from the overall analysis of this test section and from relationships between this and other test sections. The premature asphalt failure may have been due to rapid cooling of asphalt during transportation, placing and compaction. Asphalt paving was done on the last week of the paving season, when the outside temperature was approximately 7 °C (45 °F) and it was raining. Although the FERF experimental facility is equipped with a powerful heating system, the gates were kept open to allow access to the paving equipment. Despite efforts to clean the truck tires, the asphalt base course surface may have received some soil contamination at the locations where the premature failure developed during traffic.

The dynamic strains at failure at the top of the subgrade are compared with the current Asphalt Institute and Shell subgrade failure criteria in Figure 67. As explained

above, our experiments were conducted at constant speed of 12 km/hour (7.46 miles/hour). In order to compare with these results to those from the AASHTO Road tests, where the test speed was 48 km/hr, a reduction factor of 0.63 was applied to the strain data. This correction factor was based on results from experiments at the MnRoad experimental facility (Dai and Van Deusen, 1998). In order to compare to our data to that of a reference highway speed of 88 km/hour (55 miles/hour), a reduction factor of 0.48 would be needed. Figure 67 contains data from the current test section and from each of the previously tested test sections included in this subgrade performance study. Figure 67 confirms the hypothesis that soil behavior is dependent on soil type and moisture condition. Three of the four soil types included in this study are represented in this figure each at optimum moisture content and at two moisture contents wet of optimum. Experiments on the remaining soil type are currently in progress.

Figure 67 shows that the AASHTO type A-2-4 soil is significantly less susceptible to moisture content than the other soil types. Subgrade soil AASHTO type A-4 is most susceptible to moisture variations. This is a silty soil, and therefore, it is also most susceptible to frost heaving and spring thaw weakening. Unfortunately, this is also the most abundant subgrade soil type found in the United States and in the world (Rollings, R., 2004).

Many other relationships of subgrade soil behavior will be elaborated when the complete set of experiments on the twelve test section of this study become available. This will lead to the development of suitable criteria and subgrade performance models in support to the new AASHTO Mechanistic-Empirical Pavement Design Guide.

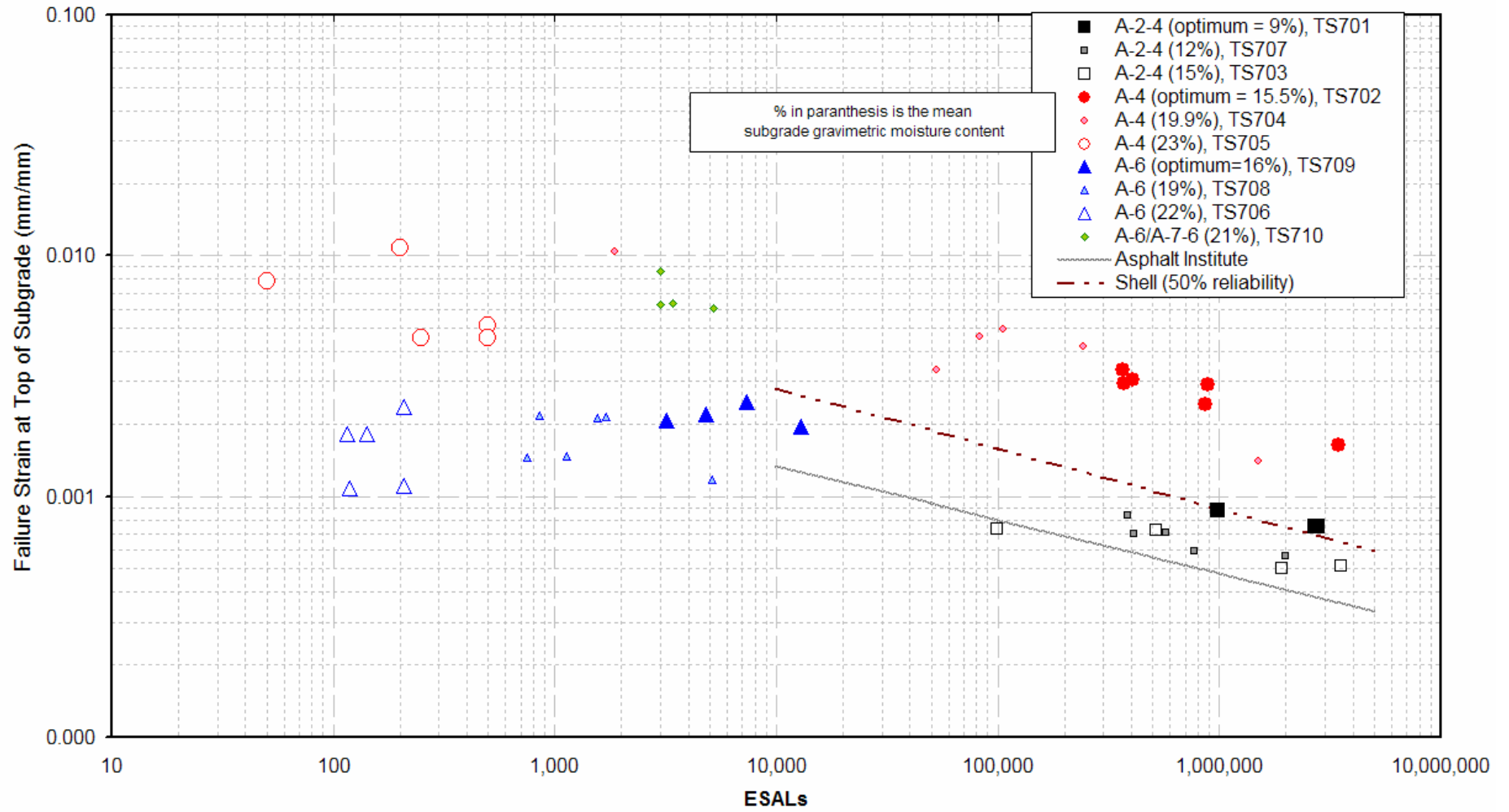


Figure 67. Effect of soil type and moisture content on subgrade failure criteria.

ACKNOWLEDGEMENTS

The authors acknowledge the sponsorship by the Federal Highway Administration (FHWA), and the Departments of Transportation of following states:

New York (lead state), Texas, California, Minnesota, Florida, Pennsylvania, Montana, Ohio, Connecticut, New Hampshire, Indiana, Idaho, Alaska, Kansas, Oregon, Georgia, Nebraska, Connecticut, Alabama, North Dakota.

The following CRREL team members have made significant contributions to this research project: Stephen Flanders, Vincent Janoo, Nathan Lamie, John Gagnon, Kurt Knuth, Richard Roberts, Troy Arnold, Charles Schelewa, Terry Melendy, Sherry Orchino, Christopher Berini, Jack Bayer, David Plumley, Russell Desclos, James Branch, Gregory Benthrop, and Claudia Grant.

REFERENCES

Dai, S.T., D.Van Deusen, D.Rettner and G.Cochran. "Investigation of Flexible Pavement Response to Truck Speed and FWD Load Through Instrumented Pavements", Proceedings of the 8th International Conference on Flexible Pavements. Seattle, Washington, pp.141-160. 1997.

Hilderbrand & Irwin, "Theoretical Analysis of Pavement Test Sections in the FERF", Internal Report, 1994.

Janoo, V. C, L. Irwin, R. Eaton, and R. Haehnel, "Pavement Subgrade Performance Study: Project Overview, ERDC Report TR15, 2002.

Perkins, S. and E. R. Cortez, "Evaluation of Base-Reinforced Pavement Using a Heavy Vehicle Simulator", 83rd. Annual Meeting of the Transportation Research Board, Washington, DC, January 2004.

AASHTO, "Guide for Mechanistic-Empirical Design of New and Rehabilitated Pavement Structures", July 2004.

APPENDIX A

SURFACE PROFILE TEST RESULTS

Table A1. Surface rut measurements in 709C1 in millimeters.

Cross Section Number	Traffic Passes								
	0	250	1000	5000	10000	25000	35000	50000	75000
1	0	-1.5	-2.3	-3.7	-5.3	-9.5	-10.6	-11.5	-14.2
2	0	-0.9	-1.9	-3.0	-4.6	-7.6	-9.0	-10.9	-12.3
3	0	-1.3	-1.7	-3.0	-4.5	-7.3	-8.2	-10.2	-11.8
4	0	-1.5	-2.0	-4.0	-6.1	-9.1	-9.9	-11.7	-13.1
5	0	-1.4	-2.6	-5.1	-7.5	-10.3	-11.9	-13.7	-16.1
6	0	-1.6	-2.2	-4.6	-6.0	-9.3	-10.8	-12.6	-15.1
7	0	-0.6	-1.6	-4.2	-5.6	-8.7	-10.4	-12.2	-14.8
8	0	-1.4	-1.8	-4.3	-6.2	-9.5	-11.1	-13.0	-14.2
9	0	-1.5	-2.3	-4.0	-6.2	-10.3	-11.6	-13.7	-15.9
10	0	-1.6	-2.4	-4.5	-7.3	-11.9	-13.7	-15.5	-17.1
11	0	-1.7	-1.9	-5.4	-6.5	-11.8	-13.4	-15.3	-17.5
12	0	-1.3	-1.9	-4.4	-5.2	-9.3	-10.7	-13.2	-14.2
13	0	-0.8	-2.0	-4.1	-4.8	-8.6	-9.7	-11.3	-13.3
14	0	-0.8	-1.4	-2.6	-4.5	-7.9	-9.2	-11.0	-12.5
15	0	-0.9	-1.6	-2.7	-4.6	-7.8	-9.2	-10.7	-12.8
16	0	-1.1	-1.2	-1.9	-3.6	-7.3	-8.6	-10.2	-11.1
17	0	-0.6	-2.2	-3.2	-4.8	-6.8	-8.1	-9.7	-11.6
18	0	-1.2	-1.4	-1.9	-3.0	-6.4	-7.8	-9.6	-10.0
19	0	-0.7	-3.7	-4.2	-4.5	-5.2	-6.4	-7.7	-9.7
20	0	-0.7	-0.5	-0.6	-2.4	-3.7	-5.2	-6.9	-11.8

Table A2. Surface rut measurements in 709C2 in millimeters.

Cross Section Number	Traffic Passes				
	0	250	1000	2500	5000
1	0	-5.0	-8.7	-12.6	-15.8
2	0	-4.8	-7.6	-11.9	-15.1
3	0	-4.6	-7.5	-12.1	-15.6
4	0	-5.1	-7.2	-11.3	-15.8
5	0	-4.7	-7.6	-12.6	-16.0
6	0	-4.3	-7.2	-12.2	-14.5
7	0	-3.5	-6.2	-10.4	-13.4
8	0	-3.3	-5.6	-9.0	-12.6
9	0	-3.4	-5.9	-10.5	-12.6
10	0	-3.9	-6.4	-8.6	-13.2
11	0	-3.6	-6.3	-10.5	-12.8
12	0	-3.5	-5.7	-8.5	-12.7
13	0	-2.7	-4.7	-7.4	-11.2
14	0	-3.3	-5.4	-9.3	-12.6
15	0	-3.7	-6.6	-9.9	-13.3
16	0	-2.9	-4.5	-7.4	-10.9
17	0	-2.5	-4.3	-8.3	-11.1
18	0	-2.3	-3.7	-6.5	-10.1
19	0	-2.3	-3.8	-6.0	-8.7
20	0	-2.9	-4.7	-6.8	-9.8

Table A3. Surface rut measurements in 709C3 in millimeters.

Cross Section Number	Traffic Passes		
	0	250	1000
1	0	-5.4	-14.4
2	0	-5.1	-15.1
3	0	-5.2	-14.9
4	0	-4.5	-14.6
5	0	-5.0	-14.8
6	0	-5.4	-14.1
7	0	-4.1	-13.1
8	0	-4.6	-13.6
9	0	-4.1	-14.1
10	0	-3.8	-12.5
11	0	-3.1	-11.6
12	0	-4.2	-12.0
13	0	-4.2	-12.2
14	0	-3.3	-11.6
15	0	-4.5	-12.2
16	0	-4.0	-10.7
17	0	-3.7	-11.7
18	0	-3.4	-8.7
19	0	-4.1	-8.7
20	0	-4.0	-9.4

Table A4. Surface rut measurements in 709C4 in millimeters.

Cross Section Number	Traffic Passes					
	0	250	1000	5000	10000	22000
1	0	-2.5	-2.5	-4.7	-5.6	-10.7
2	0	-1.3	-2.5	-4.5	-6.2	-10.8
3	0	-1.8	-3.2	-5.7	-8.2	-12.0
4	0	-2.4	-4.0	-7.1	-10.4	-14.1
5	0	-3.2	-4.7	-7.1	-12.5	-17.3
6	0	-2.9	-5.1	-7.9	-12.1	-17.0
7	0	-2.3	-3.9	-7.4	-10.6	-15.4
8	0	-2.2	-3.0	-7.7	-10.3	-16.1
9	0	-2.0	-3.3	-6.1	-9.6	-15.7
10	0	-1.5	-2.3	-5.1	-8.2	-14.1
11	0	-1.6	-2.8	-6.8	-8.8	-15.0
12	0	-1.6	-3.6	-7.4	-9.4	-16.9
13	0	-2.1	-3.6	-5.5	-8.4	-14.8
14	0	-2.1	-3.6	-6.3	-8.9	-15.8
15	0	-2.0	-3.4	-7.4	-9.5	-13.3
16	0	-1.5	-2.5	-4.8	-7.5	-10.3
17	0	-1.5	-2.7	-4.6	-6.6	-10.2
18	0	-0.9	-2.7	-4.5	-6.5	-9.3
19	0	-1.0	-2.9	-4.9	-6.3	-9.9
20	0	-1.6	-2.0	-3.5	-5.4	-8.9

Table A5. Surface rut measurements in 709C5 in millimeters.

Cross Section Number	Traffic Passes			
	0	250	500	800
1	0	-4.7	-6.3	-7.3
2	0	-5.1	-6.8	-8.5
3	0	-5.0	-6.7	-8.2
4	0	-5.3	-6.8	-8.0
5	0	-5.6	-7.5	-10.4
6	0	-6.8	-8.9	-9.2
7	0	-6.9	-8.7	-10.8
8	0	-6.2	-8.8	-11.1
9	0	-6.5	-9.0	-10.0
10	0	-6.5	-8.6	-11.4
11	0	-7.0	-10.0	-11.3
12	0	-7.2	-10.9	-17.0
13	0	-7.4	-9.5	-19.3
14	0	-7.5	-8.7	-11.3
15	0	-7.9	-11.6	-11.5
16	0	-8.0	-10.3	-12.0
17	0	-8.1	-15.3	-17.3
18	0	-8.3	-14.0	-16.4
19	0	-8.1	-9.8	-11.4
20	0	-8.9	-11.1	-12.9

Table A6. Surface rut measurements in 709C6 in millimeters.

Cross Section Number	Traffic Passes					
	0	250	1000	5000	10000	25000
1	0	-1.5	-2.2	-3.0	-3.2	-4.9
2	0	-1.7	-3.0	-3.6	-3.9	-5.6
3	0	-1.8	-2.4	-3.5	-3.8	-4.6
4	0	-2.2	-3.2	-4.1	-4.5	-6.4
5	0	-2.7	-2.9	-3.4	-4.7	-6.5
6	0	-3.1	-4.0	-4.5	-6.8	-8.7
7	0	-3.3	-4.1	-6.2	-7.6	-9.5
8	0	-2.9	-4.4	-6.1	-7.5	-10.3
9	0	-3.1	-3.6	-5.5	-6.6	-9.4
10	0	-2.9	-4.3	-5.3	-6.4	-9.0
11	0	-3.6	-4.2	-5.5	-6.4	-8.9
12	0	-4.0	-4.6	-6.1	-7.2	-9.9
13	0	-3.5	-4.5	-5.5	-6.7	-9.6
14	0	-3.7	-4.5	-6.0	-6.7	-9.8
15	0	-3.8	-4.7	-5.2	-6.0	-10.1
16	0	-3.7	-4.8	-5.7	-7.4	-9.4
17	0	-4.0	-4.4	-5.5	-6.5	-10.9
18	0	-3.2	-4.5	-6.3	-7.5	-10.9
19	0	-3.7	-4.3	-5.2	-6.6	-11.8
20	0	-3.8	-5.6	-6.8	-8.1	-11.8

APPENDIX B

PERMANENT DEFORMATION MEASUREMENTS

Table B 1. Vertical permanent deformation (mm) in 709C1.

Depth (mm)	Traffic Passes								
	0	250	1000	5000	10000	25000	35000	50000	75000
0-76	0	-0.323	-0.770	-1.395	-1.518	-1.641	-1.824	-1.885	-2.066
76-190	0	-0.247	-0.474	-1.083	-1.499	-2.273	-2.508	-2.674	-3.061
190-305	0	-0.180	-0.388	-1.141	-1.786	-2.799	-3.083	-3.389	-3.801
305-457	0	-0.047	-0.098	-0.503	-0.700	-1.230	-1.515	-1.445	-2.012
457-610	0	-0.084	-0.175	-0.551	-0.712	-1.080	-1.115	-1.151	-1.541
610-762	0	-0.008	-0.057	-0.297	-0.345	-0.533	-0.542	-0.325	-0.517
762-914	0	-0.004	-0.029	-0.149	-0.172	-0.267	-0.271	-0.162	-0.259
914-1067	0	-0.002	-0.014	-0.074	-0.086	-0.133	-0.135	-0.081	-0.129
1067-1219	0	-0.001	-0.007	-0.037	-0.043	-0.067	-0.068	-0.041	-0.065
1219-1372	0	0.000	-0.004	-0.019	-0.022	-0.033	-0.034	-0.020	-0.032
1372-1524	0	0.000	-0.002	-0.009	-0.011	-0.017	-0.017	-0.010	-0.016

Semi-axial load was 26.7 kN.

Table B 2. Vertical permanent deformation (mm) in 709C2.

Depth (mm)	Traffic Passes				
	0	250	1000	2500	5000
0-76	0	-0.397217	-0.83057	-1.20754	-1.66865
76-190	0	-0.658652	-1.4373	-2.24701	-3.05436
190-305	0	-1.159806	-2.31677	-3.39602	-4.25945
305-457	0	-0.436618	-0.95007	-1.72706	-2.44953
457-610	0	-0.119057	-0.25867	-0.47381	-0.73978
610-762	0	-0.059528	-0.12933	-0.2369	-0.36989
762-914	0	-0.029764	-0.06467	-0.11845	-0.18495
914-1067	0	-0.014882	-0.03233	-0.05923	-0.09247
1067-1219	0	-0.007441	-0.01617	-0.02961	-0.04624
1219-1372	0	-0.003721	-0.00808	-0.01481	-0.02312
1372-1524	0	-0.00186	-0.00404	-0.0074	-0.01156

Semi-axial load was 40.0 kN.

Table B 3. Vertical permanent deformation (mm) in 709C3.

Depth (mm)	Traffic Passes			
	0	250	1000	1500
0-76	0	-0.40332	-1.34783	-1.57895
76-190	0	-0.78241	-1.88117	-2.1525
190-305	0	-1.6232	-4.58647	-5.54373
305-457	0	-0.58634	-1.39835	-1.78441
457-610	0	-0.37557	-0.80716	-1.08514
610-762	0	-0.2071	-0.26175	-0.18046
762-914	0	-0.10355	-0.13087	-0.09023
914-1067	0	-0.05178	-0.06544	-0.04511
1067-1219	0	-0.02589	-0.03272	-0.02256
1219-1372	0	-0.01294	-0.01636	-0.01128
1372-1524	0	-0.00647	-0.00818	-0.00564

Semi-axial load was 53.4 kN.

Table B 4. Vertical permanent deformation (mm) in 709C4.

Depth (mm)	Traffic Passes					
	0	250	1000	5000	10000	22000
0-76	0	-0.22	-0.56	-1.07	-1.48	-2.26
76-190	0	-0.44	-1.00	-2.20	-3.33	-5.17
190-305	0	-0.22	-0.46	-1.01	-1.62	-2.66
305-457	0	-0.27	-0.53	-0.95	-1.37	-1.87
457-610	0	-0.10	-0.21	-0.45	-0.69	-0.91
610-762	0	-0.05	-0.11	-0.22	-0.35	-0.46
762-914	0	0.03	0.02	0.01	0.04	-0.03
914-1067	0	0.01	0.01	0.00	0.02	-0.02
1067-1219	0	0.01	0.00	0.00	0.01	-0.01
1219-1372	0	0.00	0.00	0.00	0.01	0.00
1372-1524	0	0.00	0.00	0.00	0.00	0.00

Semi-axial load was 31.1 kN.

Table B 5. Vertical permanent deformation (mm) in 709C5.

Depth (mm)	Traffic Passes			
	0	250	500	800
0-76	0	-2.97	-3.53	-3.97
76-190	0	-1.21	-1.50	-1.83
190-305	0	-2.36	-1.77	-2.51
305-457	0	-1.31	-1.31	-1.58
457-610	0	-0.70	-0.71	-0.78
610-762	0	-0.39	-0.29	-0.37
762-914	0	-0.45	-0.39	-0.47
914-1067	0	-0.38	-0.16	-0.15
1067-1219	0	-0.19	-0.08	-0.08
1219-1372	0	-0.09	-0.04	-0.04
1372-1524	0	-0.05	-0.02	-0.02

Semi-axial load was 40.0 kN.

Table B 6. Vertical permanent deformation (mm) in 709C6.

Depth (mm)	Traffic Passes					
	0	250	1000	5000	10000	25000
0-76	0	-0.23	-0.78	-1.34	-2.00	-2.43
76-190	0	-0.45	-2.11	-1.60	-1.13	-0.97
190-305	0	-0.59	-0.95	-1.42	-1.75	-3.08
305-457	0	-0.22	-0.36	-0.67	-0.87	-1.72
457-610	0	-0.13	-0.29	-0.41	-0.49	-1.11
610-762	0	-0.07	-0.14	-0.20	-0.24	-0.55
762-914	0	-0.03	-0.07	-0.10	-0.12	-0.28
914-1067	0	-0.02	-0.04	-0.05	-0.06	-0.14
1067-1219	0	-0.01	-0.02	-0.03	-0.03	-0.07
1219-1372	0	0.00	-0.01	-0.01	-0.02	-0.03
1372-1524	0	0.00	0.00	-0.01	-0.01	-0.02

Semi-axial load was 20.0 kN.

Test Section 709 AASHTO A-6 subgrade soil at optimum moisture content (16 %)

APPENDIX C

PERMANENT STRAIN MEASUREMENTS

Table C 2. Vertical permanent strain (microstrains) in 709C1.

Depth (mm)	Traffic Passes								
	0	250	1000	5000	10000	25000	35000	50000	75000
38	0	4245	10103	18306	19924	21534	23936	24733	27113
133	0	2288	4407	10101	14072	21421	23832	25472	29216
248	0	1708	3680	10858	17134	27035	30110	33192	37353
381	0	301	623	3201	4464	7862	9715	9286	12924
533	0	587	1220	3832	4966	7548	7809	8068	10807
686	0	51	378	1963	2284	3533	3591	2154	3425
838	0	6	45	233	275	426	437	261	412
991	0	2	15	76	88	136	138	83	132
1143	0	1	8	44	67	84	80	48	76
1295	0	1	5	27	32	48	50	30	48
1448	0	2	12	61	72	111	112	67	107

Semi-axial load was 26.7 kN.

Table C 2. Vertical permanent strain (microstrains) in 709C2.

Depth (mm)	Traffic Passes				
	0	250	1000	2500	5000
38	0	5213	10900	15847	21898
133	0	5921	13003	20482	28061
248	0	11104	22446	33298	42239
381	0	2765	6033	11006	15692
533	0	863	1876	3440	5380
686	0	358	777	1424	2223
838	0	213	462	846	1321
991	0	108	235	430	670
1143	0	47	103	188	293
1295	0	25	55	101	157
1448	0	13	28	52	81

Semi-axial load was 40.0 kN.

Table C 3. Vertical permanent strain (microstrains) in 709C3.

Depth (mm)	Traffic Passes			
	0	250	1000	1500
38	0	5293	17688	20721
133	0	7720	18732	21713
248	0	13313	38215	47571
381	0	4141	9925	12752
533	0	2730	5887	7944
686	0	1310	1659	1144
838	0	604	765	528
991	0	390	494	341
1143	0	165	209	145
1295	0	81	103	72
1448	0	19	26	41

Semi-axial load was 53.4 kN.

Table C 4. Vertical permanent strain (microstrains) in 709C4.

Depth (mm)	Traffic Passes					
	0	250	1000	5000	10000	22000
38	0	2855	7373	14035	19486	29596
133	0	4173	9471	21008	32210	50664
248	0	1904	3899	8660	13956	23097
381	0	1716	3382	6096	8814	12073
533	0	707	1565	3256	5081	6708
686	0	150	332	690	1075	1416
838	0	-170	-95	-55	-274	218
991	0	-40	-22	-13	-64	51
1143	0	-37	-20	-12	-59	47
1295	0	-26	-14	-8	-41	33
1448	0	-10	-6	-3	-17	13

Semi-axial load was 31.1 kN.

Table C 5. Vertical permanent strain (microstrains) in 709C5.

Depth (mm)	Traffic Passes			
	0	250	500	800
38	0	38968	46311	52085
133	0	11605	14451	17720
248	0	20832	15909	22521
381	0	8465	8550	10354
533	0	5096	5220	5715
686	0	2594	1982	2486
838	0	2845	2471	2941
991	0	2252	935	914
1143	0	813	337	330
1295	0	621	290	284
1448	0	341	142	139

Semi-axial load was 40.0 kN.

Table C 6. Vertical permanent strain (microstrains) in 709C6.

Depth (mm)	Traffic Passes					
	0	250	1000	5000	10000	25000
38	0	2956	10297	17569	26206	31911
133	0	4786	22386	16779	12015	10321
248	0	4901	7912	11859	14594	25756
381	0	1423	2341	4400	5698	11309
533	0	988	2157	3068	3674	8373
686	0	438	957	1360	1628	3709
838	0	180	393	558	668	1522
991	0	73	160	228	273	621
1143	0	39	85	121	145	329
1295	0	24	52	74	89	203
1448	0	13	28	40	48	109

Semi-axial load was 20.0 kN.

APPENDIX D

DYNAMIC STRAIN MEASUREMENTS

Table D 3. Vertical dynamic strain (microstrains) in 709C1.

Depth (mm)	Traffic Passes								
	0	250	1000	5000	10000	25000	35000	50000	75000
133	3280	3011	2982	3015	3098	3158	3183	2957	3114
248	2751	2528	2749	2686	2839	2939	2982	2657	2954
381	3716	3507	4076	4413	5127	5987	6253	5749	6533
533	2591	2334	2730	3084	3799	4781	5202	4722	5499
686	1135	1125	1233	1257	1414	1623	1724	1548	1705
838	0	0	0	0	0	0	0	0	0
991	0	0	0	0	0	0	0	0	0
1143	0	0	0	0	0	0	0	0	0
1295	0	0	0	0	0	0	0	0	0
1448	213	214	260	191	214	223	229	190	217

Semi-axial load was 26.7 kN.

Table D 2. Vertical dynamic strain (microstrains) in 709C2.

Depth (mm)	Traffic Passes				
	0	250	1000	2500	5000
133	3463	3453	3536	3244	3494
248	3598	3448	3333	2801	3058
381	6122	6898	7786	7778	9086
533	3451	4038	4938	5263	6694
686	2063	2242	2487	2482	2915
838	1223	1360	1515	1550	1812
991	868	995	1009	1124	1261
1143	627	375	85	317	477
1295	383	130	408	476	476
1448	293	313	296	298	366

Semi-axial load was 40.0 kN.

Table D 3. Vertical dynamic strain (microstrains) in 709C3.

Depth (mm)	Traffic Passes			
	0	250	1000	1500
133	3207	3548	3488	3297
248	5003	5812	6087	6267
381	7095	9405	11244	11993
533	3797	5793	7703	8434
686	2113	2477	2921	3165
838	1938	2252	2732	2991
991	0	0	0	0
1143	608	721	801	1000
1295	528	589	703	989
1448	0	0	0	0

Semi-axial load was 53.4 kN.

Table D 4. Vertical dynamic strain (microstrains) in 709C4.

Depth (mm)	Traffic Passes					
	0	250	1000	5000	10000	22000
133	3011	2998	2962	3166	3542	3907
248	3230	3543	3654	4247	4647	5374
381	5661	6983	7438	9165	10026	10985
533	3431	4221	4403	4834	4821	5362
686	0	0	0	0	0	0
838	805	1074	929	1183	1260	1563
991	0	0	0	0	0	0
1143	0	0	0	0	0	0
1295	0	0	0	0	0	0
1448	256	324	320	342	156	360

Semi-axial load was 31.1 kN.

Table D 5. Vertical dynamic strain (microstrains) in 709C5.

Depth (mm)	Traffic Passes			
	0	300	500	950
133	8501	4395	2590	4717
248	7806	7971	5953	5988
381	10239	10500	10867	11256
533	5677	5577	5605	5735
686	2500	2558	2661	2850
838	2146	2089	2222	2324
991	476	867	983	1086
1143	0	0	0	0
1295	930	534	525	547
1448	468	360	411	369

Semi-axial load was 40.0 kN.

Table D 6. Vertical dynamic strain (microstrains) in 709C6.

Depth (mm)	Traffic Passes						
	0	250	1000	5000	10000	25000	35000
133	2595	0	0	0	0	0	0
248	3379	2888	2945	2976	3085	3616	2027
381	6392	6958	6878	7047	7160	7830	6912
533	0	0	0	0	0	0	0
686	899	915	877	909	899	966	929
838	0	0	0	0	0	0	0
991	0	0	0	0	0	0	0
1143	0	0	0	0	0	0	0
1295	407	155	250	179	322	11	0
1448	47	240	22	75	0	79	17

Semi-axial load was 20.0 kN.

APPENDIX E

STRESS MEASUREMENTS

Table E 4. Vertical stress (kPa) in 709C1.

Depth	Traffic Passes								
	0	250	1000	5000	10000	25000	35000	50000	75000
76 mm below top of subgrade	41.4	40.4	40	40.8	41.8	48.1	48.1	51.4	55.5

Semi-axial load was 26.7 kN.

Table E 2. Vertical stress (kPa) in 709C2.

Depth	Traffic Passes				
	0	250	1000	2500	5000
Middle of Base Course	136.2	123.1	123.4	118.3	124.9
76 mm below top of subgrade	64.8	62.2	61.3	58	61.9
381 mm below top of subgrade	39.3	38.1	39	37.6	40.6

Semi-axial load was 40.0 kN.

Table E 3. Vertical stress (kPa) in 709C3.

Depth	Traffic Passes			
	0	250	1000	1500
76 mm below top of subgrade	75.3	78.2	78.9	79.2

Semi-axial load was 53.4 kN.

Table E 4. Vertical stress (kPa) in 709C4.

Depth	Traffic Passes					
	0	250	1000	5000	10000	22000
76 mm below top of subgrade	45.3	44.9	43.2	42.7	42.9	44.8

Semi-axial load was 31.1 kN.

Table E 5. Vertical stress (kPa) in 709C5.

Depth	Traffic Passes			
	0	250	500	800
Middle of Base Course	137.9	144.4	143.5	145.3
76 mm below top of subgrade	68.4	68.3	68.3	68.1

Semi-axial load was 40.0 kN.

Table E 6. Vertical stress (kPa) in 709C6.

Depth	Traffic Passes						
	0	250	1000	5000	10000	25000	35000
Top of Base Course	95.5	83.2	88.7	85.7	88.2	100.6	96.7
Bottom of Base Course	50.6	46.9	48.0	47.5	49.1	56.5	51.4
76 mm below top of subgrade	37.8	36.7	35.9	37	37.4	39.4	42.4
76 mm below top of subgrade	40.0	37.4	39.1	38.9	40.0	46.9	43.1

Semi-axial load was 20.0 kN.

APPENDIX F

FALLING WEIGHT DEFLECTOMETER MEASUREMENTS

Table F 1. FWD deflections at 21 locations within Test Section 709.

Sensor		W1	W2	W3	W4	W5	W6	W7
Radial Distance:	(m)	0	0.30	0.61	0.91	1.22	1.52	1.83
	(in.)	0	12	24	36	48	60	72
STATION	LOAD	Deflection (mil)						
1	5953	84.7	49.5	7.7	3.4	2.6	1.7	1.3
2	6366	90.2	35.5	8.7	3.2	2.0	1.5	1.0
3	6274	78.4	40.5	8.8	3.9	2.5	1.4	1.0
4	6211	82.8	44.6	8.6	4.2	2.9	1.9	1.3
5	6027	109.1	70.0	5.6	2.6	1.9	0.9	0.8
6	6562	99.5	68.9	3.0	2.1	1.3	0.5	0.8
7	6366	90.1	40.0	7.8	4.3	2.6	1.8	1.3
8	6451	89.5	39.1	8.1	3.9	3.1	4.0	1.7
9	6680	92.9	51.2	9.1	4.1	3.4	2.3	1.4
10	6673	84.7	50.5	8.8	4.1	3.4	2.3	1.4
11	6211	99.3	53.7	5.5	2.4	1.9	1.0	0.9
12	6414	92.4	63.3	7.2	4.0	2.6	1.4	0.8
13	6477	94.6	60.8	6.7	3.9	3.0	1.8	0.8
14	5923	90.9	73.3	1.1	4.4	2.8	1.3	1.3
15	5923	114.6	68.4	7.1	1.5	1.7	1.0	1.0
16	6477	94.7	61.5	7.4	2.3	3.4	2.2	1.2
17	6163	87.4	35.0	6.9	3.4	3.1	2.3	1.6
18	6200	72.2	38.7	8.4	4.4	3.2	2.3	1.7
19	6145	79.5	48.0	9.8	3.5	2.9	2.0	1.1
20	6008	80.2	50.1	10.2	3.3	3.0	1.9	0.9
21	5547	98.3	60.0	5.0	1.4	2.0	0.9	0.5

Test parameters:

Plate radius.....5.95 in (151 mm)

Air and pavement temperature..... 65 °F (18.3 °C)

For layer thickness see figures 55 through 60.